SANDIA NATIONAL LABORATORIES
WASTE ISOLATION PILOT PLANT

ANALYSIS REPORT FOR THE 2026 COMPLIANCE RECERTIFICATION APPLICATION PERFORMANCE ASSESSMENT: FINAL STATE REPOSITORY

REVISION 0

TODD ZEITLER
(Affiliate)

Digitally signed by TODD ZEITLER (Affiliate)
Date: 2025.12.10 12:49:17 -07'00'

Authentication

Author:	Todd R. Zeitler	Org.	8612
Author:	Sarah Brunell	Org.	8881
Author:	Brad Day	Org.	8881
Author:	Paul Docherty	Org.	8881
Author:	Dwayne Kicker	Org.	8881
Author:	Sungtae Kim	Org.	8881
Author:	Seth King	Org.	8881
Author:	Jennifer Long	Org.	8881
Author:	Justin Wilgus	Org.	8881
Technical Reviewer:	Clifford Hansen	Org.	8824
Technical Reviewer:	Kate Weiksnar	Org.	8855
QA Reviewer:	Shelly R. Nielsen	Org.	8883
Management Reviewer:	Steve Wagner	Org.	8881

DECEMBER 2025

Information Only

Executive Summary

The Waste Isolation Pilot Plant (WIPP) was initially certified as a repository consisting of 10 panels, which were excavated for the long-term storage and placement of transuranic waste (U.S. EPA 1998). However, due to operational constraints, the entire volume of the 10 panels is no longer available for waste disposal. In March 2024, the U.S. Department of Energy (DOE) submitted the Replacement Panels Planned Change Request (RPPCR) to the U.S. Environmental Protection Agency (EPA) for approval of waste emplacement in two new panels. These panels, referred to as replacement panels, are located to the west of the existing operations area. The RPPCR received EPA approval in July of 2025 (U.S. EPA 2025).

The addition of the two replacement panels is not expected to provide adequate space for the disposal of the allowable waste volume designated for WIPP under the Land Withdrawal Act (LWA); thus, the 12-panel configuration is regarded as an interim state (IS) of the repository. The DOE may pursue approval for waste disposal in seven additional panels to accommodate the full allowable volume of waste. This hypothetical 19-panel configuration is considered the anticipated final state (FS) of the repository.

The DOE demonstrates compliance with containment requirements as outlined in the Certification Criteria of Title 40 CFR Part 191.13 through performance assessment (PA). PA calculations estimate the probability and consequences of potential radionuclide releases from the repository to the accessible environment over a regulatory period of 10,000 years following facility closure. WIPP PA models are utilized to support the periodic recertification of WIPP.

The 2026 Compliance Recertification Application (CRA-2026) represents the fifth recertification application submitted to the EPA. A PA has been carried out by Sandia National Laboratories to support the DOE's submission of the CRA-2026. The results presented in the CRA-2026 PA include those from the CRA-2026 interim state PA (CRA26_IS) (Brunell et al. 2025), which consider a 12-panel repository representation, and are compared to those from the RPPCR PA, the most recent regulatory submission.

This report documents the CRA-2026 supplemental PA for the final state repository (CRA26_FS) and details the effects of an increased waste inventory and additional repository footprint to accommodate the disposal of the full LWA allowable waste volume. In comparison to the CRA26_IS, the primary effects of these changes are an increased number of intrusions into the repository footprint, coupled with decreased radionuclide activity concentrations (in both mobilized and nonmobilized forms). The results of these effects include similar or higher mean total releases, driven by increased waste area brine pressures and saturations (leading to higher spallings and direct brine releases). The increased number of intrusions leads to an increased probability of intersecting a high-concentration waste stream (increasing cuttings and cavings releases). Releases through the Culebra are also increased but remain at negligible levels.

Information Only

TABLE OF CONTENTS

EXECUTIVE SUMMARY ..... **II**

1.0 INTRODUCTION **1**

2.0 CHANGES RELATIVE TO THE CRA26_IS **2**

2.1 Repository Design 2

2.2 Parameters Related to Repository Dimensions 3

2.3 Salado Flow and Transport Computational Grid 4

2.4 Waste Inventory 4

2.5 Baseline Actinide Solubilities 5

2.6 Humic Colloidal Enhancement Parameters 5

2.7 Minimum Brine Volume Needed for a DBR 5

2.8 Culebra Release Point Location 6

3.0 METHODOLOGY FOR THE CRA26_FS **8**

3.1 Review of FEPs and Conceptual Models 8

3.2 Salado Flow 9

3.2.1 Repository Representation in BRAGFLO 9

3.2.2 Salado Flow Modeling Scenarios 10

3.3 Radionuclide Activities for Solid Releases 11

3.4 Cuttings, Cavings, and Spallings 11

3.5 Direct Brine Release Volumes 12

3.5.1 Initial Conditions 13

3.5.2 Modeling Scenarios 14

3.6 Mobilized Radionuclide Concentrations 15

3.7 Salado Transport 15

3.8 Culebra Flow and Transport 16

3.9 Calculation of CCDFs for Releases 18

3.10 Sensitivity Analysis 19

3.11 Run Control 19

4.0 RESULTS **20**

4.1 Inventory 20

Information Only

4.1.1 Total Waste Volume 20
4.1.2 Inventory by EPA Units 21
4.1.3 Waste Stream Activity Concentration 22
4.1.4 Total Radionuclide Activity 23
4.2 Salado Flow 25
4.3 Cuttings, Cavings, and Spallings 39
4.3.1 Cuttings and Cavings 39
4.3.2 Spallings 40
4.4 Direct Brine Release Volumes 44
4.5 Mobilized Radionuclide Concentrations 49
4.6 Salado Transport 53
4.7 Culebra Flow and Transport 57
4.8 Releases by Release Mechanism 62
4.8.1 Undisturbed Repository Releases 63
4.8.2 Cuttings and Cavings Releases 63
4.8.3 Spallings Releases 67
4.8.4 Direct Brine Releases 71
4.8.5 Long-Term Radionuclide Transport 74
4.9 Total Releases 80
4.9.1 Sensitivity Analysis for Total Releases 84
4.9.2 Comparison to RPPCR 87

5.0 CONCLUSIONS 88

6.0 REFERENCES 90

Information Only

LIST OF FIGURES

Figure 1. Final State Repository Layout 3
Figure 2. Culebra Release Point Locations 7
Figure 3. BRAGFLO Grid for the CRA26_FS with Modeled Area Descriptions 10
Figure 4. CRA26_FS and CRA26_IS DBR Grid with Simulated Intrusion Locations 13
Figure 5. Regions Used to Transfer Initial Pressure and Saturation from the BRAGFLO Salado Grid to the DBR Grid 14
Figure 6. Culebra Modeling Domain (Derived from Wilgus and Bethune 2025) 18
Figure 7. Total Activity in WIPP CH- and RH-TRU Waste from Closure to 10,000 Years After Closure, in Units of (a) Curies (Ci) and (b) EPA Units. 25
Figure 8. Mean Net Brine Flow into the Waste Panel 28
Figure 9. Mean Net Brine Flow into the South Rest-of-Repository 28
Figure 10. Mean Net Brine Flow into the North Rest-of-Repository 29
Figure 11. Mean Net Brine Flow into the West Rest-of-Repository 29
Figure 12. Normalized Mean Net Brine Flow into the West Rest-of-Repository 30
Figure 13. Mean Brine Consumption in the Waste Panel 30
Figure 14. Mean Brine Consumption in the South Rest-of-Repository 31
Figure 15. Mean Brine Consumption in the North Rest-of-Repository 31
Figure 16. Mean Brine Consumption in the West Rest-of-Repository 32
Figure 17. Normalized Mean Brine Consumption in the West Rest-of-Repository 32
Figure 18. Mean Brine Saturation in the Waste Panel 33
Figure 19. Mean Brine Saturation in the South Rest-of-Repository 33
Figure 20. Mean Brine Saturation in the North Rest-of-Repository 34
Figure 21. Mean Brine Saturation in the West Rest-of-Repository 34
Figure 22. Mean Total Repository Gas Generation 35
Figure 23. Mean Normalized Total Repository Gas Generation 35
Figure 24. Mean Brine Pressure in the Waste Panel 36
Figure 25. Mean Brine Pressure in the South Rest-of-Repository 36
Figure 26. Mean Brine Pressure in the North Rest-of-Repository 37
Figure 27. Mean Brine Pressure in the West Rest-of-Repository 37
Figure 28. Mean Brine Flow up the Borehole 38
Figure 29. Mean Brine Flow up the Shaft 38

Information Only

Figure 30. Mean Brine Flow in Anhydrite Layers Across the Land Withdrawal Boundary.....39
Figure 31. Non-Zero Spallings Release Volume by Scenario.....43
Figure 32. Non-Zero Spallings Release Volume by Location.....43
Figure 33. Spallings Release Concentration from Closure to 10,000 Years.....44
Figure 34. DBR Volume Frequency, All Non-Zero Releases.....46
Figure 35. DBR Volumes, All Non-Zero Releases.....48
Figure 36. DBR Volumes by Scenario, All Non-Zero Releases.....48
Figure 37. Largest Contributors in Curies to Inventory at Closure in the Waste Area.....50
Figure 38. Comparison of Mean Concentrations for Select Radionuclides.....52
Figure 39. Summed Concentration Versus Time Used for Determining DBRs, all Vectors.....52
Figure 40. Cumulative Lumped Radionuclide Release.....54
Figure 41. Cumulative Brine Releases up the Borehole.....55
Figure 42. Total Cumulative Radionuclide Releases vs Time.....56
Figure 43. Particle Travel Paths and Travel Time to the LWB Exceedance Probabilities, Full Mining Scenario (Derived from Wilgus and Bethune 2025).....59
Figure 44. Particle Travel Paths and Travel Time to the LWB Exceedance Probabilities, Partial Mining Scenario (Derived from Wilgus and Bethune 2025).....60
Figure 45. Exceedance Probability of Cumulative Mass to the LWB in 10,000 Years for Full Mining Scenario (Derived from Wilgus and Bethune 2025).....61
Figure 46. Exceedance Probability of Cumulative Mass to the LWB in 10,000 Years for Partial Mining Scenario (Derived from Wilgus and Bethune 2025).....62
Figure 47. Mean Cuttings and Cavings Excavated Volume for Replicate 1.....64
Figure 48. Mean Cuttings and Cavings Excavated Volume Scaled by the FVW Factor for Replicate 1.....65
Figure 49. Cuttings and Cavings Releases for Replicate 1 of the CRA26_FS.....65
Figure 50. Cuttings and Cavings Releases for Replicate 2 of the CRA26_FS.....66
Figure 51. Cuttings and Cavings Releases for Replicate 3 of the CRA26_FS.....66
Figure 52. Overall Mean Cuttings and Cavings Releases.....67
Figure 53. Mean Spallings Volume for Replicate 1.....68
Figure 54. Mean Spallings Volume Scaled by the FVW Factor for Replicate 1.....69
Figure 55. Spallings Releases for Replicate 1 of the CRA26_FS.....69
Figure 56. Spallings Releases for Replicate 2 of the CRA26_FS.....70
Figure 57. Spallings Releases for Replicate 3 of the CRA26_FS.....70

Information Only

Figure 58. Overall Mean Spallings Releases 71
Figure 59. Mean Direct Brine Volume for Replicate 1 72
Figure 60. Direct Brine Releases for Replicate 1 of the CRA26_FS....72
Figure 61. Direct Brine Releases for Replicate 2 of the CRA26_FS....73
Figure 62. Direct Brine Releases for Replicate 3 of the CRA26_FS....73
Figure 63. Overall Mean Direct Brine Releases 74
Figure 64. Mean Activity Entering the Culebra by Radionuclide for Replicate 1 of the CRA26_FS 75
Figure 65. Overall Mean Radionuclide Activity Entering the Culebra 76
Figure 66. Releases Through the Culebra for Replicate 1 of the CRA26_FS 77
Figure 67. Releases Through the Culebra for Replicate 2 of the CRA26_FS 78
Figure 68. Releases Through the Culebra for Replicate 3 of the CRA26_FS 78
Figure 69. Mean Replicate 1 Releases Through the Culebra by Radionuclide and Release Point79
Figure 70. Overall Mean Releases Through the Culebra....80
Figure 71. Total Releases for Replicate 1 of the CRA26_FS 81
Figure 72. Total Releases for Replicate 2 of the CRA26_FS 82
Figure 73. Total Releases for Replicate 3 of the CRA26_FS 82
Figure 74. Overall Mean Release Components for the CRA26_FS 83
Figure 75. Overall Mean Total Releases for the CRA26_FS 83
Figure 76. Overall Mean Total Releases....88

Information Only

LIST OF TABLES

Table 1. Changed Repository Parameters 4
Table 2. Inventory Iron, CPR, and Decay Heat Concentrations 5
Table 3. Updated Humic Colloid Parameters 5
Table 4. Minimum Brine Volume Parameter 6
Table 5. BRAGFLO Modeling Scenarios for the CRA26_FS 11
Table 6. DBR Scenarios 15
Table 7. WIPP CH- and RH-TRU Waste Streams by Total Scaled Volume from the CRA26_IS and CRA26_FS Inventories 21
Table 8. WIPP CH- and RH-TRU Waste Streams by Total EPA Units; At Closure (Calendar Year 2083) and After 10,000 Years (Calendar Year 12083) from the CRA26_FS Inventory 22
Table 9. WIPP CH- and RH-TRU Waste Streams Ordered by Activity Concentration at Closure (Calendar Year 2,083) and after 10,000 Years (Calendar Year 12083) from CRA26_FS Inventory 23
Table 10. Total Activity (EPA Units) for Dominant Isotopes in WIPP CH- and RH-TRU Waste at Closure and after 10,000 Years 24
Table 11. Cavings Area Statistics for CRA26_FS and CRA26_IS 40
Table 12. Spallings Volume Summary, Replicate 1 42
Table 13. DBR Volume Summary 47
Table 14. Mean Element Mobile Concentration Limits in mol/L 51
Table 15. Mean Lumped Radionuclide Mobile Concentration Limits in mol/L 51
Table 16. Mean Cumulative Lumped Radionuclides Releases Through a Borehole to the Culebra at 10,000 Years in EPA Units 55
Table 17. Statistics on the Overall Mean for Cuttings and Cavings Releases 67
Table 18. Statistics on the Overall Mean for Spallings Releases 71
Table 19. Statistics on the Overall Mean for Direct Brine Releases 74
Table 20. Statistics on the Overall Mean for Radionuclide Activity Entering the Culebra 76
Table 21. Statistics on the Overall Mean for Releases Through the Culebra 80
Table 22. Statistics on the Overall Mean for Total Releases 84
Table 23. Stepwise Ranked Regression Analysis for Mean Total Releases for Replicate 1 of the CRA26_IS and CRA26_FS 85
Table 24. Stepwise Ranked Regression Analysis for Mean Total Releases for Replicate 2 of the CRA26_IS and CRA26_FS 86

Information Only

Table 25. Stepwise Ranked Regression Analysis for Mean Total Releases for Replicate 3 of the CRA26_IS and CRA26_FS 86

Table 26. Statistics on the Overall Mean for Total Releases 88

Information Only

1.0 INTRODUCTION

The Waste Isolation Pilot Plant (WIPP), located in southeastern New Mexico, has been developed by the U.S. Department of Energy (DOE) for the geologic disposal of transuranic (TRU) waste. The containment of TRU waste at the WIPP is regulated by the U.S. Environmental Protection Agency (EPA) under Title 40 of the Code of Federal Regulations (CFR), Part 191.

The DOE demonstrates compliance with the containment requirements of 40 CFR 191.13 by means of performance assessment (PA) as described in the Certification Criteria of Title 40 CFR Part 194. Sandia National Laboratories (SNL) conducts PAs at the request of the DOE. The PA calculations estimate the probability and consequences of potential radionuclide releases from the repository to the accessible environment over a regulatory period of 10,000 years following facility closure. The PA models are continuously maintained and updated with new information, which typically leads to refinements and modifications in both the models and their parameters. Additionally, planned changes to the repository and its components necessitate updates to the WIPP PA models.

All previous WIPP certifications have been based on a repository consisting of 10 panels. In March 2024, the DOE submitted the Replacement Panels Planned Change Request (RPPCR) to seek EPA approval for waste emplacement in two new panels, referred to as replacement panels, located to the west of the existing operations area (Bollinger 2024). The RPPCR received EPA approval in July of 2025 (U.S. EPA 2025).

The addition of the two replacement panels is not expected to provide sufficient space for the disposal of the allowable waste volume designated for the WIPP under the Land Withdrawal Act (LWA). The 12-panel configuration is thus regarded as an interim state of the repository. The DOE may seek approval for waste disposal in up to seven additional panels to accommodate the full allowable volume of waste. This 19-panel configuration is considered the anticipated final state of the repository.

The CRA-2026 is the fifth recertification application for the WIPP submitted by the DOE for EPA approval. The PA executed by SNL in support of the CRA-2026 PA is described in AP-214 (Hansen et al. 2025). This report summarizes the results of the CRA-2026 PA for the final state repository (CRA26_FS) and compares them to the results of the PA performed for the interim state repository (CRA26_IS) (Brunell et al. 2025).

Information Only

2.0 CHANGES RELATIVE TO THE CRA26_IS

Several changes are incorporated in the CRA26_FS PA relative to the CRA26_IS. All changes are associated with the inclusion of seven additional waste panels beyond the 12 waste panels considered for the CRA26_IS. These changes include:

- The repository design.
- Parameters related to repository dimensions.
- The waste inventory.
- Baseline actinide solubilities.
- Colloid concentration parameters for humic colloids.
- The Salado flow and transport computational grid.
- The minimum brine volume needed for a direct brine release (DBR).
- The addition of Culebra release points for the additional waste panels.

Changes listed above are discussed in more detail in the sections that follow.

2.1 Repository Design

This analysis represents the 19-panel final state repository consisting of ten original panels, two replacement panels, and seven additional panels. The 12-panel interim state repository represented in the CRA26_IS consisted of the ten original and two replacement panels. Figure 1 depicts the final state repository. The 19-panel repository design is the same as for the RPPCR.

Information Only

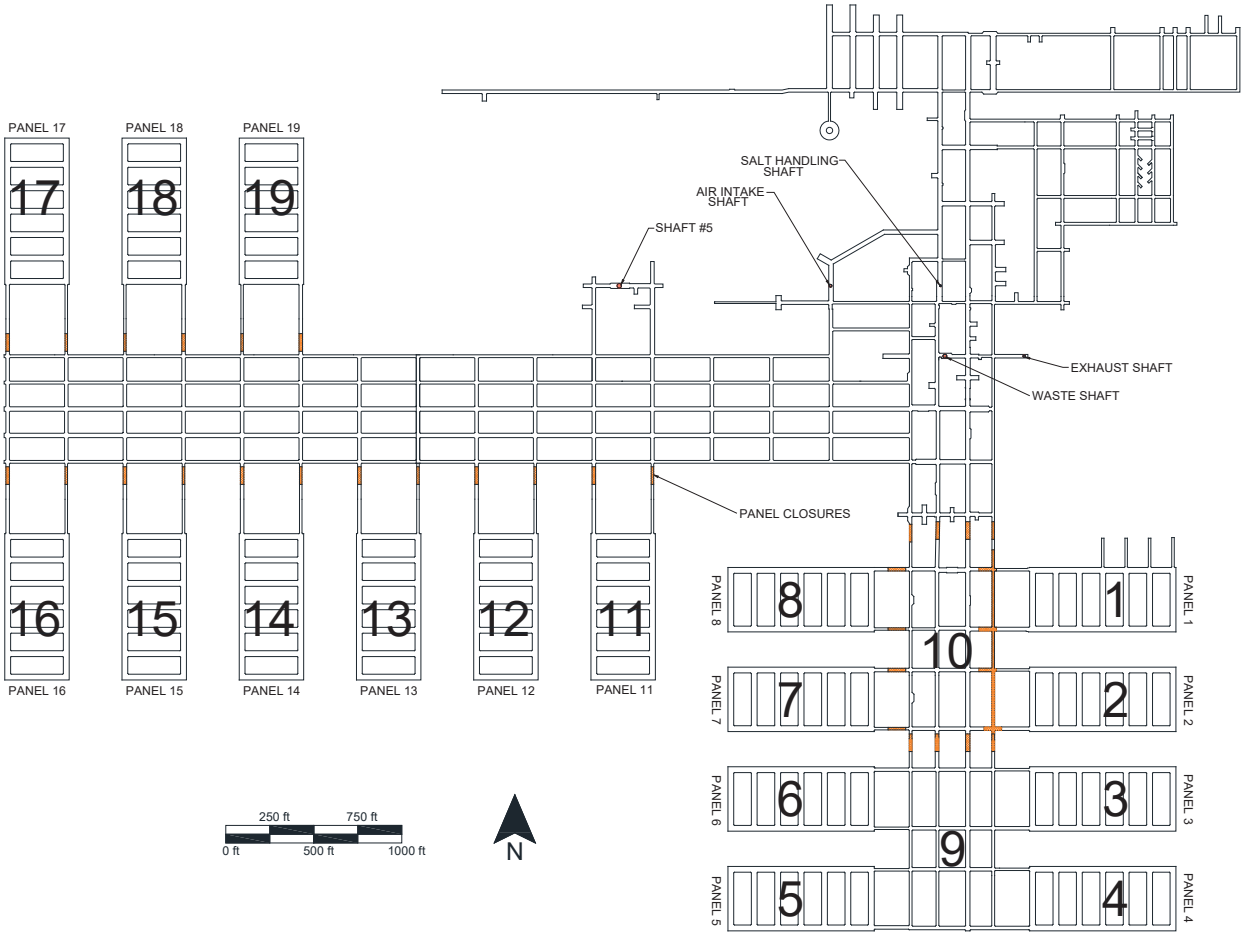


Figure 1. Final State Repository Layout

2.2 Parameters Related to Repository Dimensions

The repository design (Section 2.1) requires changes to several parameters describing repository dimensions. Brunell (2025) revises four parameters to align with the as-built dimensions of the original 10 waste panels and the planned dimensions of the replacement and additional waste panels. The parameters include:

- the waste storage volume (REFCON:VREPOS).
- the area of the berm placed over the waste panels (REFCON:ABERM).
- the area allocated for contact-handled (CH) waste disposal (REFCON:AREA_CH).
- the fraction of the repository volume occupied by CH waste (REFCON:FVW).

For the CRA26_FS PA, the value of this parameter has been increased back to the value used previous to the CRA26_IS PA. The updated values are provided in Table 1. The repository parameters REFCON:ABERM and REFCON:AREA_RH have the same values in the CRA26_FS as in the RPPCR. CRA26_FS parameters REFCON:VREPOS, REFCON:AREA_CH and

Information Only

REFCON:FVW differ from the RPPCR due to aligning the computational grid (Section 2.3) to as-built dimensions.

Table 1. Changed Repository Parameters

Material	Property	CRA26_IS Value	CRA26_FS Value	Units
REFCON	VREPOS	560,722.29	905,734.49	m^3
REFCON	ABERM	750,000	1,268,303	m^2
REFCON	AREA_CH	141,511	228,582	m^2
REFCON	FVW	0.279	0.186	-
REFCON	AREA_RH	3,528	15,760	m^2

2.3 Salado Flow and Transport Computational Grid

Dimensions in the computational grid for the Salado flow (BRAGFLO) and transport (NUTS) calculation are changed to represent the final state repository (Section 2.1). Day (2025) modified the CRA26_FS computational grid in comparison to the CRA26_IS computational grid as summarized in Section 3.2.1. The CRA26_FS grid differs from that used in the RPPCR due to aligning the grid with as-built repository dimensions.

2.4 Waste Inventory

For CRA26_IS, the waste volume was lowered from the statutory limit on the volume of waste established in the LWA to 157,837.92 m^3 (Ward 2025). As a result, the inventory estimate was scaled to this lower volume. For CRA26_FS, the repository volume is increased back to the LWA volume and the inventory estimate is scaled to this increased volume of 175,564 m^3 (6,200,000 ft^3). Based on information collected up to December 31, 2023, the Full Repository Performance Assessment Inventory Report – 2024 (FRPAIR-2024; Van Soest 2025a) offers an inventory estimate scaled to the LWA waste volume. Kicker (2025a) conducted a screening analysis of the inventory estimates for the FRPAIR-2024 to define the inventory-related input parameters for the PA calculations. The inventory differs from that used in the RPPCR.

Table 2 compares aspects of the CRA26_FS and CRA26_IS inventories, normalized by the waste storage volume of each repository (REFCON:VREPOS). The inventory aspects are iron, cellulosics, plastics, and rubber (CPR), and decay heat. The iron, CPR, and decay heat concentrations are each decreased for the CRA26_FS and the inventory volume as a percentage of repository volume is 28% and 18% for CRA26_IS and CRA26_FS, respectively.

Information Only

Table 2. Inventory Iron, CPR, and Decay Heat Concentrations

Input	Unit	CRA26_IS Value	CRA26_FS Value	CRA26_FS to CRA26_IS Ratio
Iron	kg/m^3	126.83	97.93	0.77
CPR	kg/m^3	40.48	29.09	0.72
Decay Heat	$watt/m^3$	0.43	0.31	0.73

2.5 Baseline Actinide Solubilities

Thermodynamic calculations are used to compute the baseline solubilities for actinides in the +III, +IV, and +V oxidation states in GWB and ERDA-6 brines for five multiples of the minimum brine volume for a DBR event. These baseline solubility calculations account for inventory components and thus are updated to be consistent with inventory estimates. Domski (2025a) reports the baseline solubility values based on the CRA26_FS inventory. The baseline solubilities differ from those used in the RPPCR.

Currently there is no thermodynamic model for WIPP actinides in the +VI oxidation state, so there is no inventory dependence of the baseline solubility for actinides in the +VI oxidation state. As a result, the +VI oxidation state baseline solubility is the same in the CRA26_FS and CRA26_IS.

2.6 Humic Colloidal Enhancement Parameters

Based on updates to the thermodynamic model and baseline solubility values, Mariner (2025) reevaluated the proportionality constant for humic colloids. Mariner recommends updated values for radionuclides in the +III oxidation state for Castile Salado brine (PHUMOX3:PHUMCIM) and in the +IV oxidation state for Salado brine (PHUMOX4:PHUMSIM). The humic colloidal enhancement parameters differ from those used in the RPPCR.

Table 3. Updated Humic Colloid Parameters

Material	Property	CRA-2026 IS Value	CRA-2026 FS Value	Units
PHUMOX3	PHUMCIM	0.3	0.4	-
PHUMOX4	PHUMSIM	0.02	0.01	-

2.7 Minimum Brine Volume Needed for a DBR

The parameter representing minimum brine volume required for a direct brine release (DBR), GLOBAL:DBRMINBV, is revised (Brunell 2025) to be consistent with geomechanical modeling that predicts repository porosity and with the repository geometry described in Section 2.1. The new geomechanical model predicts a smaller porosity in the repository, which results in a lower pore volume and the value for GLOBAL:DBRMINBV compared to previous assessments. The value used in the CRA-2026 FS PA is presented in Table 4. The minimum brine volume has

Information Only

increased for the CRA26_FS due to the larger repository footprint compared to the CRA26_IS. The minimum brine volume differs from that used in the RPPCR.

Table 4. Minimum Brine Volume Parameter

Material	Property	CRA-2026 IS Value	CRA-2026 FS Value	Units
GLOBAL	DBRMINBV	6,314	9,608	m^3

2.8 Culebra Release Point Location

The CRA26_FS uses four Culebra release points (CRPs). For the RPPCR, the CRP 2 was located at the centroid of Panels 11, 12, and 13 in a 19-panel representation of the WIPP repository. For the interim state repository with only replacement Panels 11 and 12 beyond the original 10, CRP 2 is relocated to the centroid of Panels 11 and 12 (Wilgus and Brunell 2025). To simplify comparison between analysis results, the 19-panel repository representation uses the same CRP 2 location as the 12-panel repository representation (Figure 2). Particle track pathways from CRP 2 in its original location (Bethune 2023) and re-calculated location (Wilgus and Bethune 2025) are highly similar for both partial mining and full mining scenarios. The locations of the other Culebra release points (CRP 1, CRP 3, and CRP 4) remain unchanged from the RPPCR. The full detailed set of CRP coordinates are provided in Wilgus and Bethune (2025).

Information Only

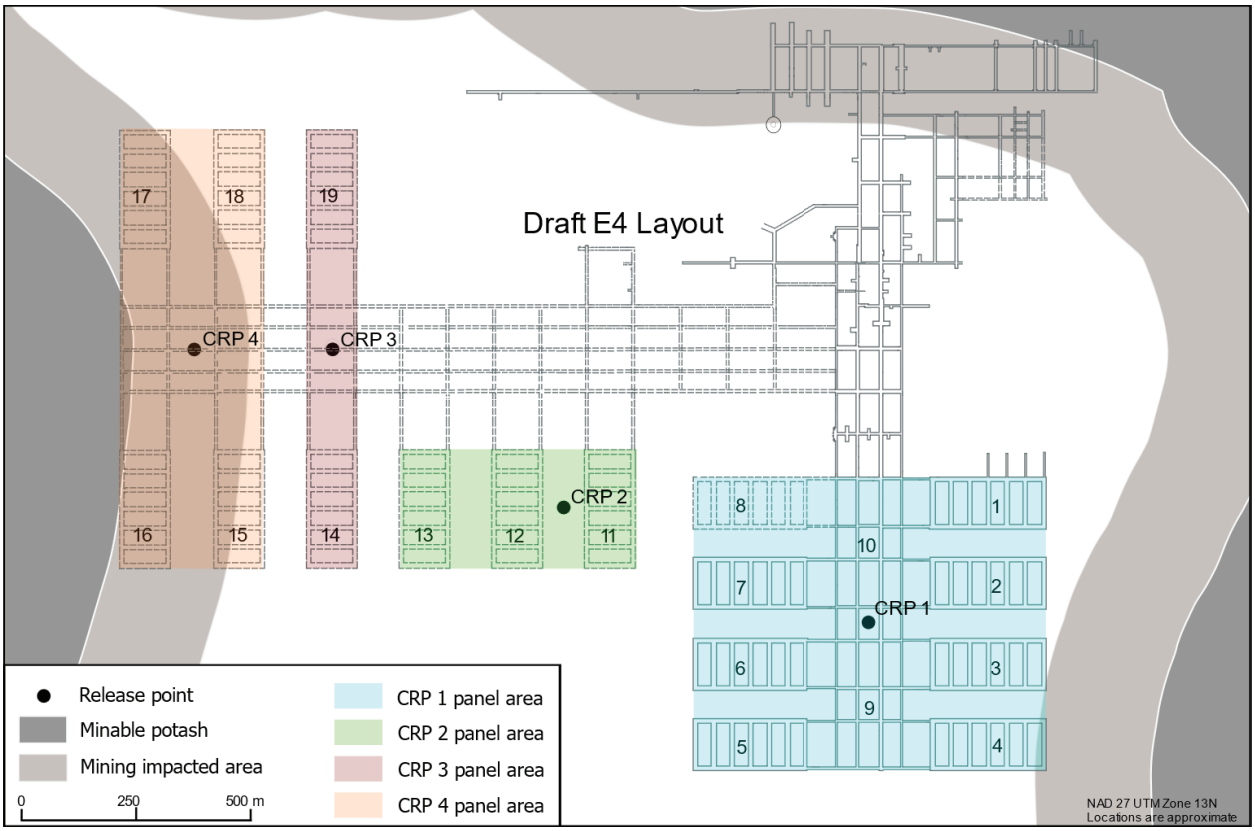


Figure 2. Culebra Release Point Locations

Information Only

3.0 METHODOLOGY FOR THE CRA26_FS

The WIPP PA calculations estimate the probability and consequence of potential radionuclide releases from the repository to the accessible environment for a regulatory period of 10,000 years after facility closure. It is conceivable that he WIPP repository might be disturbed by exploratory drilling for natural resources during the 10,000-year regulatory period. Drilling could create additional pathways for radionuclide transport, especially in the Culebra, and could potentially release material directly to the surface. In addition, hypothetical mining for potash within the Land Withdrawal Boundary (LWB) might alter flow in the overlying geologic units and may locally accelerate transport through the Culebra. The disturbed scenarios used in PA modeling are designed to capture the range of possible releases that could result from these hypothetical drilling and mining.

The PA accommodates both aleatory (i.e., stochastic) and epistemic (i.e., subjective) uncertainty in its constituent models. Aleatory uncertainty pertains to unknowable future events such as intrusion times and locations that may affect repository performance. It is accounted for by the generation of random sequences of future events. Epistemic uncertainty concerns parameter values that are assumed to be constants; the constants' true values are uncertain due to a lack of knowledge about the system. An example of a parameter with epistemic uncertainty is the permeability of a material. Epistemic uncertainty is accounted for by sampling parameter values from assigned distributions using Latin Hypercube Sampling, discussed in King and Zeitler (2025). One set of all sampled values required to run a WIPP PA calculation is termed a vector. Each set of 100 vectors is termed a replicate, and three sets of 100 vectors (e.g., three replicates) are used in a full WIPP PA analysis. For each vector, 10,000 possible sequences of future events (e.g., futures) are simulated to address aleatory uncertainty. The releases for each of the 10,000 simulated futures are tabulated for each of the 100 vectors in each of the 3 replicates.

For a random variable, the complementary cumulative distribution function (CCDF) provides the probability of the variable being greater than a particular value. By regulation, PA results are presented as a distribution of CCDFs of releases (U.S. EPA 1996). Each individual CCDF summarizes the likelihood of releases across the 10,000 futures simulated for one vector of parameter values. The uncertainty in parameter values results in a distribution of CCDFs.

3.1 Review of FEPs and Conceptual Models

An assessment of the features, events, and processes (FEPs) that could influence the long-term performance and safety of the WIPP repository was performed for the CRA-2026 analysis according to SP 9-4 (Kirkes 2024). The assessment aimed to determine if any of the changes implemented in this analysis affect current baseline FEP screening arguments or decisions. The FEPs assessment considered both the interim state and final state repositories. The FEPs assessment found that no changes to the FEP baseline were warranted (Kirkes and McCormick 2025).

The CRA-2026 conceptual models are unchanged from those of the RPPCR or CRA26_IS. The primary differences between the CRA26_FS and the CRA26_IS are:

- The inventory for the final state repository is based on the FRPAIR-2024 (Van Soest 2025a).

Information Only

- The Salado flow and transport computational grid for the final state repository is adjusted to represent 19 waste panels.

These differences do not require changes to the conceptual models on which the CRA-2026 (including the CRA26_IS and the CRA26_FS) and RPPCR are based.

3.2 Salado Flow

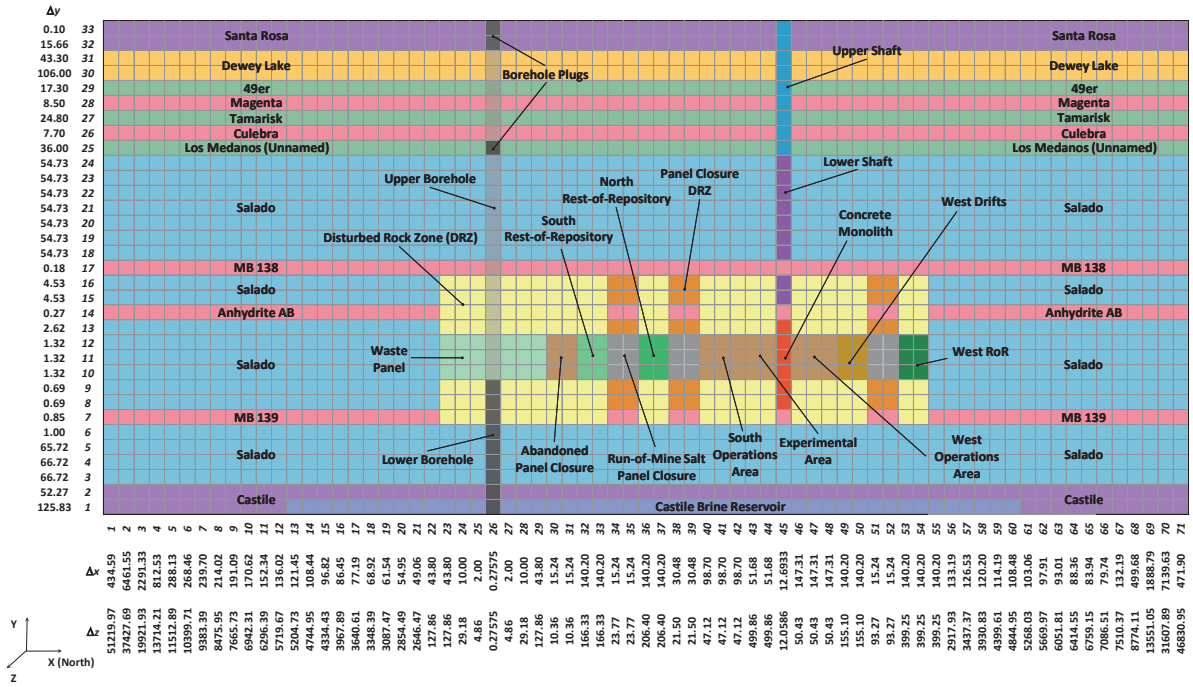
The BRAGFLO code calculates the flow of brine and gas in the vicinity of the WIPP repository over a 10,000-year regulatory compliance period. The results of these calculations are used by other WIPP PA codes to calculate potential radionuclide releases to the accessible environment.

The following subsections summarize the approach and methodology for Salado flow modeling as described by Day and King (2025).

3.2.1 Repository Representation in BRAGFLO

The computational grid and associated material map used by BRAGFLO for the CRA26_FS includes changes from the CRA26_IS BRAGFLO grid to the planned represent the extension of the West Drifts and seven additional waste panels located to the west of the existing Operations area (e.g., the West Rest-of-Repository). The flaring of the far-field Salado was re-calculated based on expanded dimensions of the WIPP repository with the distance to the North LWB calculated as the minimum distance from the westernmost edge of the excavated repository to the nearest land withdrawal boundary (to the west) and the distance to the South LWB calculated as the minimum distance from the southernmost edge of the excavated repository to the nearest land withdrawal boundary (to the south) (Day 2025). The generic BRAGFLO computational grid with modeled area descriptions and cell dimensions for the CRA26_FS is shown in Figure 3. Detailed material maps associated with the six modeling scenarios are provided for the CRA26_IS in Section 4.2 of Day and King (2025). The CRA26_IS maps apply to the CRA26_FS with the exception of modified Δx and Δz dimensions as given in Figure 3.

Information Only



Δx, Δy, and Δz dimensions in meters.

Figure 3. BRAGFLO Grid for the CRA26_FS with Modeled Area Descriptions

3.2.2 Salado Flow Modeling Scenarios

The six BRAGFLO modeling scenarios used in the CRA26_FS are unchanged from those used for the CRA26_IS. Results obtained in the six scenarios are used to initialize flow and material properties in subsequent codes in the PA computational suite (e.g., in the calculation of direct brine release volumes). The scenarios include one undisturbed scenario (S1-BF), four scenarios that include a single inadvertent drilling intrusion into the repository (S2-BF to S5-BF), and one scenario investigating the effect of two intrusions into a single waste panel (S6-BF). Two types of intrusions, denoted as E1 and E2, are considered. An E1 intrusion assumes the borehole passes through a waste-filled panel and into a region of pressurized brine that may exist under the repository in the Castile formation, while an E2 intrusion assumes that the borehole passes through the repository but does not encounter pressurized brine. BRAGFLO results obtained in Scenario S6-BF are only used to calculate radionuclide transport to the Culebra (Section 3.8). Table 5 summarizes the six scenarios used in the Salado flow calculation. A total of 1,800 separate Salado flow simulations are run (3 replicates × 6 scenarios × 100 vectors). Section 4.2 describes results from scenarios S1-BF, S2-BF, S4-BF, and S6-BF. Results from scenarios S2-BF and S3-BF are generally similar to each other, as are results from S4-BF and S5-BF.

Information Only

Table 5. BRAGFLO Modeling Scenarios for the CRA26_FS

Scenario	Description
S1-BF	Undisturbed Repository
S2-BF	E1 intrusion at 350 years
S3-BF	E1 intrusion at 1,000 years
S4-BF	E2 intrusion at 350 years
S5-BF	E2 intrusion at 1,000 years
S6-BF	E2 intrusion at 1,000 years; E1 intrusion at 2,000 years.

Table 3 from Day and King (2025).

3.3 Radionuclide Activities for Solid Releases

Waste stream activity data for the CRA26_FS based on the FRPAIR-2024. Activity in waste encountered during a hypothetical drilling event is quantified using the metric of EPA units. The activity in EPA units for a radionuclide is the initial source term activity (in Ci) of that radionuclide divided by the product of the waste unit factor (WUF) and the release limit (in Ci/unit of waste) for the same radionuclide (Sanchez et al. 1997). Release limits and the number of Ci in an EPA unit vary by radionuclide.

The activity in EPA units at each time interval for interest of each of the major radionuclides in each waste stream is calculated by the WIPP PA code EPAUNI. EPAUNI also calculates the activity of the entire waste stream in EPA units (at each of the specified time intervals) and the probability of encountering each waste stream during a drilling intrusion.

EPAUNI models ten radionuclides (^{241}Am, ^{244}Cm, ^{137}Cs, ^{238}Pu, ^{239}Pu, ^{240}Pu, ^{241}Pu, ^{90}Sr, ^{233}U, and ^{234}U), which account for 99.83% of the EPA units at the time of repository closure in the CRA26_FS inventory (Kicker 2025a). For a full description of the EPAUNI calculation methodology, see Kim and Kicker (2025).

3.4 Cuttings, Cavings, and Spallings

The conceptual structure of the solids volume calculations in the CRA26_FS remains consistent with the methodology used in the CRA26_IS. The volume of solid material (in m^3) brought to the surface due to inadvertent human intrusion through drilling is assessed using the WIPP PA code CUTTINGS_S. This code calculates the volume of material removed through three distinct release mechanisms: cuttings, cavings, and spallings.

Cuttings refer to the repository waste that is directly impacted by the drill bit. These materials are immediately transported to the surface via the cooling fluid circulated through the borehole during drilling. The volume of cuttings corresponds to the repository material intersected by the borehole.

Cavings occur when waste materials that originally bordered the borehole on its exterior erode into the cooling fluid due to frictional effects. If the shear stresses exerted by the cooling fluid at the borehole wall exceed the shear strength of the surrounding matrix materials, erosion will take

Information Only

place, resulting in the removal of wall material. This process can lead to a local increase in the borehole diameter, which may cause the volume of waste removed to exceed the volume of the borehole initially cut through the waste. As the borehole diameter increases, the fluid shear stresses at the outer boundary decrease. If these stresses diminish to a point where the failure stress of the wall material equals or exceeds the fluid shear stress, the caving process will cease.

Spallings occur when the repository is pressurized at the time of intrusion. If the internal pressure within the repository exceeds the hydrostatic pressure of the cooling fluid column, materials originally surrounding the borehole but located interior to the repository-fluid interface may deform inward to replace the materials removed by the cutting bit and erosive brine. The solid fraction of these materials is referred to as spallings. In cases where repository materials are more permeable, pressurized gas may seep through the matrix, carrying loose particles with it. Conversely, if the repository pressures are too low, spalling events will not occur.

Additionally, the CUTTINGS_S code calculates information about the pressure, saturation, porosity, and crushed panel height, which is used as initial conditions for direct brine release calculations.

3.5 Direct Brine Release Volumes

If the WIPP repository were to be penetrated by a borehole while under conditions of sufficient repository brine pressure and saturation, brine could migrate up through the intruding borehole to reach the land surface. Such an event is defined as a DBR. As with previous WIPP PAs, the BRAGFLO DBR analysis uses the BRAGFLO code to numerically evaluate the volumetric flux of brine that enters the borehole over the duration of the release.

Pressure and saturation from the Salado flow simulations are initial conditions in the DBR calculation. The approach and methodology for DBR volume modeling in the CRA26_FS is the same as in the CRA26_IS, as described by Zeitler (2025). The following subsections summarize the approach and methodology.

The BRAGFLO_DBR model explicitly represents the vicinity of the waste panels, including specific repository features like individual panels and panel closures, in a 2-dimensional rectilinear grid. Like the BRAGFLO Salado Model (Section 3.2.1), the grid dips 1º to the south.

The DBR numerical grid and material map used in the CRA26_FS PA is the same as that used in the CRA26_IS calculations and is shown in Figure 4. The increased repository area included in the CRA26_FS representation of the WIPP in Salado flow calculations did not result in a change to the DBR grid representation, as the DBR grid already adequately considers the connections between the Salado flow results and DBR initial conditions for each of the waste regions. With the short duration of DBR simulations, there is very little communication across panel closures; therefore, there is not a need to have an explicit representation of repository volume outside of the panel closures containing the intrusion locations. Four drilling locations are considered in the CRA26_FS PA: “U” (for upper, since it is up-dip), “M” (for middle), and “L” (for lower, since it is down-dip), and “O” (for other). These intrusion locations are shown in Figure 4. Additional details on the DBR model are described in Zeitler (2025).

Information Only

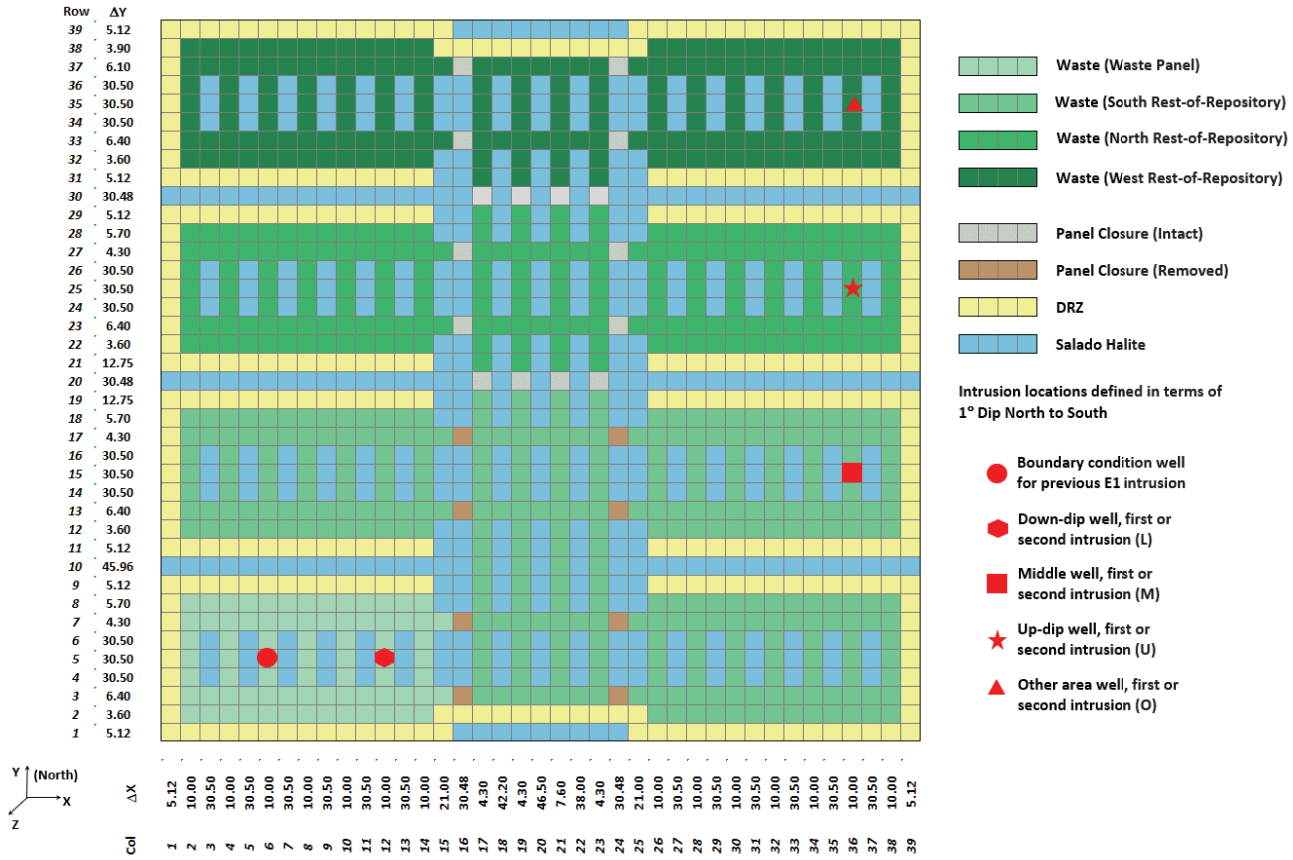


Figure 4. CRA26_FS and CRA26_IS DBR Grid with Simulated Intrusion Locations

3.5.1 Initial Conditions

The methodology for using brine pressures and brine saturations in the CRA26_FS DBR volume calculations remains unchanged from that used for the CRA26_IS. Brine pressures and brine saturations calculated during the BRAGFLO Salado flow simulations (Section 4.2) are volume-averaged and used as initial conditions in the DBR simulations. Figure 5 illustrates the method used to transfer initial conditions in the waste for the CRA26_FS. The BRAGFLO grid aggregates waste panels into four waste-bearing regions: Waste Panel, South Rest-of-Repository, North Rest-of-Repository, and West Rest-of-Repository (Day and King 2025). In Figure 5, these regions are denoted Waste Panel, SRoR, NRoR and WRoR, respectively. At the time of the intrusion, the volume-averaged pressure and saturation from the four waste-filled regions in the BRAGFLO grid are used as the initial pressure and saturation for corresponding waste regions in the DBR grid. Consistent with the designations L, M, U and O for the intrusion locations, the DBR grid waste regions will be referred to as Lower, Middle, Upper, and Other. As indicated in Figure 5, conditions in the BRAGFLO Waste Panel map to the Lower waste region in the DBR grid; likewise, BRAGFLO SRoR conditions map to the Middle DBR region, NRoR to the Upper DBR region, and WRoR to the Other DBR region. Note that pressure and saturation are allowed to change during the DBR volume calculations.

Information Only

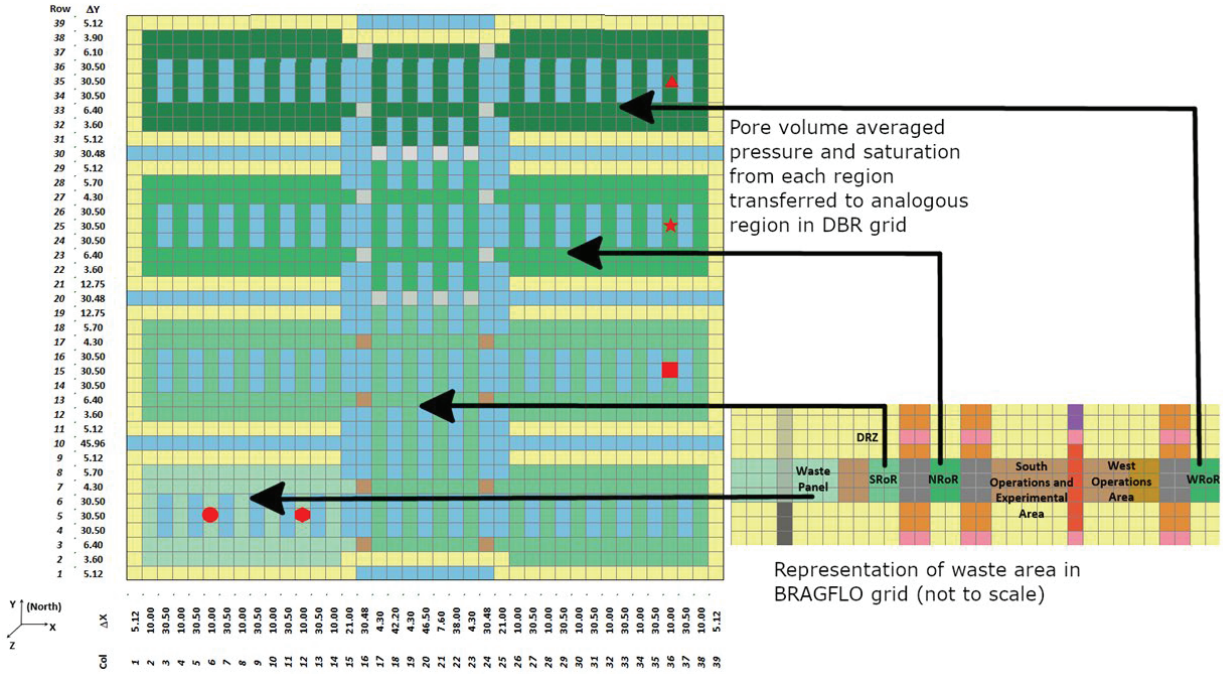


Figure 5. Regions Used to Transfer Initial Pressure and Saturation from the BRAGFLO Salado Grid to the DBR Grid

3.5.2 Modeling Scenarios

In performing DBR volume calculations, five of the BRAGFLO Salado flow model scenarios, S1-BF to S5-BF, are used to set the initial conditions for the DBR volume calculations at the time of intrusion. The five modeling scenarios used in the CRA26_FS are unchanged from those used for the CRA26_IS. These five BRAGFLO Salado flow scenarios (Section 3.2.2) capture the long-term behavior of the repository under three different conditions: undisturbed (E0); intersected by a borehole that continues down to a hypothetical pressurized brine reservoir below the repository (E1); and intersected by a borehole that does not intersect pressurized regions below the repository (E2). The DBR volume calculations map the resulting BRAGFLO pressure and saturation conditions at a suite of intrusion times onto the DBR model grid and simulate flow to the intrusion.

The scenarios and intrusion times used for the CRA26_FS, presented in Table 6, are the same as those used for the CRA26_IS. There are a total of 104 combinations, or DBR simulations, for each parameter vector. The BRAGFLO scenario S6-BF, which represents multiple intrusion scenarios, is not used for DBR calculations but is instead reserved for long-term transport modeling (Section 3.7).

Information Only

Table 6. DBR Scenarios

Scenario	Description
S1-DBR	Initially undisturbed repository (E0 conditions). Intrusion at the L, M, U, or O location at 100; 350; 1,000; 3,000; 5,000; or 10,000 years: 24 combinations.
S2-DBR	Initial E1 intrusion at 350 years followed by a second intrusion at the L, M, U, or O location at 550; 750; 2,000; 4,000; or 10,000 years: 20 combinations.
S3-DBR	Initial E1 intrusion at 1,000 years followed by a second intrusion at the L, M, U, or O location at 1,200; 1,400; 3,000; 5,000; or 10,000 years: 20 combinations.
S4-DBR	Initial E2 intrusion at 350 years followed by a second intrusion at the L, M, U, or O location at 550; 750; 2,000; 4,000; or 10,000 years: 20 combinations.
S5-DBR	Initial E2 intrusion at 1,000 years followed by a second intrusion at the L, M, U, or O location at 1,200; 1,400; 3,000; 5,000; or 10,000 years: 20 combinations.

3.6 Mobilized Radionuclide Concentrations

The methodology for mobilized radionuclide concentrations calculations is the same in the CRA26_FS DBR as for the CRA26_IS. The PANEL code simulates radionuclide decay and mobilization in brine in the repository throughout the 10,000-year regulatory period. PANEL performs three essential functions in PA. First, it determines radionuclide concentrations in brine as a function of time. Second, it calculates radionuclide transport releases to the Culebra for the E2E1 scenario, which involves a borehole intrusion into the repository followed by a borehole intrusion into a hypothetical pressurized brine reservoir beneath the repository. Third, PANEL determines the mobile concentration limits of five "lumped" radionuclides. The lumped radionuclides, namely, AM241L, PU238L, PU239L, U234L, and TH230L are described by Leigh and Trone (2005).

Kicker (2025a) reports a total of 168 radionuclides in the repository for the CRA-2026_FS. PANEL models decay and ingrowth for 30 of the radionuclides; and, for 26 of the 30, PANEL determines both concentrations and E2E1 transport releases.

The PANEL code reports the sum of radionuclide concentrations for use by code CCDFGF in calculating DBRs. The code also combines E2E1 releases determined for individual radionuclides to form releases for the five lumped radionuclides. Lumped E2E1 releases are PANEL's contribution to *to Culebra* releases. Lumped radionuclide mobile concentration limits determined by PANEL are used by code NUTS.

3.7 Salado Transport

The methodology for calculating radionuclide transport in the Salado in the CRA26_FS DBR remains unchanged from that used for the CRA26_IS. The NUTS code simulates transport in the Salado formation for BRAGFLO scenarios S1-BF through S5-BF. PANEL determines lumped radionuclide *to Culebra* releases for all vectors in BRAGFLO scenario S6-BF (Table 5).

Information Only

The NUTS transport model accounts for contaminant advection in the aqueous phase, dissolution and precipitation, and radioactive decay (Shinta 1997). The transport equations are solved on the same two-dimensional computational grid used by BRAGFLO. Additionally, NUTS relies on BRAGFLO for values of brine flow rate, brine saturation, and porosity, all of which are functions of space and time.

NUTS considers three pathways for potentially significant transport releases: (i) along anhydrite marker beds to the LWB; (ii) up the repository shaft to the Culebra; and (iii) up through an intruding borehole to the Culebra. Releases through the marker beds and shaft are effectively zero, as discussed in Section 4.8.1. Releases up the borehole to the Culebra are the NUTS contribution to *to Culebra* releases (Section 4.8.5.1).

For efficiency, NUTS works with the lumped radionuclides. In addition, NUTS uses screening simulations to identify vectors likely to contribute appreciably to transport releases. Only screened-in vectors take part in full transport simulations. PANEL calculates both radionuclide concentrations and transport to the Culebra for S6-BF (E2E1 scenario), as described in Section 3.6. The NUTS and PANEL *to Culebra* releases are used by CCDFGF to calculate *from Culebra* releases at the LWB.

3.8 Culebra Flow and Transport

The methodology for flow and transport calculations in the Culebra Dolomite Member (Culebra) of the Rustler Formation is the same in the CRA26_FS and the CRA26_IS. The Culebra is the most likely subsurface release pathway of radionuclides to the LWB (Beauheim and Holt 1990; Holt 1997). It is hypothesized that subsidence of the Culebra due to potash mining leads to fracturing, resulting in higher Culebra transmissivities and altered groundwater flow patterns (Wallace 1996). WIPP PA accounts for these potential changes in transmissivity by simulating flow and transport within the Culebra under full and partial mining conditions.

Conceptual handling of Culebra flow and transport is unchanged since 2008 (Hart et al. 2008; Burgess et al. 2008). Consequently, the model domain and discretization are the same for CRA26_FS as in the CRA26_IS and the RPPCR calculations (Kuhlman 2010; Bethune 2023; Figure 6). Groundwater flow in the Culebra is calculated with MODFLOW6 simulating steady state flow using mining modified transmissivity fields at two resolutions:

1) A 100-m grid used in the T-field calibrations (Bowman et al. 2023) and particle tracking simulations.
2) A 50-m grid used in the mass transport simulations.

Other key model domain features shown in Figure 6 include no flow (inactive cells) and constant head boundaries, recharge cells (Kuhlman 2010), and the extent of mineable potash (Cranston 2009).

Radionuclide transport is simulated by placing a 1 kg source term (^{241}Am, ^{239}Pu, ^{230}Th, and ^{234}U) into the Culebra at discrete release points above the waste panels then tabulating the cumulative fraction of mass that crosses the LWB at 50-year intervals. Transport of the ^{230}Th daughter product of ^{234}U decay is calculated and tracked as a separate species. In the results section (see Section 4.7), ^{230}Th refers to the ^{234}U daughter product and ^{23A}Th refers to the ^{230}Th released at the release

Information Only

point. Mass transport of radionuclides in the 19-panel final state repository is represented with CRP 1, 2, 3, and 4 (Figure 6). For the CRA-2026 (both CRA26_IS and CRA26_FS), CRP 2 was relocated to the centroid of Panels 11 and 12 (Wilgus and Brunell 2025; see Section 2.8).

Flow field patterns from each CRP are characterized by tracking a single, non-sorbing particle through the modified flow fields to the LWB for each combination of release point, transmissivity field, parameter vector, and mining scenario with code DTRKMF. Radionuclide transport is simulated with code SECOTP2D and accounts for physical processes not modeled in particle track simulations.

There are five steps in estimating radionuclide transport through the Culebra, including:

Step 1. Construction of 1,000 base geostatistical realizations of Culebra hydraulic transmissivity (T), anisotropy, storativity, and recharge fields (collectively referred to as "T-fields");

Step 2. Calibration of the T-fields to observed head and pumping drawdowns including selection of a final set of the 100 best fit realizations;

Step 3. Modification of the T-fields to account for potential subsidence due to potash mining beneath the Culebra;

Step 4. Calculation of steady-state groundwater flow-fields for each mining-modified T-field using MODFLOW6; and

Step 5. Calculation of radionuclide transport through the Culebra to the LWB for each simulated flow-field and release location using SECOTP2D.

Steps 1 and 2 produce 100 equally likely T-fields that are input to Step 3. The work presented in this analysis report is limited to Step 3 through Step 5. The output of Step 5 is used by the WIPP PA code CCDFGF to calculate potential radionuclide releases through the Culebra to the accessible environment (King et al. 2025; see Section 4.8.5.2). A more complete overview of the methodology is described in Wilgus and Bethune (2025).

Information Only

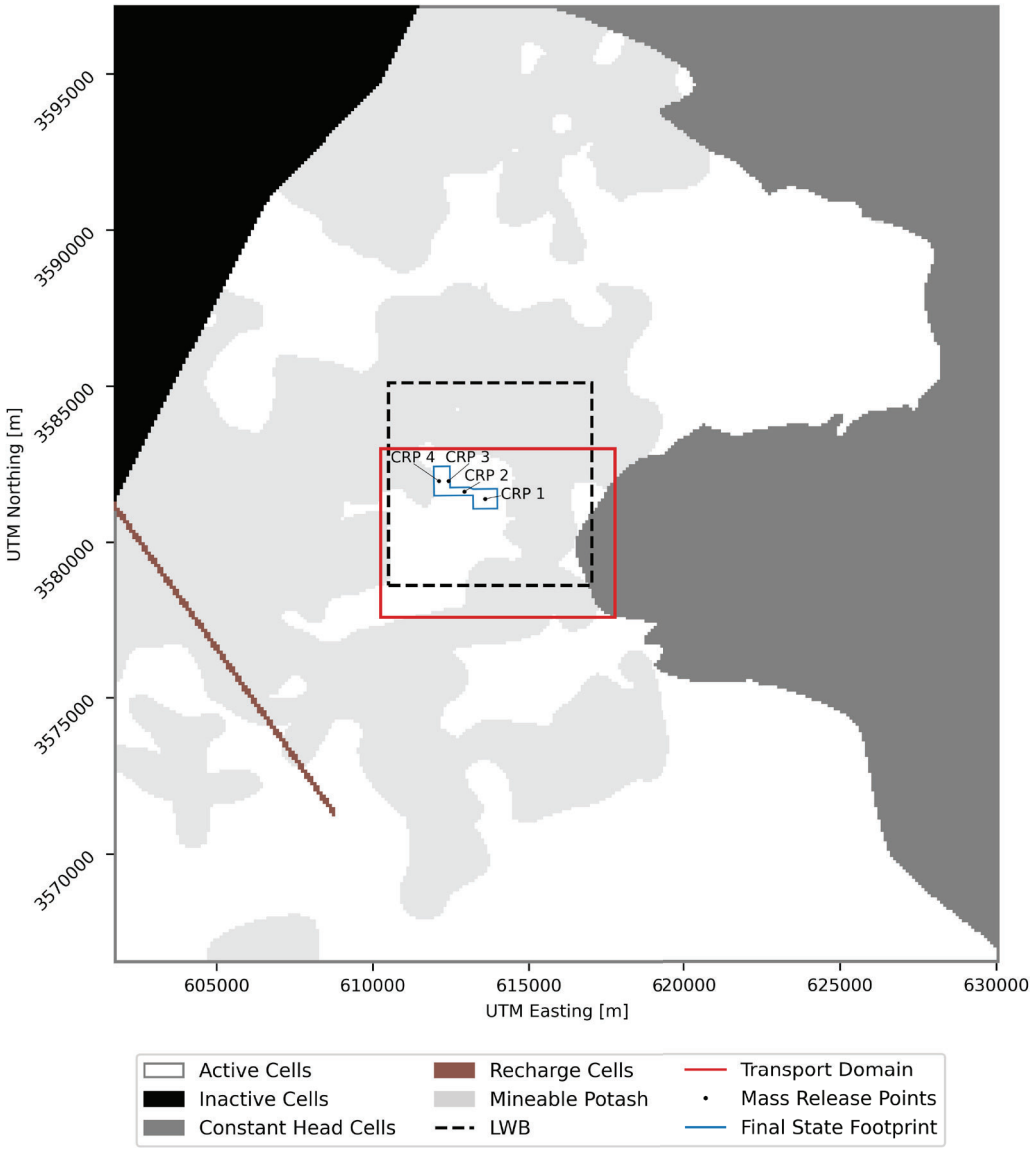


Figure 6. Culebra Modeling Domain (Derived from Wilgus and Bethune 2025)

3.9 Calculation of CCDFs for Releases

The conceptual structure of the CCDFGF calculation in the CRA26_FS remains consistent with the methodology used in the CRA26_IS. For each member of a sample of uncertain parameters, many 10,000-year futures are randomly generated. Each future comprises a sequence of simulated drilling intrusions and mining events. Drilling location, whether a brine pocket is penetrated, and the type of plugging pattern are randomly determined. The simulation of many possible realizations, or futures, characterizes the aleatory uncertainty of the results.

Information Only

For each drilling intrusion, direct releases are tabulated using output from the other models described in Section 3.0. Over the course of the entire future, releases through the Salado and Culebra to the LWB are recorded using output from the Salado and Culebra transport models. The switch from partial mining to full mining conditions occurs randomly with a probability of 1% per 100 years. The total of these various releases at the end of the 10,000-year period yields a datum for total releases. The collection of total release data points, over all futures, comprises one CCDF of releases.

The code CCDFGF generates the random futures and constructs the CCDFs. A more complete description of the CCDF calculation methodology can be found in King et al. (2025). The following subsection describes the changes to the panel neighboring assignments for the CRA26_FS.

The CRA26_FS classifies each pair of waste panels into one of four groups based on the number of panel closures separating the waste panels: same, connected, adjacent, and non-adjacent. For the CRA26_FS, the panel neighbor assignments differ from the CRA26_IS due to the interim state calculation only including 12 panels, whereas the CRA26_FS includes 19 panels. The panel neighboring relationships for the CRA26_FS are identical to those used in the RPPCR. For CRA26_FS, panel intrusion probabilities were updated using area ratios from Day (2025).

3.10 Sensitivity Analysis

Stepwise linear multiple rank regression analyses are performed to determine the relative importance of the sampled parameters in the uncertainty in releases using the code STEPWISE. Sensitivity analysis results for the CRA26_FS analysis are compared to the results of the CRA26_IS analysis. The sensitivity analysis identifies parameters which contribute most to the uncertainty in a model result (King et al. 2025). Note the CRA26_FS uses the same sampled input parameters in the STEPWISE analysis as the CRA26_IS.

3.11 Run Control

A full description of the run control for CRA26_FS, including names and locations of input and output files, can be found in Long (2025). The WIPP PA Parameter Database (PAPDB), ParamDB, is used as the source for parameter values. Parameter specifications and sampled values can be found in Feng and Kicker (2025).

Information Only

4.0 RESULTS

This section summarizes the CRA26_FS process model results and release calculations. Unlike for the CRA26_IS (Brunell et al. 2025), no individual analysis reports were created for the CRA26_FS process model results. PA process model results are discussed here for the inventory, repository conditions, direct release mechanisms, and subsurface transport mechanisms. Results of PA process models are compared to the CRA26_IS, and are shown for Replicate 1 only, unless otherwise stated. Finally, CCDFs of cumulative releases for each release mechanism, total releases, and the sensitivity analysis for total releases are discussed.

4.1 Inventory

Inventory analysis results for the CRA26_FS (based on inventory data from Van Soest 2025a) are presented in this section and compared to inventory analysis results for the CRA26_IS (Kim and Kicker 2025).

4.1.1 Total Waste Volume

Table 7 presents the 10 largest (out of a total of 590) waste streams in the CRA26_IS and CRA26_FS inventories, which account for approximately 51.71% and 52.60% of the total waste volume, respectively. In both inventories, the top two waste streams by volume are SR-CH-PP and LA-MHD01.001. These waste streams contribute 22.33% of the total volume in CRA26_IS and 24.44% in CRA26_FS.

The assessments of waste stream volumes in the respective PAIRs use different scaling factors, which are rounded to three significant figures. In the ISPAIR-2024 report (Van Soest 2025b), the scaling factors are 1.11 for CH waste streams and 0.587 for RH waste streams, resulting in a total inventory volume of 157,873 m^3. In the FRPAIR-2024 (Van Soest 2025a), the scaling factors are 1.36 for CH waste streams and 6.57 for RH waste streams, leading to a total inventory volume of 175,508 m^3, as shown in Table 7. The discrepancies between the WIPP waste capacity and the total volumes in Table 7 are 41 m^3 in the CRA26_IS (from 157,832 m^3 to 157,873 m^3) and 66 m^3 in the CRA26_FS (from 175,508 m^3 to 175,574 m^3). These discrepancies are attributed to the scale factors, which were rounded to three significant figures.

Information Only

Table 7. WIPP CH- and RH-TRU Waste Streams by Total Scaled Volume from the CRA26_IS and CRA26_FS Inventories

Rank Order	CRA26_IS Waste Stream ID	CRA26_IS Stream Type	CRA26_IS Volume (m^3)	CRA26_FS Waste Stream ID	CRA26_FS Stream Type	CRA26_FS Volume (m^3)
1	SR-CH-PP	CH	2.55E+04	SR-CH-PP	CH	3.11E+04
2	LA-MHD01.001	CH	9.75E+03	LA-MHD01.001	CH	1.18E+04
3	WP-BN510	CH	9.63E+03	RL200-02	CH	1.03E+04
4	RL200-02	CH	8.48E+03	WP-BN510	CH	9.63E+03
5	RLPFP-01	CH	6.16E+03	LA-MHD01-Pits	CH	6.66E+03
6	LA-MHD01-Pits	CH	5.46E+03	RLPFP-01	CH	6.16E+03
7	WP-ID-SDA-SLUDGE	CH	5.20E+03	WP-ID-SDA-SLUDGE	CH	5.20E+03
8	WP-RF029.01	CH	4.31E+03	WP-RF029.01	CH	4.31E+03
9	WP-LA-MHD01.001	CH	3.65E+03	WP-LA-MHD01.001	CH	3.65E+03
10	WP-BNINW216	CH	3.50E+03	WP-BNINW216	CH	3.50E+03
•	•	•	•	•		•
•	•	•	•	•		•
•	•	•	•	•		•
590	WP-LA-OS-00-04	CH	2.69E-03	WP-LA-OS-00-04	CH	2.69E-03
	Total		157873	Total		175508

4.1.2 Inventory by EPA Units

Table 8 presents the 10 waste streams that predominantly contribute to the total EPA units in CRA26_FS, which account for approximately 87.95% of the total inventory at closure and 93.08% at 10,000 years post-closure. In both the CRA26_IS and CRA26_FS inventories, the top two waste streams are SR-KAC-PuOx-2 and SR-KAC-PuOx. These waste streams contribute 36.18% and 22.47%, respectively, of the total EPA units at closure in the CRA26_FS (see Table 8), while they account for 34.91% and 21.87% in the CRA26_IS (Kim and Kicker, 2025). At the closure year of 2083, the CRA26_IS inventory contains 10,000 EPA units (Kim and Kicker, 2025) and the CRA26_FS waste inventory contains 10,024 EPA units (Table 8).

For the SR-KAC-PuOx-2 waste stream, which has the highest activity, CRA26_FS reports a total of 3.32E+06 Ci. This total includes 2.13+06 Ci of ^{239}Pu, 4.90E+05 Ci of ^{241}Am, 4.67E+05 Ci of ^{240}Pu, 1.73E+05 Ci of ^{241}Pu, and 6.08E+04 Ci of ^{238}Pu (Van Soest 2025a, Table 5-1). In CRA26_IS, this waste stream has a total of 2.72E+06 Ci, which includes 1.74+06 Ci of ^{239}Pu, 4.01E+05 Ci of ^{241}Am, 3.82E+05 Ci of ^{240}Pu, 1.41E+05 Ci of ^{241}Pu, and 4.98E+04 Ci of ^{238}Pu (Van Soest 2025b, Table 5-1).

Information Only

By 10,000 years post-closure, the total number of EPA units decreases to 4,005 in the CRA26_IS (Kim and Kicker 2025, Table 3) and 4,050 in the CRA26_FS (see Table 2). The top two waste streams at that time continue to be SR-KAC-PuOx-2 and SR-KAC-PuOx, which together provide 73.97% of the total remaining EPA units (see Table 2). Overall, ten waste streams account for approximately 93.08% of the repository activity at the end of the regulatory period.

Table 8. WIPP CH- and RH-TRU Waste Streams by Total EPA Units; At Closure (Calendar Year 2083) and After 10,000 Years (Calendar Year 12083) from the CRA26_FS Inventory

Rank Order	Waste Stream ID at Closure	Stream Type at Closure	EPA Units at Closure	Waste Stream ID after 10,000 Years	Stream Type after 10,000 Years	EPA Units after 10,000 Years
1	SR-KAC-PuOx-2	CH	3.63E+03	SR-KAC-PuOx-2	CH	2.03E+03
2	SR-KAC-PuOx	CH	2.25E+03	SR-KAC-PuOx	CH	9.70E+02
3	SR-CH-PP	CH	1.21E+03	SR-CH-PP	CH	3.72E+02
4	LA-MHD01.001	CH	6.86E+02	LA-MHD01-Pits	CH	1.03E+02
5	LA-MHD01-Pits	CH	3.76E+02	LA-MHD01.001	CH	9.95E+01
6	WP-LA-MHD01.001	CH	2.03E+02	WP-RF118.01	CH	6.45E+01
7	WP-RF009.01	CH	1.52E+02	WP-LA-MHD01.001	CH	5.70E+01
8	WP-RF118.01	CH	1.20E+02	WP-RF009.01	CH	5.28E+01
9	WP-SR-W027-221H-HET	CH	1.12E+02	WP-BN510	CH	1.29E+01
10	WP-SR-MD-PAD1	CH	7.82E+01	WP-RF003.01	CH	1.22E+01
•	•	•	•	•		•
•	•	•	•	•		•
•	•	•	•	•		•
590	LB-T002	CH	1.73E-07	WP-OR-LWT-CH-HET	CH	1.93E-12
	Total		10024	Total		4050

4.1.3 Waste Stream Activity Concentration

The activity concentration (EPA units/m^3) for each waste stream is calculated at closure and at 10,000 years post-closure. The ten waste streams that exhibit the highest activity concentrations in the CRA26_FS at each time point are listed in Table 9. Due to radioactive decay, the number of EPA units for each waste stream, and, thus, the concentration of activity in the waste, decreases at 10,000 years post-closure. The varying distributions of radionuclides within each waste stream, along with their different decay rates, lead to a variable decrease in activity concentration.

Information Only

Consequently, the group of the top ten waste streams by activity concentration at closure will vary at 10,000 years post-closure. The activity concentration in EPA units/m^3 decreases by about 10% from the CRA26_IS to the CRA26_FS due to the approximately 10% increase in waste volume.

Table 9. WIPP CH- and RH-TRU Waste Streams Ordered by Activity Concentration at Closure (Calendar Year 2,083) and after 10,000 Years (Calendar Year 12083) from CRA26_FS Inventory

Rank Order	Waste Stream ID at Closure	Stream Type at Closure	EPA units per m^3 at Closure	Waste Stream ID after 10,000 Years	Stream Type after 10,000 Years	EPA units per m^3 after 10,000 Years
1	OR-OXIDE-CH-HET	CH	5.73E+00	WA-SR-KAC-PUOX	CH	1.40E+00
2	WA-SR-KAC-PUOX	CH	2.91E+00	SR-KAC-PuOx-2	CH	1.27E+00
3	SR-KAC-PuOx	CH	2.88E+00	SR-KAC-PuOx	CH	1.24E+00
4	SR-KAC-PuOx-2	CH	2.27E+00	WP-SR-KAC-PUOX	CH	1.14E+00
5	WP-SR-KAC-PUOX	CH	2.06E+00	OR-OXIDE-CH-HET	CH	6.17E-01
6	WP-LA-OS-00-01.001	CH	1.32E+00	WP-LA-OS-00-04	CH	6.02E-01
7	LA-OS-00-01.001	CH	1.08E+00	LA-OS-00-01.001	CH	2.84E-01
8	WP-LA-OS-00-04	CH	1.03E+00	WP-RLRFETS.001	CH	2.36E-01
9	WP-RF005.02	CH	5.99E-01	WP-RF118.01	CH	1.92E-01
10	WP-RLHMOX.001	CH	5.64E-01	WP-RLHMOX.001	CH	1.81E-01
• • •	• • •	• • •	• • •	• • •	• • •	• • •
590	LB-T002	CH	3.50E-07	WP-OR-LWT-CH-HET	CH	3.06E-12
	Overall waste streams		5.71E-02	Overall waste streams		2.31E-02

4.1.4 Total Radionuclide Activity

Figure 7 compares the total activity (in Ci and EPA units) as a function of time for the CH and RH waste inventories. The RH waste provides a minimal contribution in terms of both Ci and EPA units. In Figure 7(a), the total activity in Ci for CRA26_FS is higher than that for CRA26_IS over the regulatory period due to increased scale factors for the 19-panel repository (CRA26_FS) compared to the 12-panel repository (CRA26_IS). The scale factor applied to CH waste is 1.11 for CRA26_IS (Van Soest 2025b) and 1.36 for CRA26_FS (Van Soest 2025a).

Information Only

In Figure 7(b), however, the total activity in EPA units for CRA26_FS is nearly identical to that for CRA26_IS over the 10,000-year regulatory period. This is attributed to the fact that the EPA unit value represents radioactivity in curies normalized by the WUF, defined as the total curies of the transuranic radionuclides at closure divided by a million curies. The WUFs used are 7.37 for CRA26_IS and 8.68 for CRA26_FS.

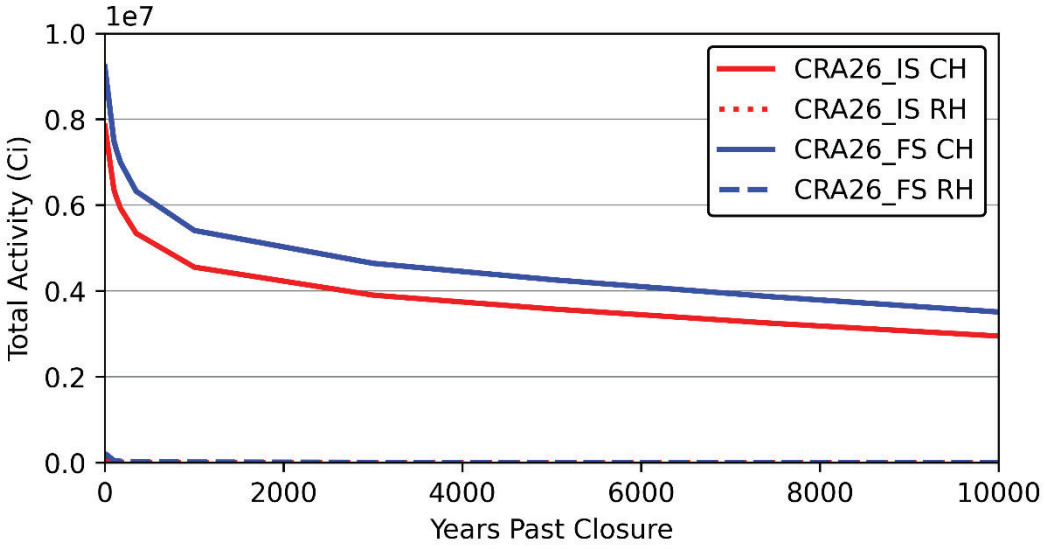
The total activity for the dominant WIPP radionuclides in EPA units at closure and at 10,000-years post-closure is displayed in Table 10. The activities of these radionuclides are similar between CRA26_IS and CRA26_FS, except for ^{137}Cs and ^{90}Sr, which are dominant radionuclides in RH waste. This difference for ^{137}Cs and ^{90}Sr is attributed to the scale factor applied to RH waste, which is 0.587 for CRA26_IS (Van Soest 2025b) and 6.57 for CRA26_FS (Van Soest 2025a).

As shown in Table 10, the initial activity of the inventory is dominated by ^{241}Am, ^{238}Pu, ^{239}Pu and ^{240}Pu. Since the inventories of ^{241}Am and ^{238}Pu decay rapidly, the total activity of the inventory is dominated at later times primarily by ^{239}Pu, with a smaller contribution from ^{240}Pu. The radionuclides ^{244}Cm, ^{137}Cs, ^{241}Pu, ^{90}Sr, ^{233}U and ^{234}U do not appreciably contribute to the total activity at any time throughout the 10,000-year regulatory period.

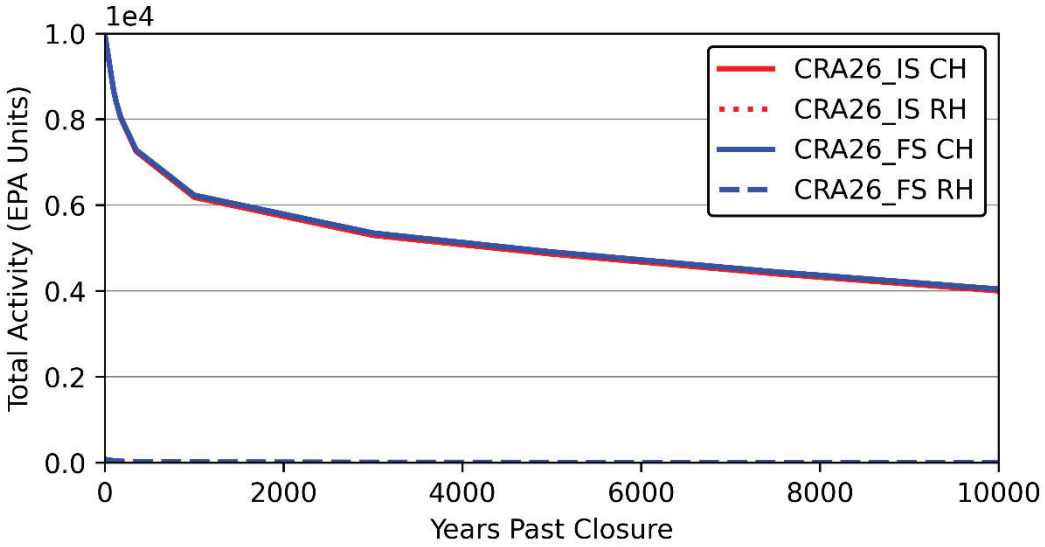
Table 10. Total Activity (EPA Units) for Dominant Isotopes in WIPP CH- and RH-TRU Waste at Closure and after 10,000 Years

Radionuclide	Half-life (y)	CRA26_IS Activity at Closure (EPA Units)	CRA26_IS Activity after 10,000 Years (EPA Units)	CRA26_FS Activity at Closure (EPA units)	CRA26_FS Activity after 10,000 Years (EPA units)
^{241}Am	432.7	2.11E+03	2.31E-04	2.08E+03	2.28E-04
^{244}Cm	18.1	-	-	-	-
^{137}Cs	30.07	4.32E+00	0.00E+00	9.51E+00	0.00E+00
^{238}Pu	87.7	1.87E+03	0.00	1.84E+03	0.00
^{239}Pu	24100	4.76E+03	3.57E+03	4.81E+03	3.61E+03
^{240}Pu	6560	1.26E+03	4.37E+02	1.27E+03	4.41E+02
^{241}Pu	14.29	-	-	-	-
^{90}Sr	28.8	2.64E+00	0.00E+00	7.01E+00	0.00E+00
^{233}U	159200	4.46E-01	4.27E-01	5.55E-01	5.31E-01
^{234}U	246000	8.89E-01	1.52E+00	8.71E-01	1.49E+00
Total		1.00E+04	4.00E+03	1.00E+04	4.05E+03

Information Only



(a) Total activity (in Ci)



(b) Total activity (in EPA units)

Figure 7. Total Activity in WIPP CH- and RH-TRU Waste from Closure to 10,000 Years After Closure, in Units of (a) Curies (Ci) and (b) EPA Units.

4.2 Salado Flow

Repository conditions influencing releases, including brine pressures and saturations within the waste areas of the repository, are summarized for CRA26_FS and compared with corresponding results for CRA26_IS. Changes introduced in CRA26_FS to accommodate seven additional waste

Information Only

panels have an impact on the Salado flow results. Changes included in the CRA26_FS that most substantially affect Salado flow results as compared to the CRA26_IS are the following:

- Decreased concentrations of inventory iron mass, CPR mass, and decay heat (Table 2) leading to decreased gas generation and brine consumption on a per waste area volume basis.
- Increased areas and volumes for the West Rest-of-Repository and associated access drifts that impact net brine flow into these areas from the adjacent DRZ.

Net brine inflow for the waste areas is shown in Figure 8 through Figure 11. The mean net brine inflows into the representative waste panel, South Rest-of-Repository, and North Rest-of-Repository are highly similar between CRA26_FS and CRA26_IS due to the equivalent area/volume of these regions and adjacent DRZ. On a per panel basis, the net brine inflow into the West Rest-of-Repository is also highly similar (Figure 12), but the West Rest-of-Repository in CRA26_FS consists of nine panels whereas for CRA26_IS it consists of only two panels. Thus, the net brine inflow for the West Rest-of-Repository is significantly larger for CRA26_FS and contributes such that the total net brine flow into the repository is greater for CRA26_FS in comparison to CRA26_IS. It is also observed that CRA26_FS scenarios with a Castile intrusion experience less net brine inflow for areas which are not separated by an intact panel closure from the intrusion borehole.

The mean brine consumption resulting from chemical reactions within the representative waste panel, South Rest-of-Repository, and North Rest-of-Repository is less for CRA26_FS in comparison to CRA26_IS because of the decreased gas generation rates due to lower concentrations of iron, CPR, and decay heat in these areas. The larger size of the West Rest-of-Repository for CRA26_FS results in greater brine consumption in this area as compared to CRA26_IS. On a volume-normalized basis, CRA26_FS experiences less brine consumption than CRA26_IS in all waste areas due to lower inventory concentrations of reactants for brine-consuming, gas-generating reactions. Brine consumption in the waste areas is shown in Figure 13 through Figure 16 with normalized results for the WRR shown in Figure 17.

Again, on a volume-normalized basis the reduced brine consumption in concert with similar net brine inflow for CRA26_FS results in mean brine saturation increases for all waste areas and scenarios in comparison to CRA26_IS. Brine saturation for the waste areas is shown in Figure 18 through Figure 21.

Primarily due to the increased size of the West Rest-of-Repository, mean total repository gas generation from all sources is greater for CRA26_FS in comparison to CRA26_IS. However, when gas generation is normalized to the repository waste volume (REFCON:VREPOS), all CRA26_FS sources of gas generation are observed to be roughly equivalent for scenarios without a Castile intrusion and less for scenarios with a Castile intrusion. Mean total and mean normalized total repository gas generation from all sources are shown in Figure 22 and Figure 23, respectively. Inventory concentrations contributing to gas generation are lower in CRA26_FS such that with available brine, volume-normalized gas generation generally lags that seen in CRA26_IS.

Mean brine pressures over all waste areas and scenarios without a Castile intrusion are generally higher for CRA26_FS in comparison to CRA26_IS, due primarily to the increased brine saturation facilitated by decreased brine consumption in relation to similar net brine inflow. However, for

Information Only

scenarios with a Castile intrusion, the increased brine saturation and reduced volume-normalized gas generation for CRA26_FS leads to highly similar but variable pressure trend comparisons with CRA26_IS. Mean brine pressure in the waste areas is shown in Figure 24 through Figure 27.

Brine flows away from the repository (up the borehole, shaft, and out through anhydrite layers across the land withdrawal boundary) are similar yet generally slightly greater for CRA26_FS in comparison to CRA26_IS, as shown in Figure 28 through Figure 30. Note that the cumulative brine flows shown in Figure 30 consider only the movement of brine and not radionuclides.

Information Only

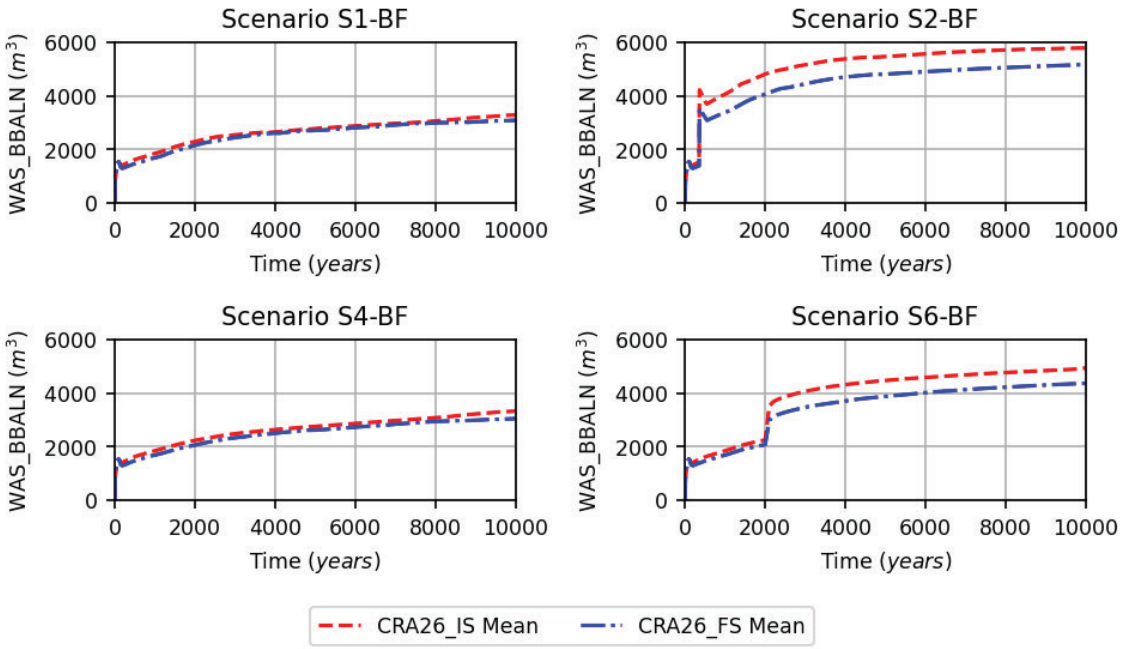


Figure 8. Mean Net Brine Flow into the Waste Panel

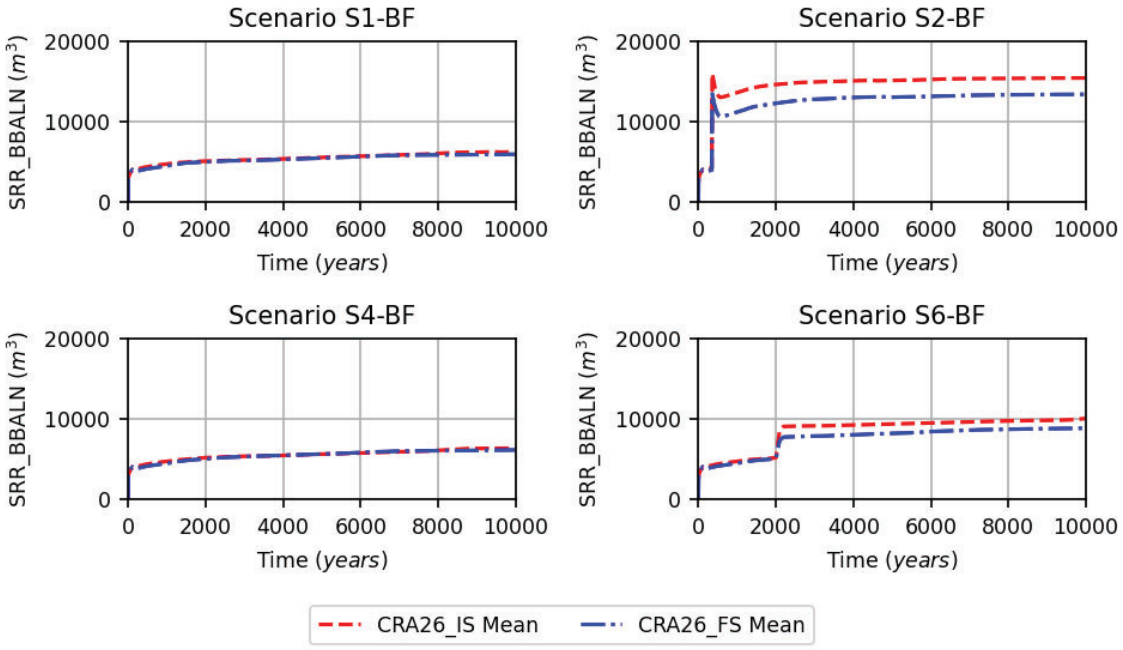


Figure 9. Mean Net Brine Flow into the South Rest-of-Repository

Information Only

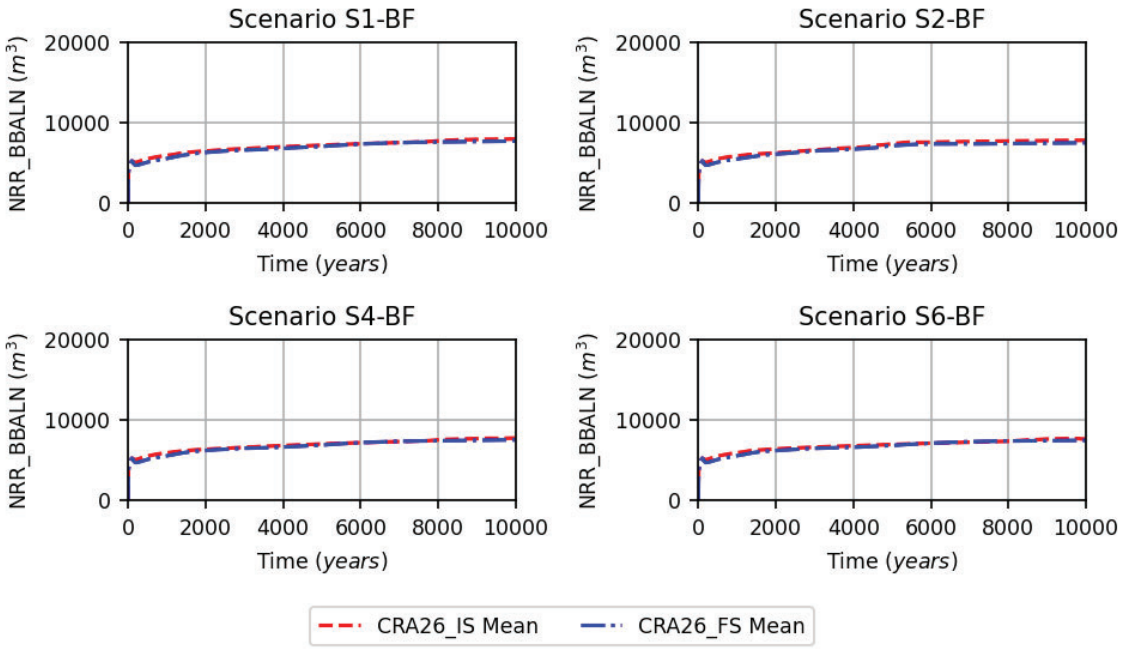


Figure 10. Mean Net Brine Flow into the North Rest-of-Repository

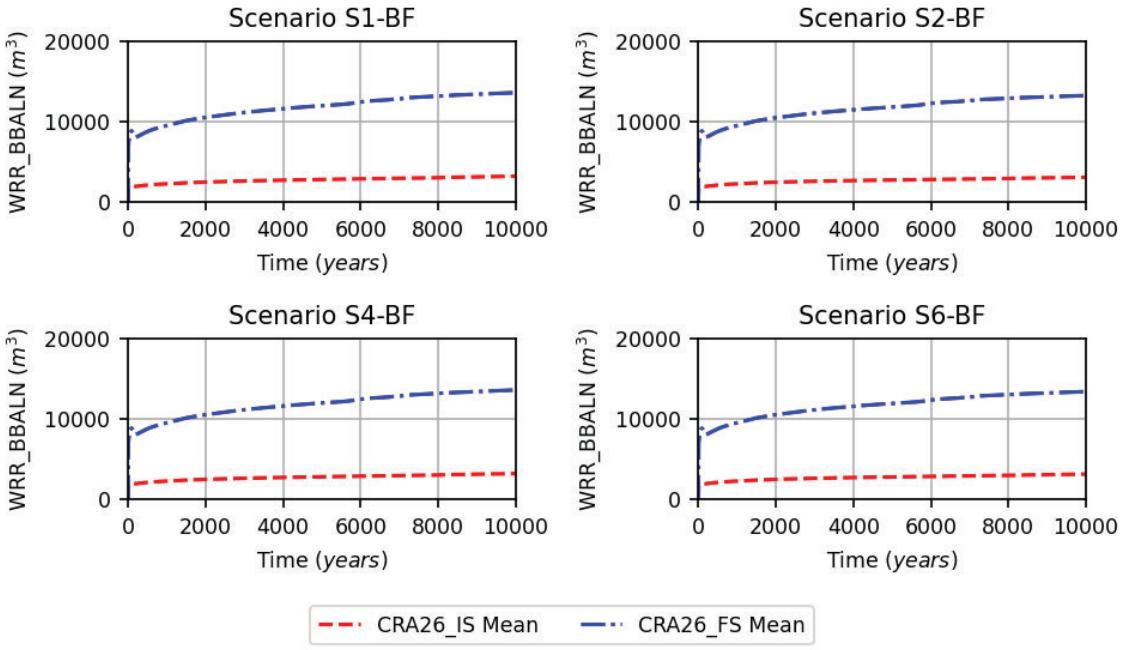


Figure 11. Mean Net Brine Flow into the West Rest-of-Repository

Information Only

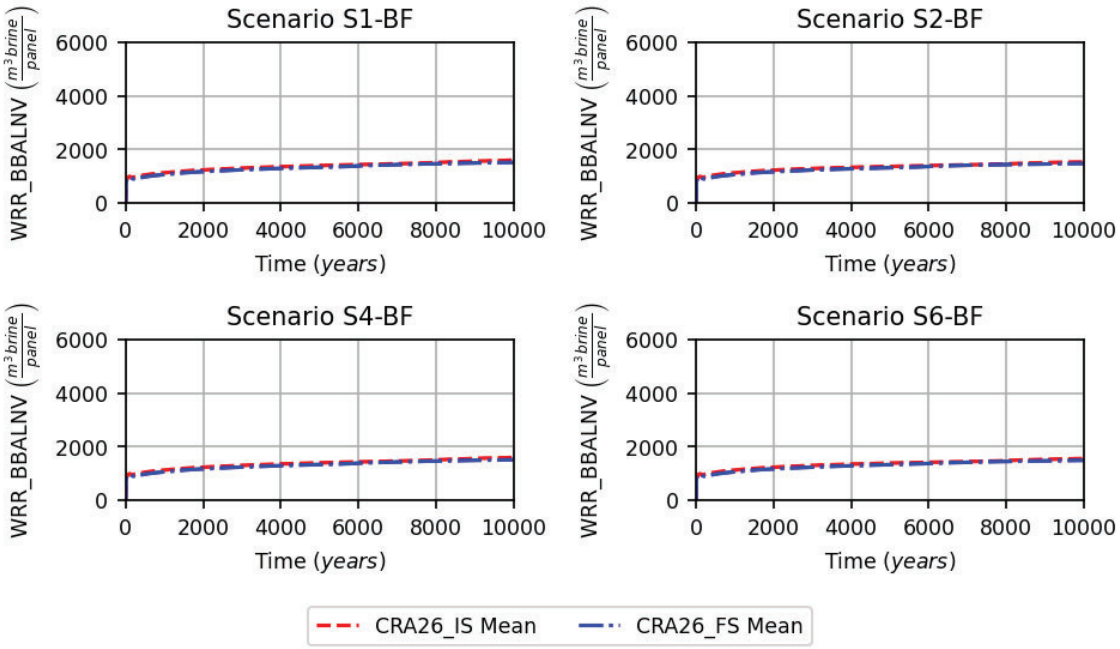


Figure 12. Normalized Mean Net Brine Flow into the West Rest-of-Repository

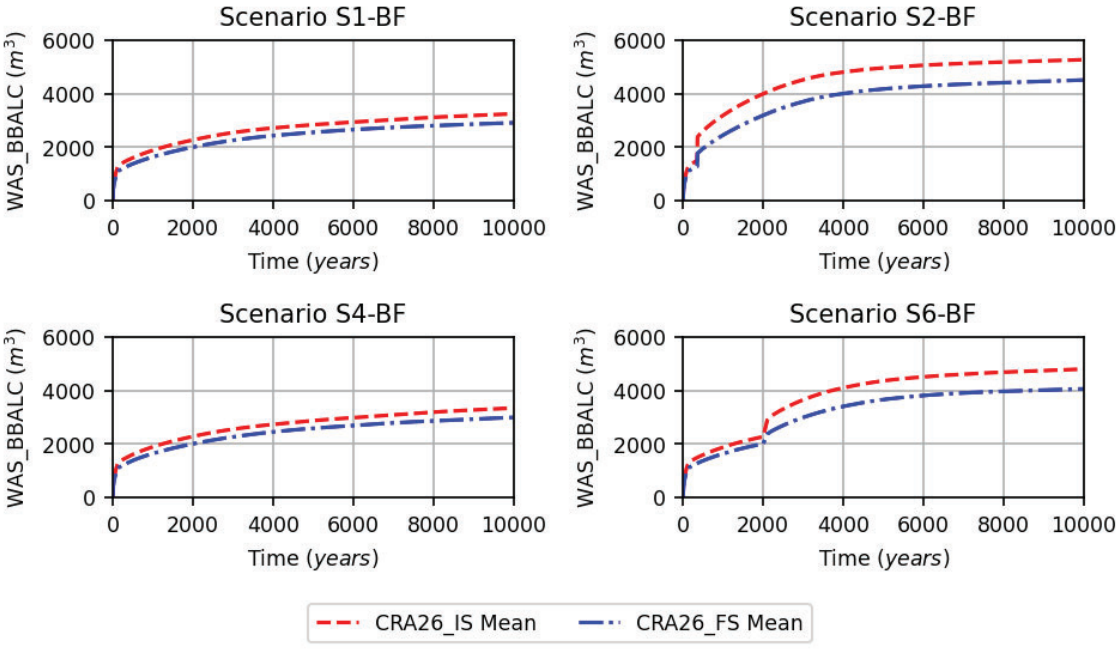


Figure 13. Mean Brine Consumption in the Waste Panel

Information Only

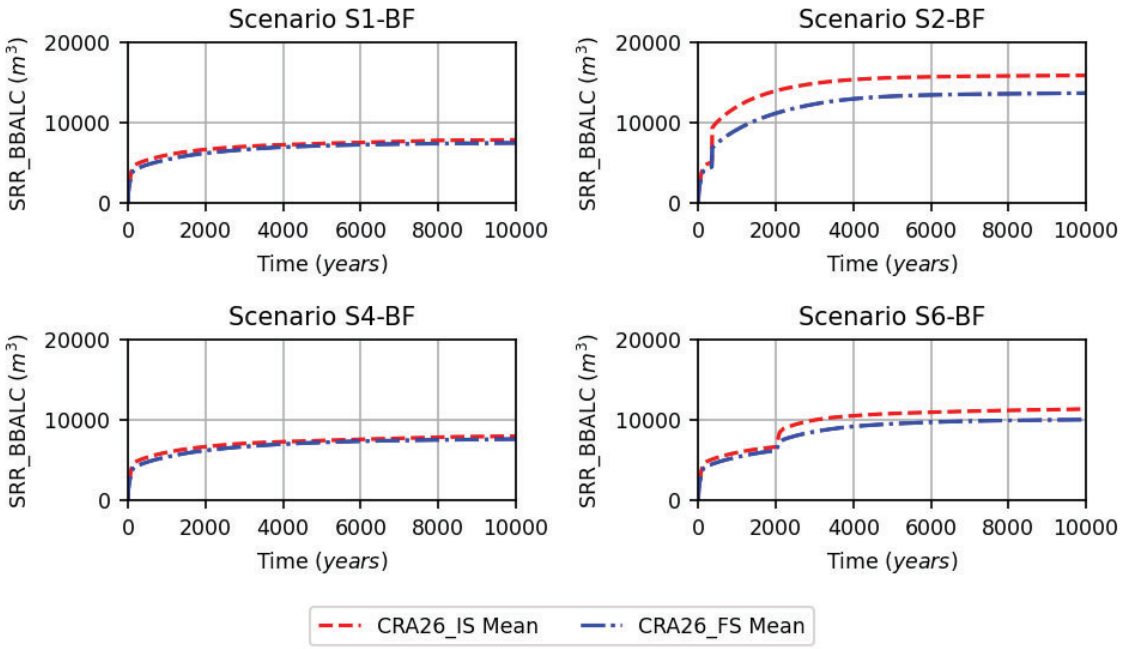


Figure 14. Mean Brine Consumption in the South Rest-of-Repository

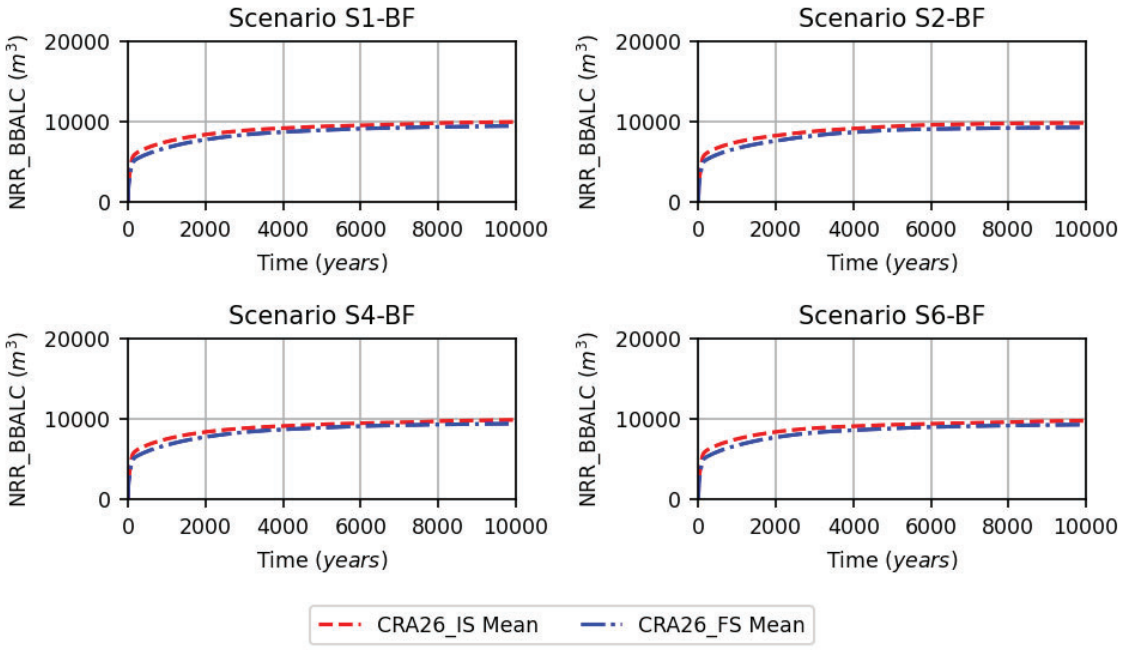


Figure 15. Mean Brine Consumption in the North Rest-of-Repository

Information Only

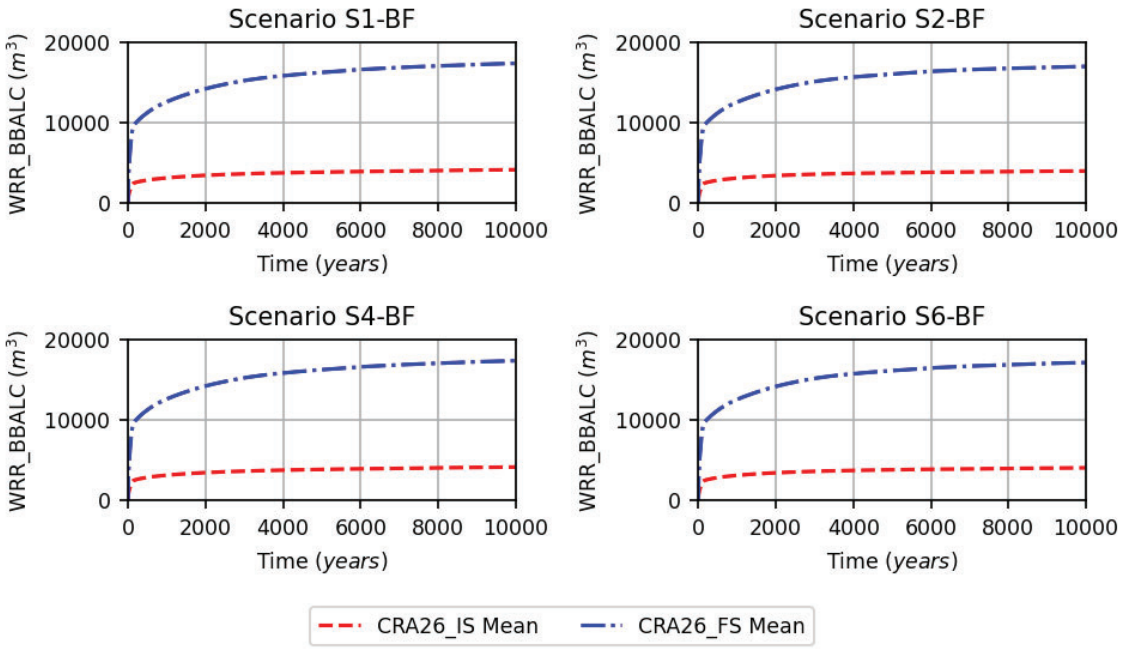


Figure 16. Mean Brine Consumption in the West Rest-of-Repository

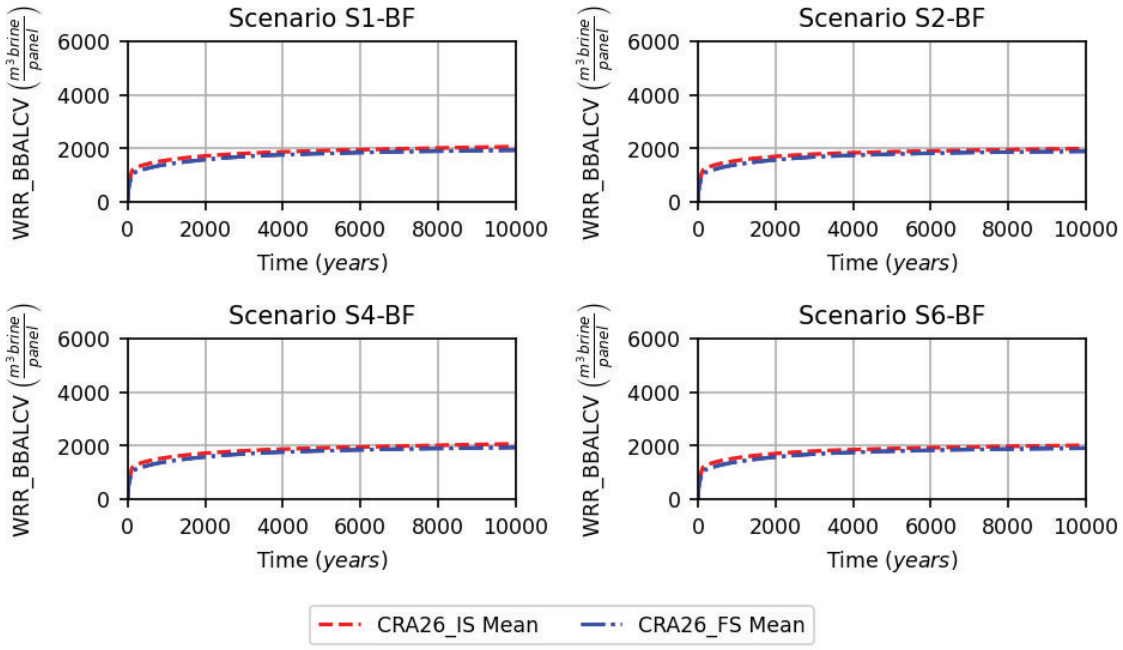


Figure 17. Normalized Mean Brine Consumption in the West Rest-of-Repository

Information Only

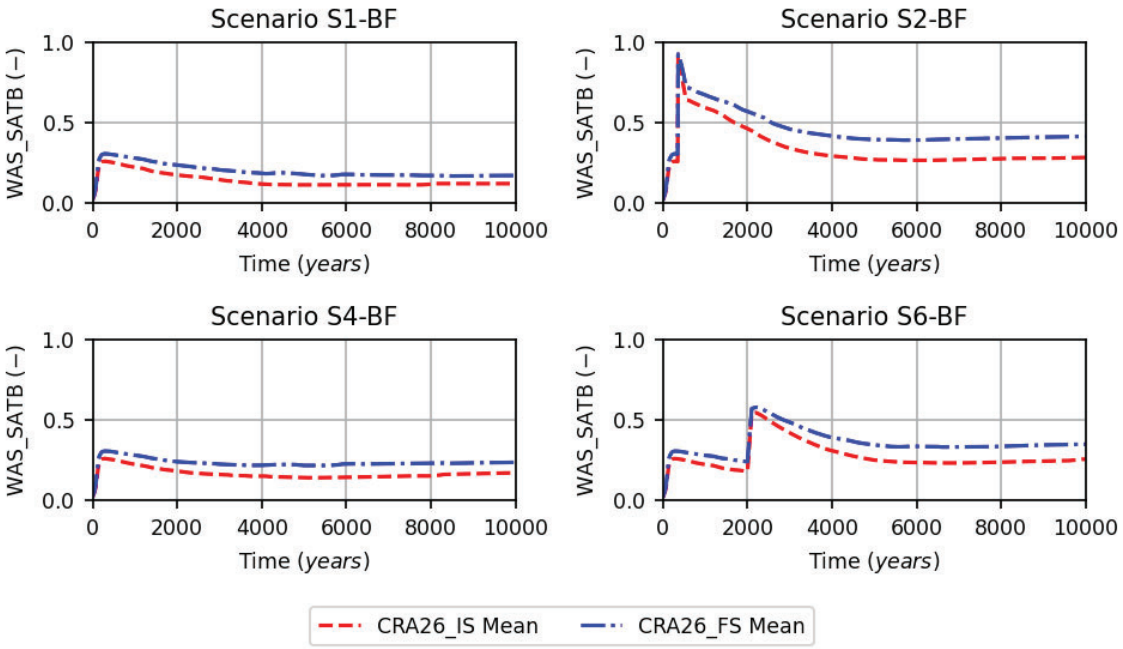


Figure 18. Mean Brine Saturation in the Waste Panel

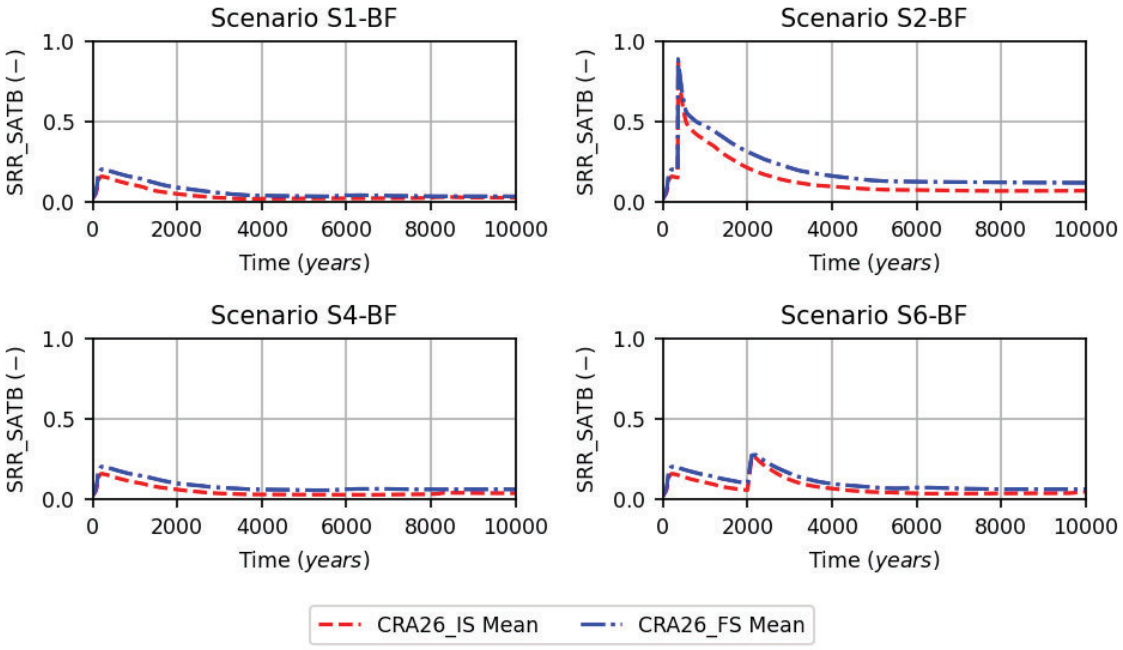


Figure 19. Mean Brine Saturation in the South Rest-of-Repository

Information Only

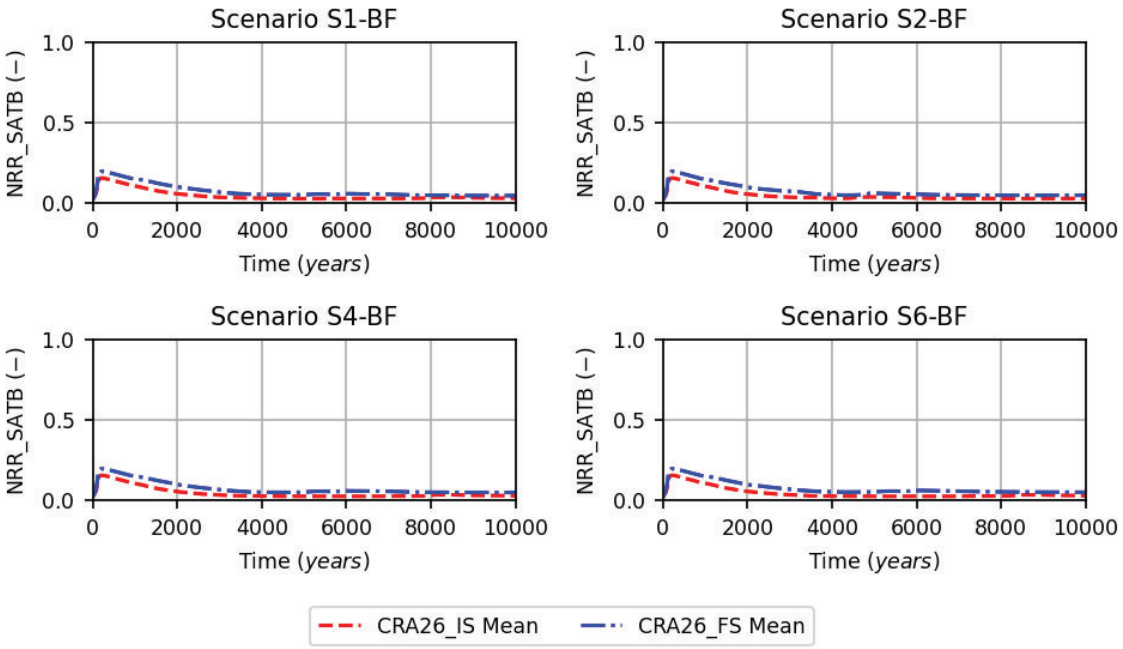


Figure 20. Mean Brine Saturation in the North Rest-of-Repository

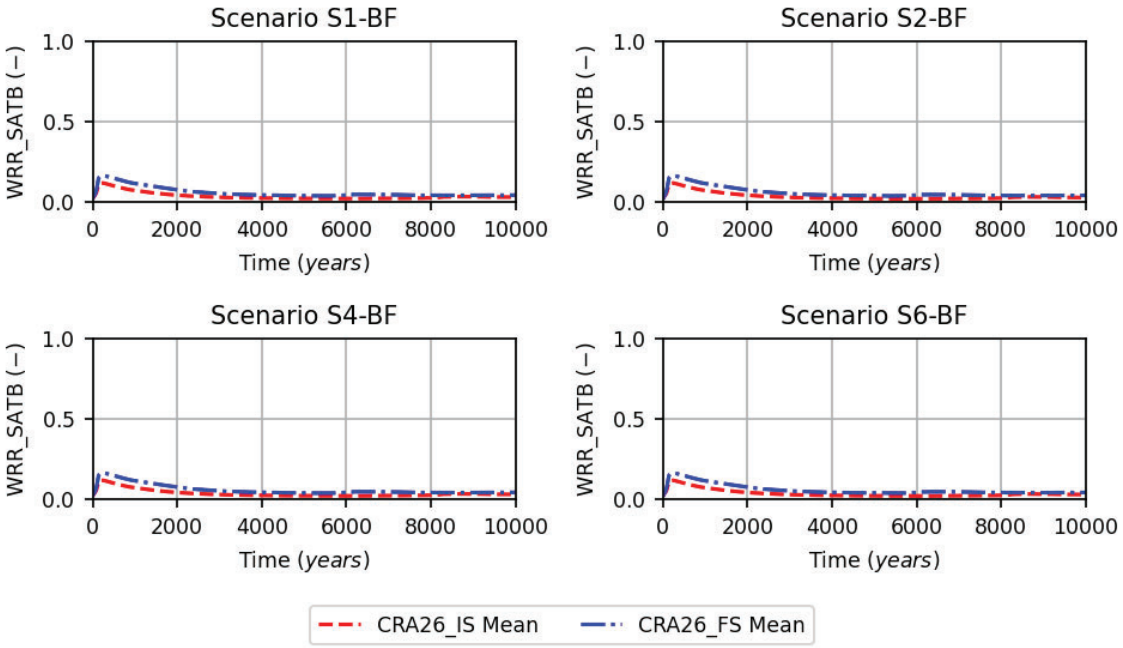


Figure 21. Mean Brine Saturation in the West Rest-of-Repository

Information Only

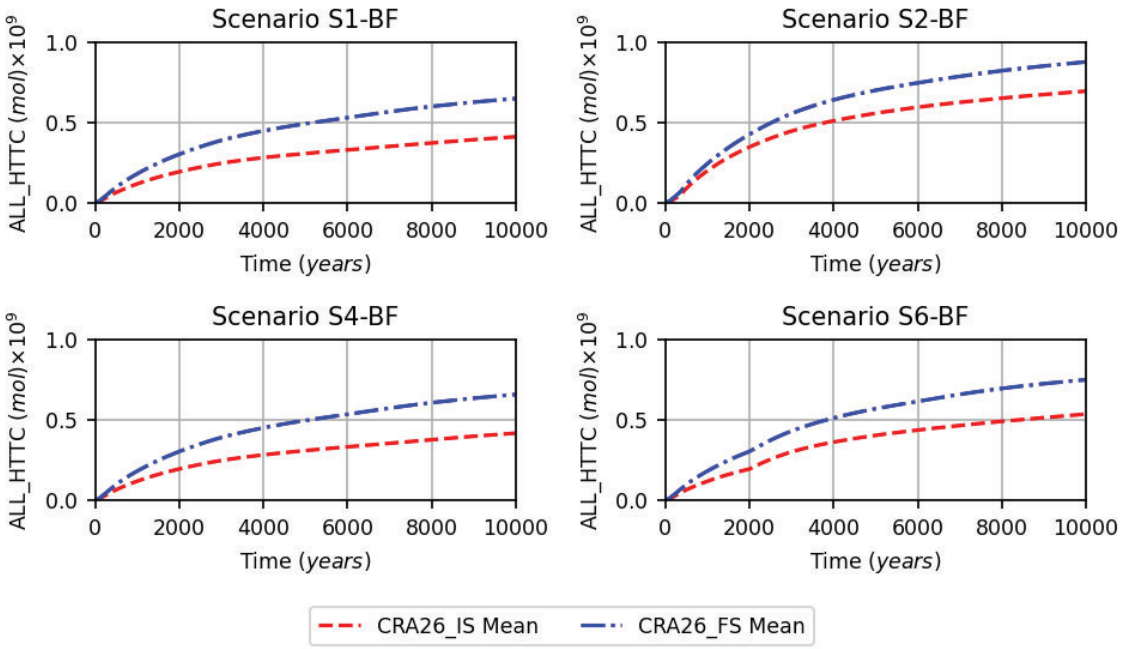


Figure 22. Mean Total Repository Gas Generation

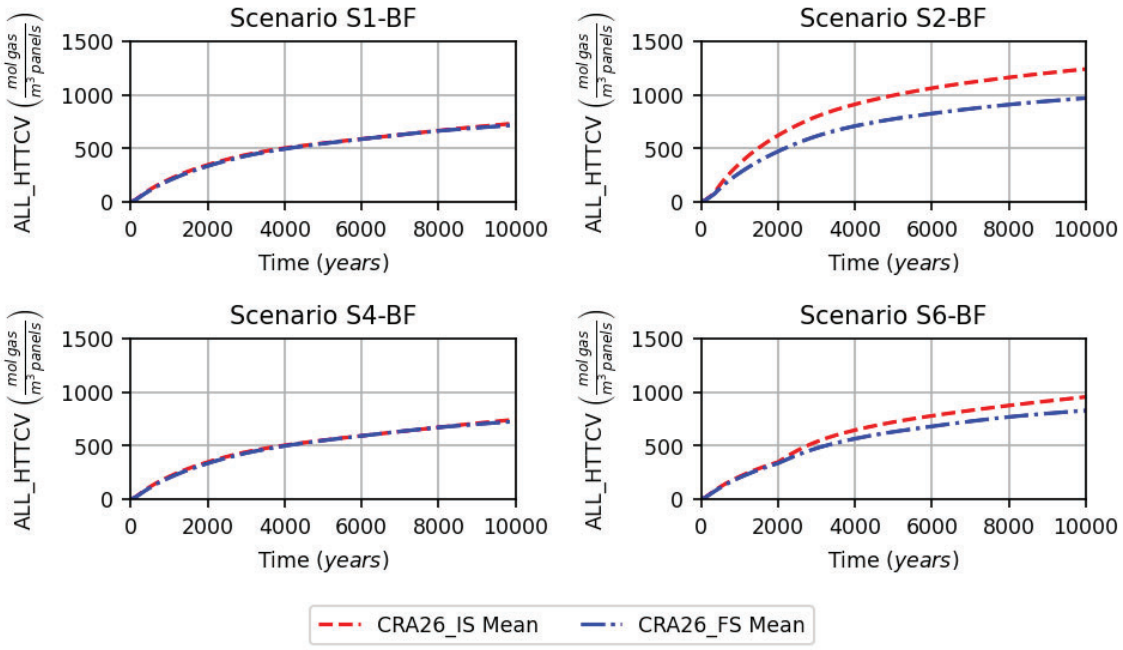


Figure 23. Mean Normalized Total Repository Gas Generation

Information Only

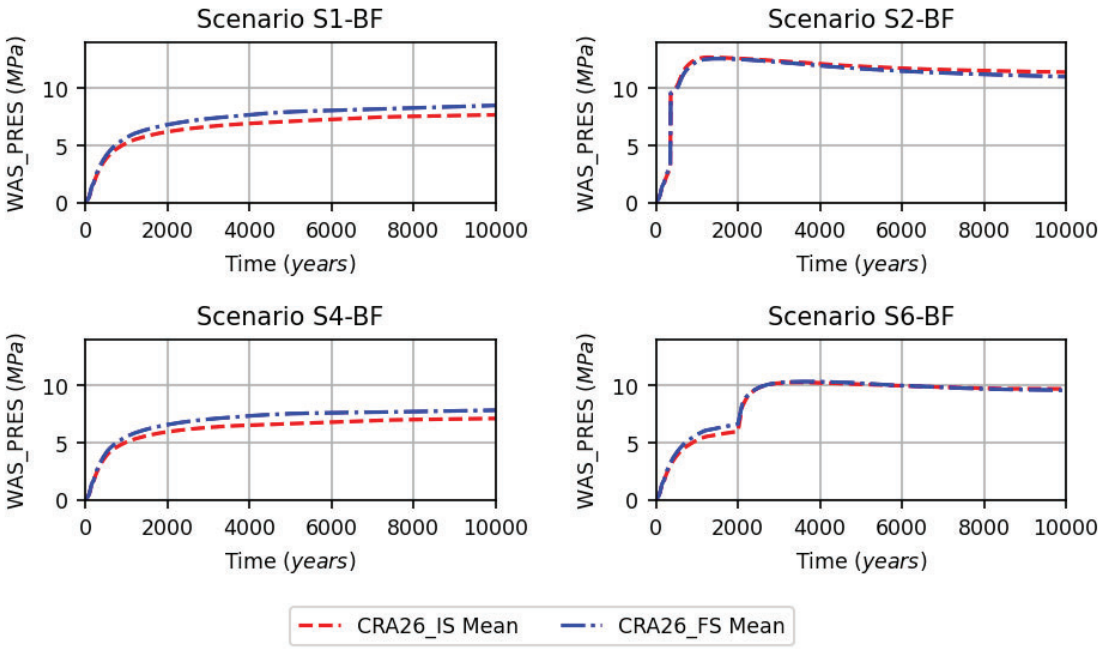


Figure 24. Mean Brine Pressure in the Waste Panel

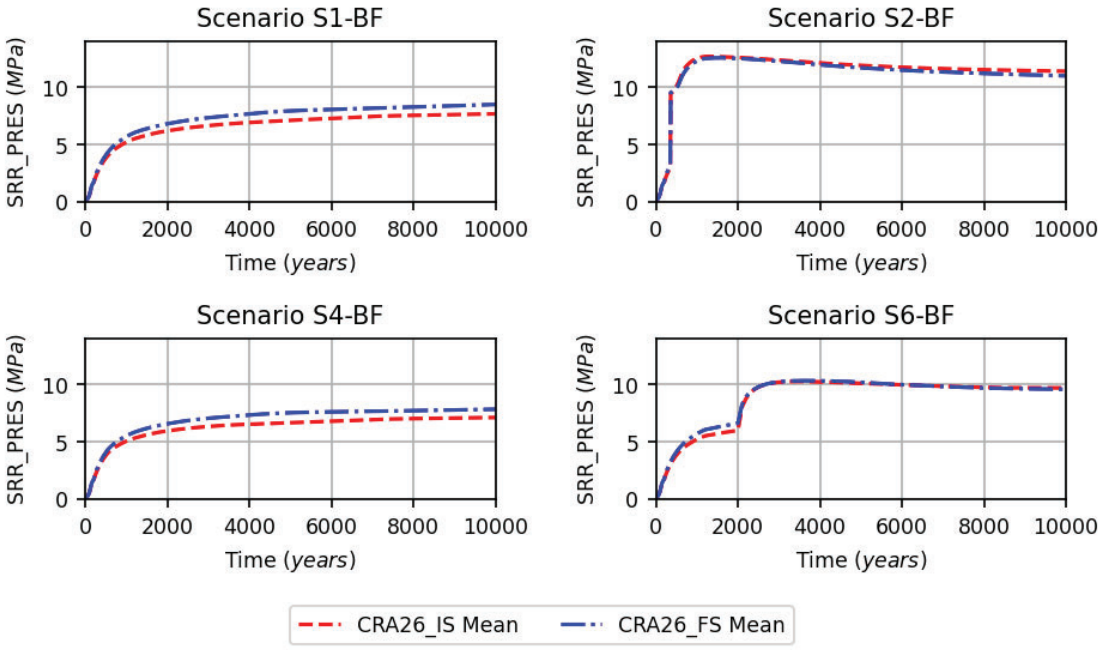


Figure 25. Mean Brine Pressure in the South Rest-of-Repository

Information Only

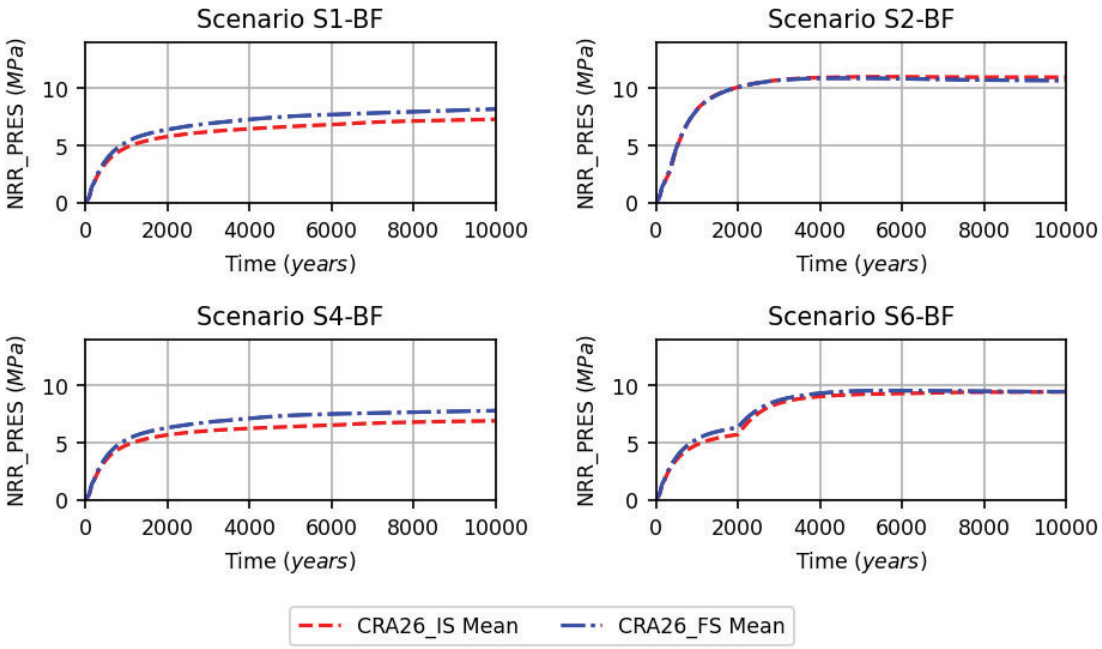


Figure 26. Mean Brine Pressure in the North Rest-of-Repository

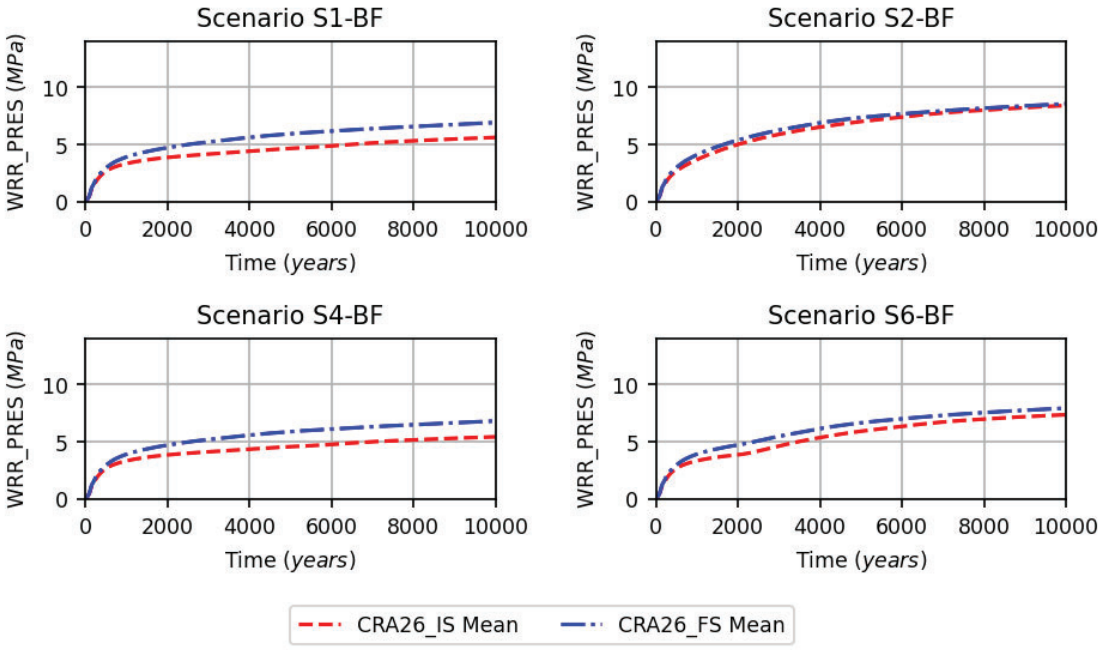


Figure 27. Mean Brine Pressure in the West Rest-of-Repository

Information Only

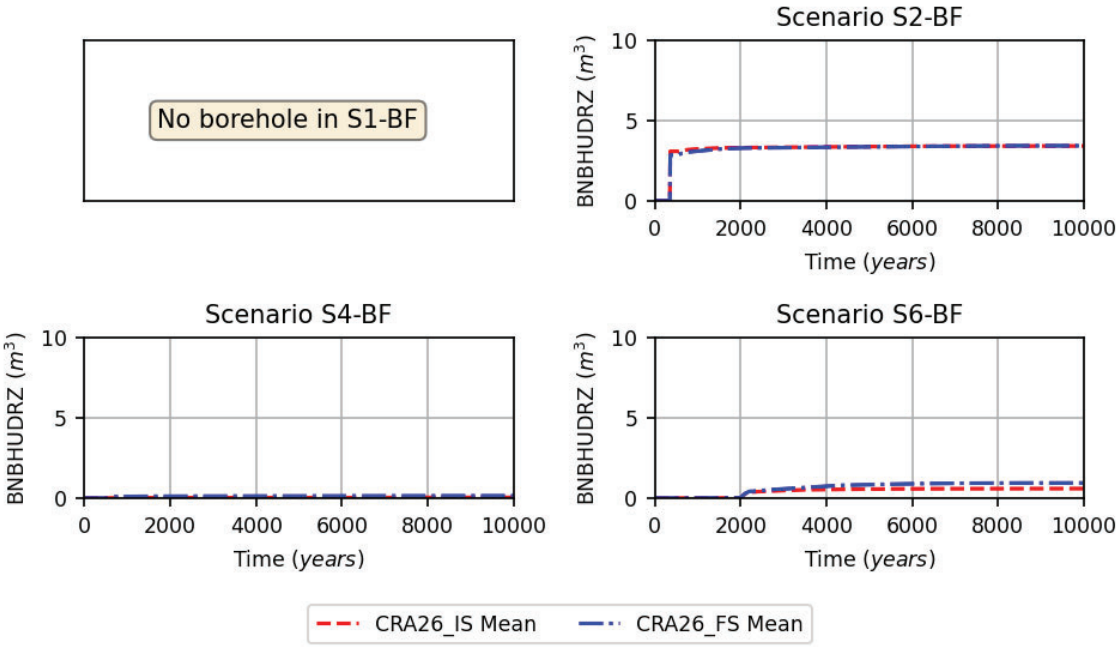


Figure 28. Mean Brine Flow up the Borehole

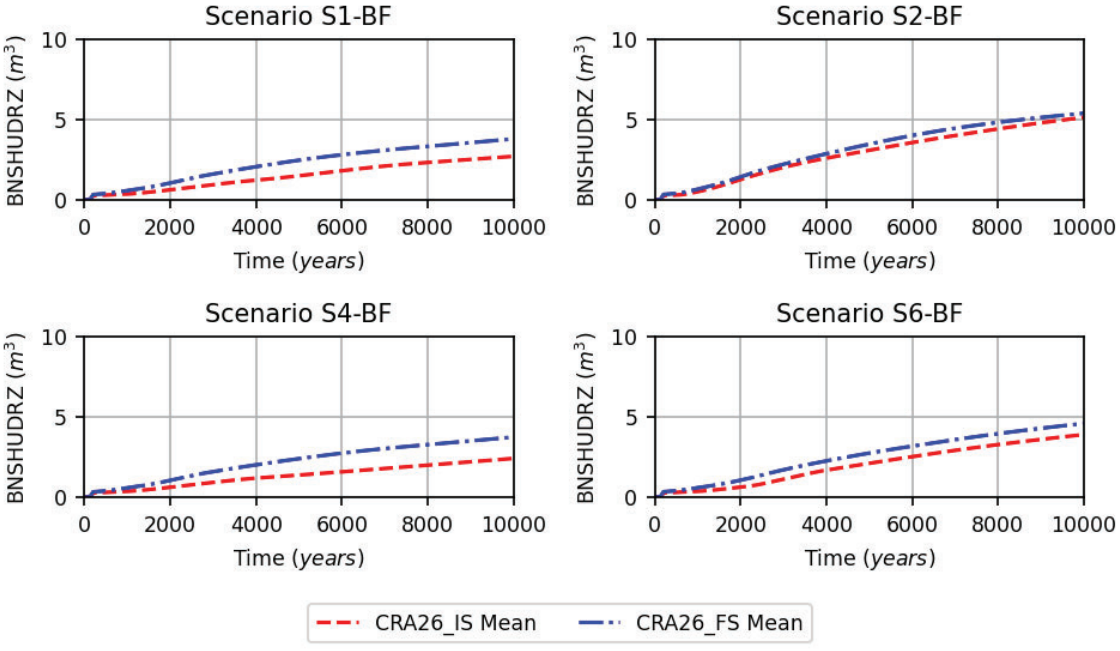


Figure 29. Mean Brine Flow up the Shaft

Information Only

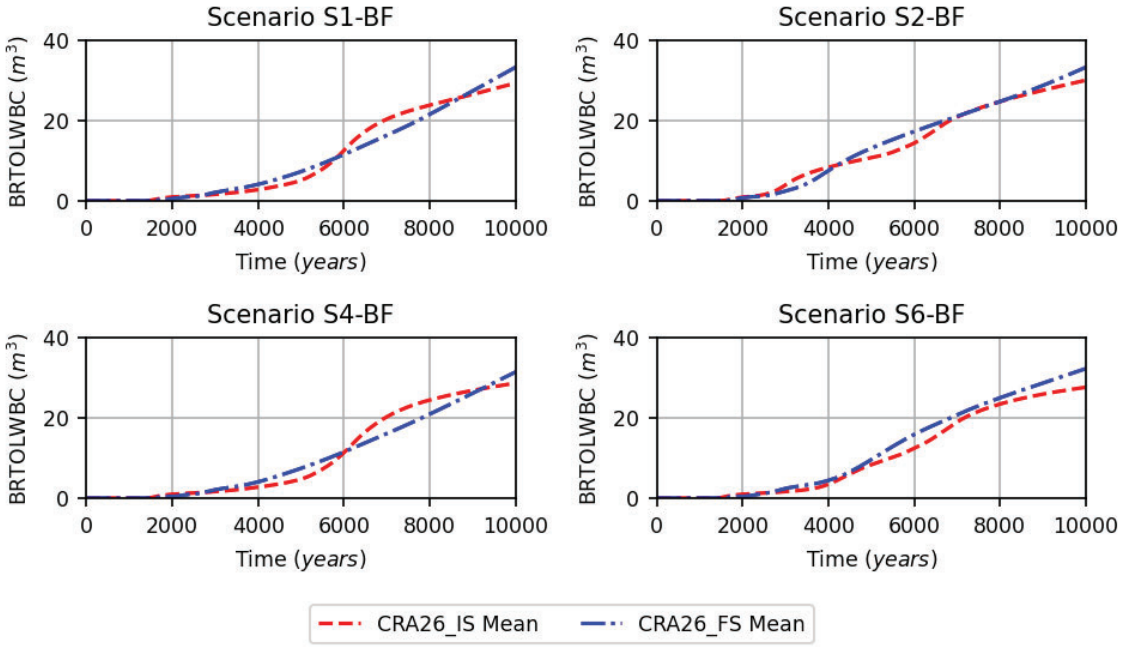


Figure 30. Mean Brine Flow in Anhydrite Layers Across the Land Withdrawal Boundary

4.3 Cuttings, Cavings, and Spallings

This section describes the volumes of solids released from the WIPP repository from an intrusion borehole. The PA codes CUTTINGS_S and DRSPALL are used to calculate these volumes which include cuttings, cavings, and spallings. Changes included in the CRA26_FS that are observed to most substantially affect spallings volumes (there are no changes to cuttings and cavings volumes) as compared to the CRA26_IS are (Brunell and Kicker 2025):

- Decreased gas generation and brine consumption on a per waste area volume basis, leading to similar but variable pressure trend comparisons across scenarios and intrusion locations with CRA26_IS (see Section 4.2).

Cuttings, cavings, and spallings volumes are analyzed across four distinct areas of the repository: the lower (L) area, which includes only Panel 5; the middle (M) area, comprising the connected Panels 3, 4, 6, and 9; the upper (U) repository area, consisting of Panels 1, 2, 7, 8, and 10; and the other (O) repository area, which encompasses Panels 11 through 19. For more information on the solids release calculations, see Brunell and Kicker (2025).

4.3.1 Cuttings and Cavings

The cuttings and cavings results obtained for the CRA26_FS are identical to those from the CRA26_IS. There were no changes to parameters associated with the cuttings and cavings processes in the CRA26_FS. Furthermore, cuttings and cavings volumes are independent of

Information Only

repository conditions so there are no changes between the CRA26_IS and the CRA26_FS. A summary of statistics for cavings is presented in Table 11.

Table 11. Cavings Area Statistics for CRA26_FS and CRA26_IS

Replicate	Mean Cavings Area (m^2)	Mean Non-Zero Cavings Area (m^2)	Maximum Cavings Area (m^2)	Number of Vectors without Cavings
R1	0.011	0.021	0.110	49
R2	0.010	0.019	0.107	44
R3	0.011	0.021	0.090	49

4.3.2 Spallings

Spallings releases are calculated by multiplying the estimated spallings volumes by the concentrations of radionuclides present in CH waste at the time of intrusion. This ensures that the assessment reflects the radionuclide concentrations relevant to the specific conditions in the repository during each intrusion event. The spallings volumes, as detailed in Section 4.3.2.1, are derived from the pressure conditions within the repository waste areas (Figure 3). Section 4.3.2.2 discusses the spallings concentrations, which are based on the average activity per volume of CH-TRU waste.

4.3.2.1 Spallings Volume

Spallings volumes are calculated based on pressure conditions in the repository waste areas. Time-dependent spallings volumes are determined by interpolating the spallings volumes calculated by DRSPALL to the time-dependent repository pressures calculated by BRAGFLO. The DRSPALL code uses sampled parameter values from the LHS code but has no dependencies on outputs of other PA codes (Lord and Rudeen 2003). It is for this reason that DRSPALL is not typically run during a PA calculation. Both the CRA26_FS and the CRA26_IS use DRSPALL results from a previous analysis (Kirchner et al. 2014; 2015).

The intrusion scenarios and times employed in the calculation of spallings volumes are presented in Table 6; these same scenarios are also used for calculating DBR volumes. Time-dependent spallings volumes are determined by interpolating the spallings volumes calculated by DRSPALL to align with the time-dependent repository pressures derived from BRAGFLO. Summary statistics of spallings volumes are provided in Table 12 and shown in Figure 31 and Figure 32 for the CRA26_FS and the CRA26_IS. Overall, the CRA26_IS and CRA26_FS analyses produce similar spallings results.

As discussed in Section 4.2, the larger volume of the West Rest-of-Repository (corresponding to the O location) in the CRA26_FS configuration results in greater net brine inflow and enhanced

Information Only

brine saturation. The increased brine saturation contributes to higher brine pressure, ultimately leading to larger spallings volumes from the O location compared to the CRA26_IS analysis.

Maximum volumes for the CRA26_IS and CRA26_FS are very similar for scenarios S1-DBR, S2-DBR, and S3-DBR (Figure 31) and for all locations (Figure 32). This similarity is attributed to maximum pressures in the repository being largely controlled by the porosity response surface in realizations with high pressures. In these high-pressure realizations, the intruding borehole has little impact on repository pressures (King 2023), and thus little impact on the maximum spallings volumes. As discussed in Section 4.2 and shown in Figure 24 through Figure 27, mean brine pressures in Scenarios S4-DBR and S5-DBR are higher in CRA26_FS in comparison to CRA26_IS, leading to higher maximum spallings volumes in those scenarios.

Information Only

Table 12. Spallings Volume Summary, Replicate 1

Scenario	Location	Mean Spallings Volume (m^3) CRA26_IS	Mean Spallings Volume (m^3) CRA26_FS	Fraction of Sim. with Nonzero Releases CRA26_IS	Fraction of Sim. with Nonzero Releases CRA26_FS	Mean of Non-Zero Spallings Releases (m^3) CRA26_IS	Mean of Non-Zero Spallings Releases (m^3) CRA26_FS
S1-DBR	**All**	**0.24**	**0.26**	**11.54%**	**13.96%**	**2.06**	**1.85**
S1-DBR	L	0.28	0.29	13.33%	15.83%	2.13	1.84
S1-DBR	M	0.28	0.29	13.33%	15.83%	2.12	1.84
S1-DBR	U	0.27	0.28	12.83%	14.50%	2.09	1.94
S1-DBR	O	0.12	0.17	6.67%	9.67%	1.75	1.77
S2-DBR	**All**	**0.41**	**0.42**	**34.80%**	**34.30%**	**1.18**	**1.22**
S2-DBR	L	0.60	0.57	50.60%	48.80%	1.18	1.17
S2-DBR	M	0.59	0.57	50.60%	48.80%	1.17	1.16
S2-DBR	U	0.33	0.36	26.60%	26.20%	1.26	1.38
S2-DBR	O	0.12	0.18	11.40%	13.40%	1.08	1.33
S3-DBR	**All**	**0.38**	**0.40**	**34.75%**	**34.90%**	**1.10**	**1.15**
S3-DBR	L	0.51	0.49	49.20%	48.20%	1.04	1.01
S3-DBR	M	0.51	0.49	49.20%	47.80%	1.04	1.02
S3-DBR	U	0.36	0.40	27.60%	28.40%	1.29	1.42
S3-DBR	O	0.15	0.23	13.00%	15.20%	1.13	1.51
S4-DBR	**All**	**0.20**	**0.24**	**13.15%**	**15.70%**	**1.52**	**1.50**
S4-DBR	L	0.23	0.25	15.00%	17.40%	1.54	1.42
S4-DBR	M	0.23	0.24	15.00%	17.40%	1.53	1.41
S4-DBR	U	0.23	0.28	14.80%	16.60%	1.57	1.68
S4-DBR	O	0.11	0.17	7.80%	11.40%	1.36	1.50
S5-DBR	**All**	**0.28**	**0.33**	**15.90%**	**19.15%**	**1.73**	**1.73**
S5-DBR	L	0.32	0.36	18.20%	21.00%	1.76	1.70
S5-DBR	M	0.32	0.36	18.20%	21.00%	1.76	1.69
S5-DBR	U	0.32	0.38	18.00%	20.80%	1.76	1.83
S5-DBR	O	0.14	0.23	9.20%	13.80%	1.57	1.66
All Scenarios	**All Locations**	**0.30**	**0.33**	**21.63%**	**23.23%**	**1.38**	**1.41**
All	**L**	0.38	0.39	28.65%	29.69%	1.34	1.30
All	**M**	0.38	0.39	28.65%	29.62%	1.34	1.30
All	**U**	0.30	0.34	19.69%	21.04%	1.53	1.61
All	**O**	0.13	0.19	9.50%	12.58%	1.34	1.55

Information Only

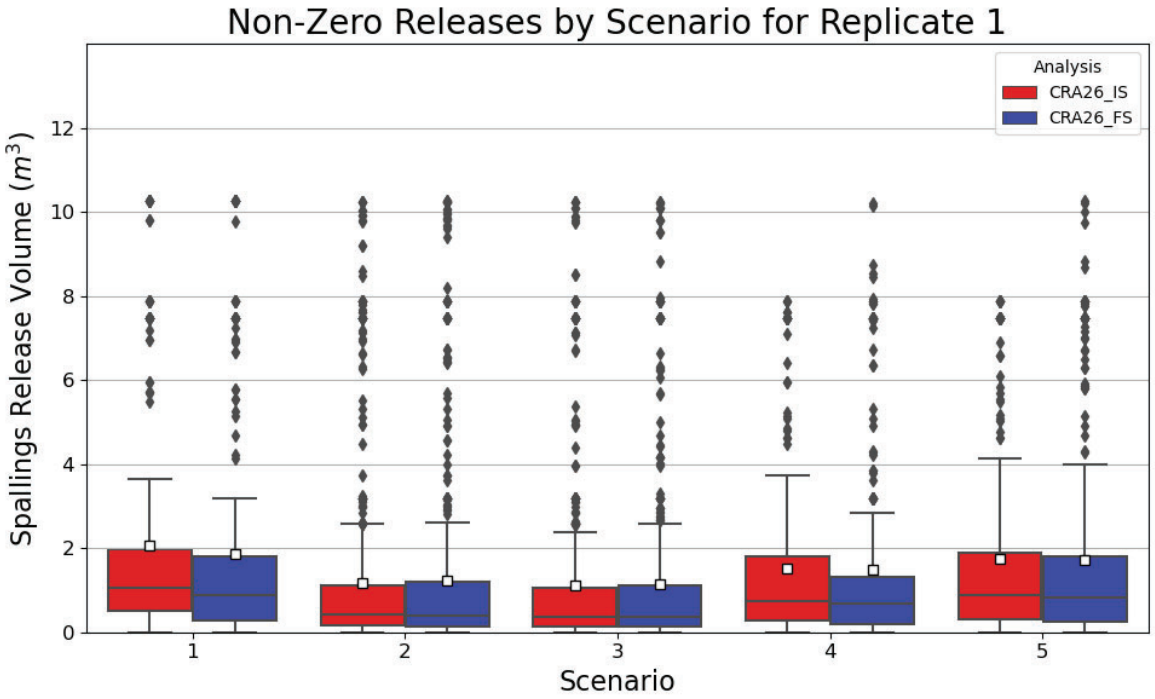


Figure 31. Non-Zero Spallings Release Volume by Scenario

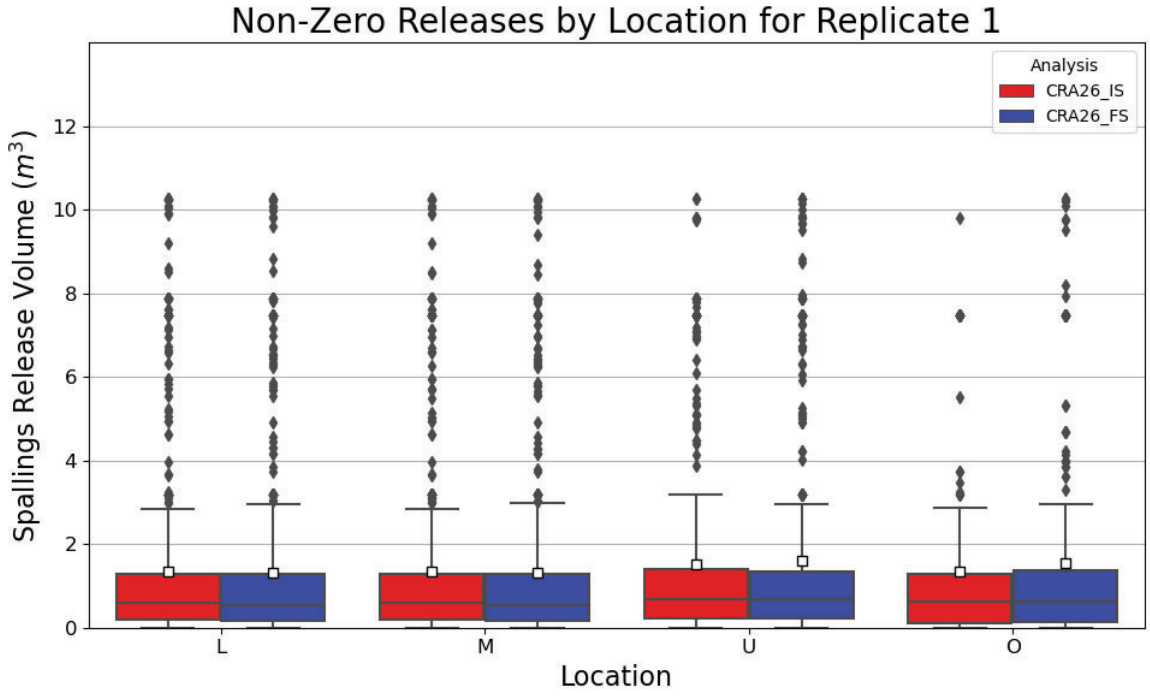


Figure 32. Non-Zero Spallings Release Volume by Location

Information Only

4.3.2.2 Spallings Concentration

Spallings releases are calculated by multiplying spallings volumes by the average concentration of radionuclides in CH waste at the time of intrusion (Section 4.8.3). Concentrations of radionuclides are calculated by the PRECCDFGF code from EPAUNI output as the volume-weighted average concentration in all CH-TRU waste streams. The inventory activity in EPA Units is relatively consistent between the CRA26_IS and the CRA26_FS (Figure 7b). The repository volume (REFCON:VREPOS; determined by the volume of waste panels), however, is increased in the CRA26_FS due to the inclusion of Panels 13 through 19. As a result, the repository-volume based spallings concentrations (i.e., in units of EPA Units per repository volume) have decreased for the CRA26_FS.

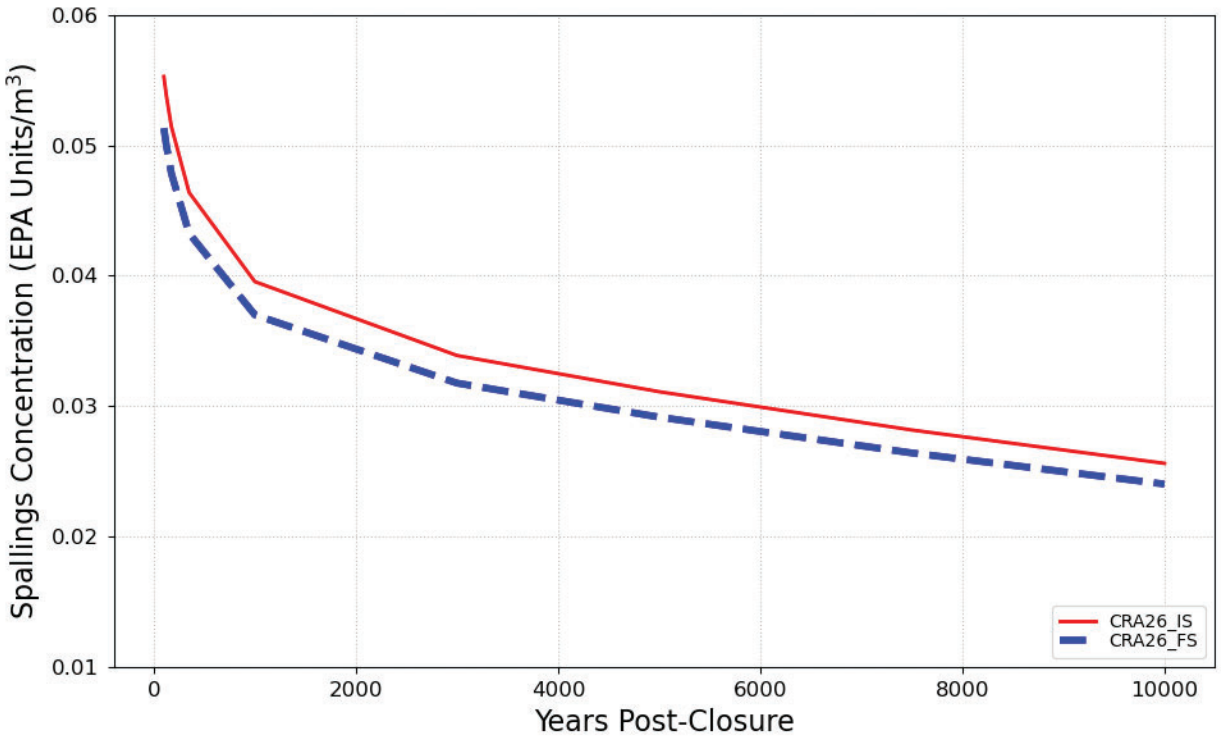


Figure 33. Spallings Release Concentration from Closure to 10,000 Years

4.4 Direct Brine Release Volumes

Mean brine releases, fraction of simulations with non-zero releases, and mean of non-zero brine releases for Replicate 1 are summarized in Table 13. The number of non-zero brine releases is plotted in Figure 34 by brine release volume, and the distribution of non-zero brine release volumes is plotted in Figure 35. Figure 36 shows the distribution of non-zero release volumes broken down by scenario. Changes included in the CRA26_FS that most substantially affect DBR results as compared to the CRA26_IS are (Zeitler 2025):

Information Only

- Decreased gas generation and brine consumption on a per waste area volume basis, leading to increased brine saturation for all scenarios in all waste areas and similar but variable pressure trend comparisons across scenarios and intrusion locations (see Section 4.2).

Comparing DBR volumes for the CRA26_IS and the CRA26_FS:

(i) The number of non-zero DBR volumes increases for the CRA26_FS across all scenarios.
(ii) In the CRA26_FS small magnitude releases increase in frequency (Figure 34), while large magnitude releases (greater than 50 m^3) decrease slightly in frequency (though they represent a very small fraction of release events) (Figure 35).
(iii) Mean and median non-zero release volumes each increase slightly for the CRA26_FS, while maximum non-zero release volumes decrease (Figure 35). Overall, the mean non-zero release volume increased by about 10% (Table 13).
(iv) For the CRA26_FS, mean non-zero release volumes increase for all scenarios except for S4-DBR (Figure 36). Median release volumes also increase for all scenarios except S4-DBR. Maximum release volumes increase for scenarios S1-DBR and S5-DBR and decrease for the other three scenarios.
(v) For both the CRA26_IS and the CRA26_FS, the largest fraction of non-zero DBR volumes occurs at the L intrusion location and decreases as the intrusion location moves to the north, that is, up dip to the M, U, and O locations (Table 13). The largest mean non-zero release volume also occurs at the L intrusion location and decreases as the intrusion location moves to the north to the M intrusion location, but then increases for the U intrusion location, and finally decreases to the lowest volume for the O intrusion location.
(vi) Releases from the O intrusion location contribute to CRA26_IS and CRA26_FS DBR volumes; however, O intrusion releases are less frequent and mean volumes are smaller compared to the L, M and U intrusion locations (Table 13).

As described in Section 4.2, the CRA26_FS Salado flow results show an increase in mean brine pressures for scenarios without an E1 intrusion and similar mean brine pressures for scenarios with an E1 intrusion. Additionally, there is an observed increase in brine saturation across all scenarios. The combination of these effects could lead to mixed impacts, but a generally higher number of non-zero DBR volumes across scenarios.

Comparing CRA26_FS and CRA26_IS DBR volumes at individual intrusion locations (in Table 13, rows directly beneath the “All Scenarios” label), DBR volumes for all intrusion locations follow the overall trend of an increased frequency of non-zero DBR volumes and with increased mean non-zero release volumes in the CRA26_FS. In both analyses, DBR volumes from the L location have the greatest frequency and mean non-zero release volume. DBR volumes at the M location have decreased frequency and mean non-zero release volumes compared to the L location, but the mean non-zero release volumes are also lower compared to the U intrusion location for Replicate 1 in both analyses.

Scenarios with an E1 intrusion (S2-DBR and S3-DBR) have an increased frequency of non-zero DBR volumes in the CRA26_FS; additionally, mean non-zero release volumes in the CRA26_FS are increased by about 12% compared with those in the CRA26_IS (Table 13). The increase in

Information Only

mean non-zero release volumes can be attributed to increased brine saturation for scenarios with E1 intrusion along with similar brine pressures (Section 4.2), despite the observed decrease in the number of large magnitude releases (Figure 35).

Scenarios without an E1 intrusion (S1-DBR, S4-DBR and S5-DBR) also saw the frequency of non-zero DBR volumes increase in the CRA26_FS. Scenarios S1-DBR and S5-DBR saw mean non-zero releases increased by about 20% and 5%, respectively, while scenario S4-DBR saw them decreased by about 10% (Table 13). The decreased mean non-zero brine releases for scenario S4-DBR is a result of larger increases in frequency for intrusions the M, U, and O locations, each of which had decreased means, compared to the L intrusion location, which did have increased mean non-zero brine releases. The decreased mean volumes for the M, U, and O locations may be due to the increased number of smaller DBR volumes (Figure 34). The increased frequency in non-zero DBR volumes can be attributed to increased brine saturation, as well as increased mean pressure for scenarios without an E1 intrusion (Section 4.2). The increased mean DBR volumes for scenarios S4-DBR and S5-DBR is a result of increased brine saturations and pressures, even when they result in an increased number of smaller DBR volumes for some location/scenario combinations in CRA26_FS.

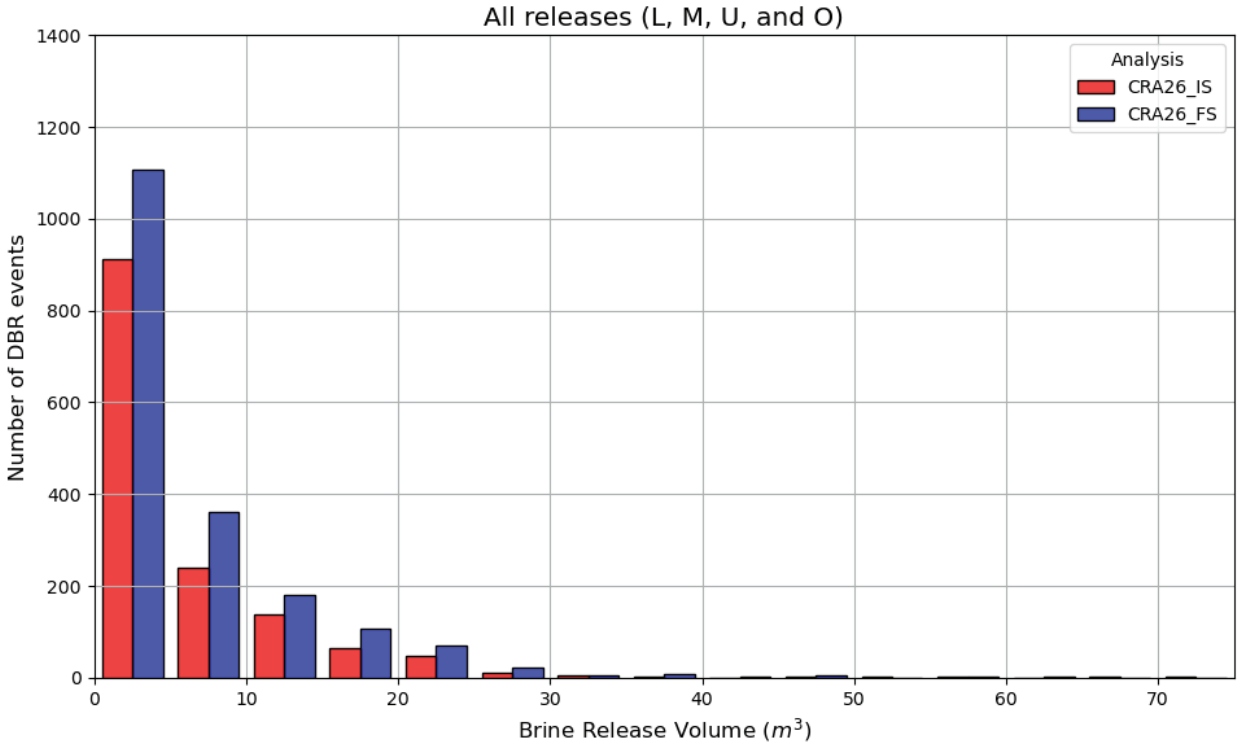


Figure 34. DBR Volume Frequency, All Non-Zero Releases

Information Only

Table 13. DBR Volume Summary

Intrusion Location	Mean Brine Released (m^3)		Fraction of Simulations with Non-Zero Releases		Mean of Non-Zero Brine Releases (m^3)	
	CRA26_IS	CRA26_FS	CRA26_IS	CRA26_FS	CRA26_IS	CRA26_FS
S1-DBR	**0.30**	**0.53**	**5.04%**	**7.12%**	**6.05**	**7.38**
L	0.78	1.38	9.67%	12.33%	8.11	11.18
M	0.20	0.30	3.67%	5.33%	5.53	5.66
U	0.19	0.31	4.83%	6.33%	3.87	4.82
O	0.05	0.12	2.00%	4.50%	2.28	2.58
S2-DBR	**1.32**	**1.77**	**27.75%**	**33.10%**	**4.77**	**5.34**
L	3.66	4.66	62.40%	68.40%	5.87	6.82
M	1.20	1.73	39.20%	46.80%	3.06	3.70
U	0.33	0.49	6.60%	11.20%	5.06	4.41
O	0.10	0.18	2.80%	6.00%	3.57	3.03
S3-DBR	**0.69**	**1.00**	**22.10%**	**28.40%**	**3.13**	**3.52**
L	1.94	2.67	51.00%	64.00%	3.81	4.17
M	0.52	0.62	27.20%	32.40%	1.91	1.90
U	0.25	0.53	6.80%	10.40%	3.68	5.08
O	0.06	0.18	3.40%	6.80%	1.70	2.67
S4-DBR	**0.68**	**0.93**	**7.75%**	**11.65%**	**8.79**	**7.94**
L	1.76	2.27	15.20%	17.80%	11.55	12.73
M	0.52	0.75	6.80%	12.40%	7.65	6.01
U	0.35	0.51	6.40%	10.40%	5.44	4.87
O	0.10	0.18	2.60%	6.00%	3.84	3.05
S5-DBR	**0.70**	**1.11**	**7.90%**	**11.70%**	**8.88**	**9.45**
L	2.07	2.79	15.20%	19.20%	13.61	14.56
M	0.40	0.81	6.60%	10.80%	6.08	7.46
U	0.28	0.62	6.40%	10.00%	4.32	6.22
O	0.06	0.20	3.40%	6.80%	1.79	2.92
All Scenarios						
L	**1.99**	**2.70**	**29.88%**	**35.42%**	**6.67**	**7.63**
M	**0.55**	**0.82**	**16.19%**	**20.92%**	**3.43**	**3.91**
U	**0.28**	**0.48**	**6.15%**	**9.54%**	**4.48**	**5.07**
O	**0.07**	**0.17**	**2.81%**	**5.96%**	**2.56**	**2.85**
ALL	**0.72**	**1.04**	**13.76%**	**17.96%**	**5.26**	**5.81**

Information Only

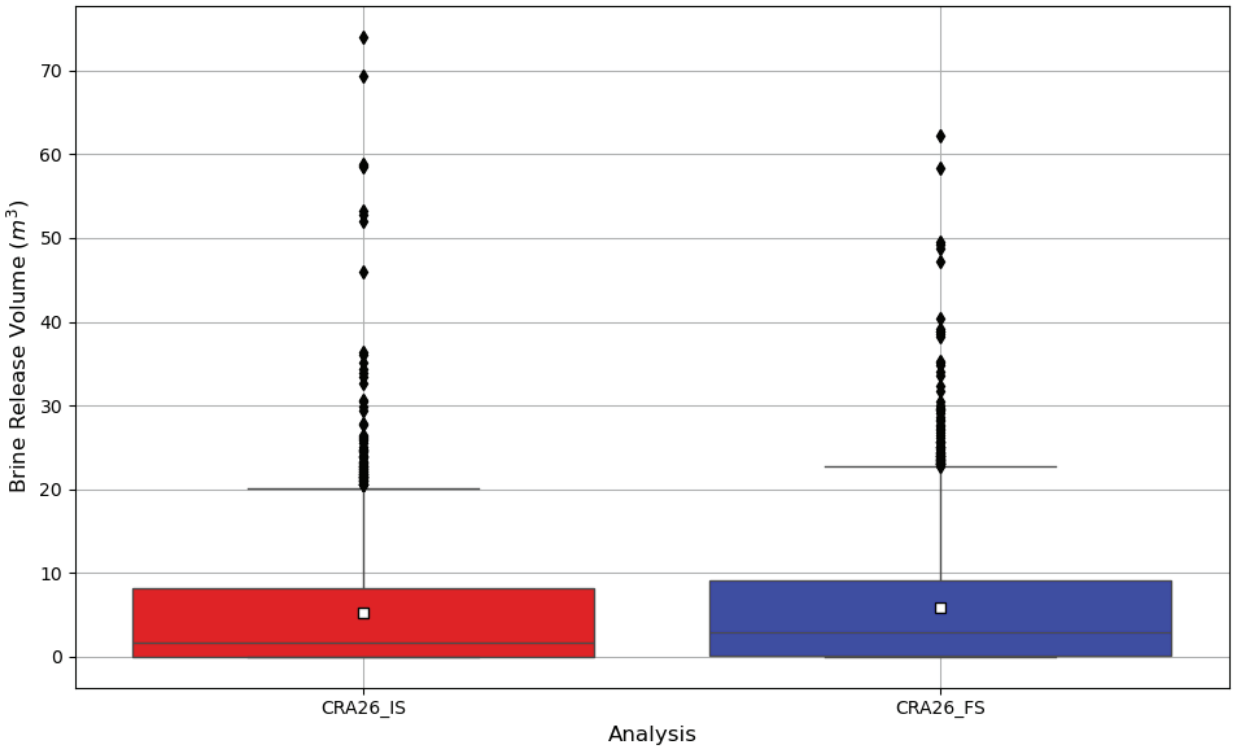


Figure 35. DBR Volumes, All Non-Zero Releases

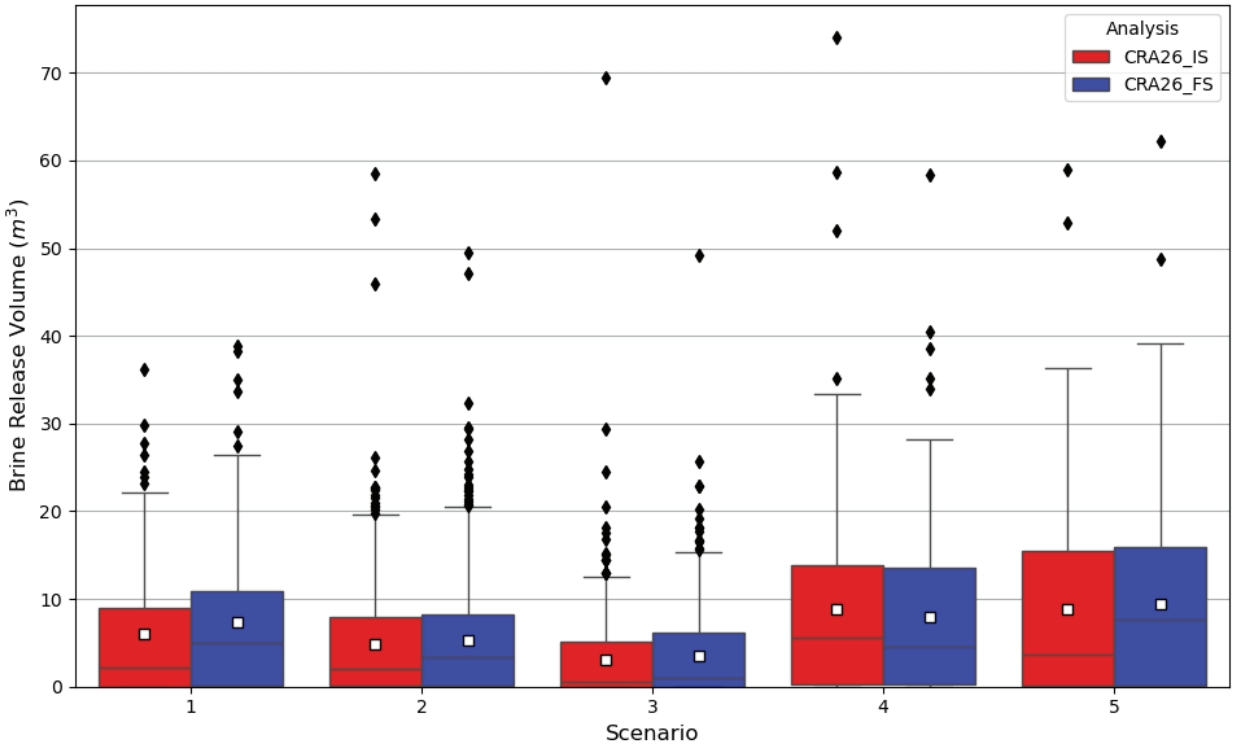


Figure 36. DBR Volumes by Scenario, All Non-Zero Releases

Information Only

4.5 Mobilized Radionuclide Concentrations

Changes included in the CRA-2026_FS that most substantially affect radionuclide mobilization results as compared to the CRA26_IS are:

- The total activity at repository closure increases from 8.05×10^6 Ci in the CRA26_IS (Kicker 2025b, Table 21) to 9.68×10^6 Ci for the CRA26_FS (Kicker 2025a, Table 21).
- The transuranic inventory of alpha-emitting radionuclides with half-lives greater than 20 years at repository closure increases from 7.37×10^6 Ci in the CRA26_IS (Kicker 2025b, Table 21) to 8.68×10^6 Ci for the CRA26_FS (Kicker 2025a, Table 21).
- DBRMINBV (the minimum brine volume for a DBR to occur, Section 2.7) increases from 6,314 m^3 in the CRA26_IS to 9,608 m^3 in the CRA26_FS, consistent with a 19-panel repository (Brunell 2025).

The PANEL code models radionuclide mobilization for a group of five interconnected waste panels, designated as the waste area (Docherty and Kim 2025, Section 5.1). Inventory in the waste area is obtained from total inventory by multiplying by the factor $5\times$REFCON:VPANLEX/REFCON:VREPOS, that is, by five times the volume of one panel, divided by the volume of the repository. Parameter REFCON:VPANLEX is 46,097.65 m^3 in both analyses; however, REFCON:VREPOS increased from 560,722.29 m^3 in the CRA26_IS to 905,734.49 m^3 in the CRA26_FS. Figure 37 illustrates the twelve largest contributors to waste area inventory, based on curies at closure, of the 30 radionuclides considered by PANEL. The five largest contributors in order, in both analyses, are ^{239}Pu, ^{241}Am, ^{238}Pu, ^{240}Pu, and ^{241}Pu. The waste area inventory of each of these radionuclides has decreased in the CRA26_FS.

Information Only

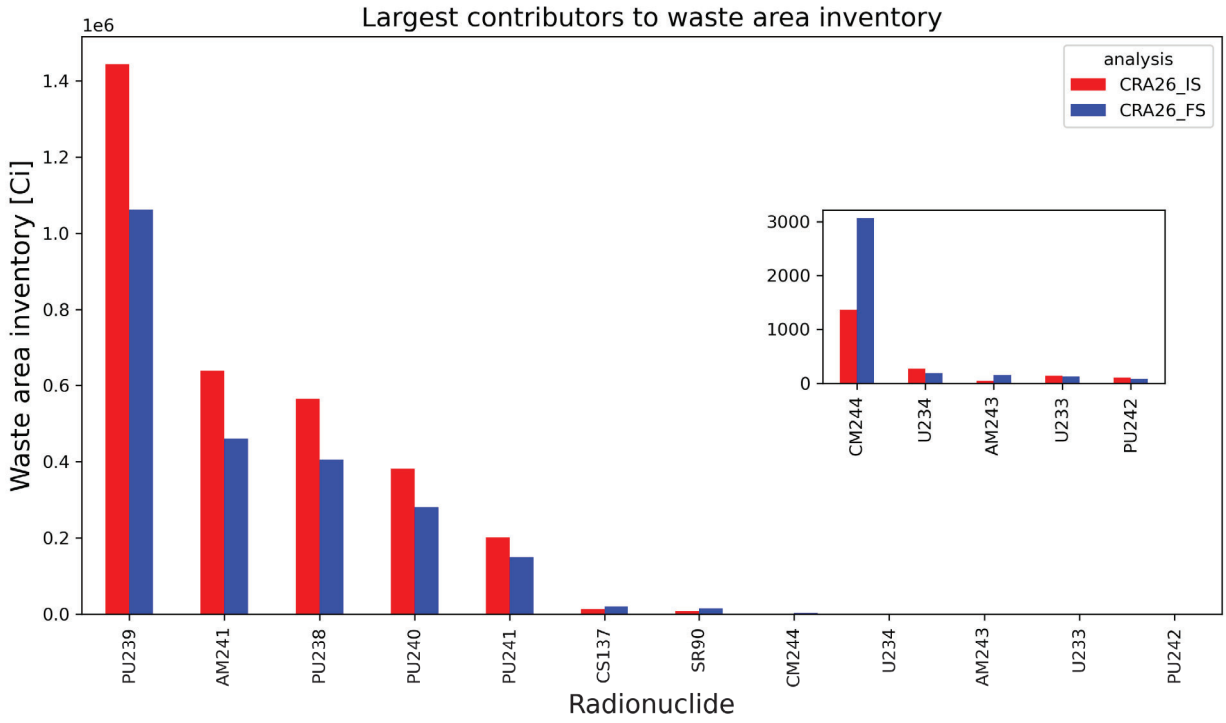


Figure 37. Largest Contributors in Curies to Inventory at Closure in the Waste Area

Domski (2025b) notes that the total moles of organic ligands are nearly the same in the CRA26_IS and the CRA26_FS. An increase in the minimum brine volume (Table 4) in the CRA26_FS thus decreases organic ligand concentrations. As a consequence, An(III) and An(V) baseline solubilities in the CRA26_FS fell to about 80% of their CRA26_IS values, for both ERDA-6 and GWB brines (Domski 2025b, Tables 16 and 17). An(IV) solubilities are not sensitive to organic ligand concentrations and remained about the same in the two analyses.

A thermodynamic model has not been developed for U(VI). Both the CRA26_IS and the CRA26_FS use a baseline solubility of 3×10^{-6} mol/L for U(VI), based on recent experimental work by Kaplan et al. (2025). U(VI) baseline solubility does not depend on brine type in the WIPP thermodynamic database (Domski 2025b).

Table 14 lists mean values of the mobile concentration limits for the primary actinides in PA, determined for the minimum volume of brine for a DBR to occur. Consistent with the changes to baseline solubilities, the mean element mobile concentration limits in both brine types decreased in the CRA26_FS for Pu, Np and Am, and remained largely unchanged for U and Th.

Information Only

Table 14. Mean Element Mobile Concentration Limits in mol/L

Brine	Analysis	PU	U	NP	AM	TH
ERDA-6	CRA26_IS	3.20E-06	3.71E-06	2.23E-06	1.66E-05	6.25E-07
ERDA-6	CRA26_FS	2.77E-06	3.71E-06	1.79E-06	1.43E-05	6.26E-07
GWB	CRA26_IS	3.22E-06	3.12E-06	6.97E-07	1.67E-05	6.19E-07
GWB	CRA26_FS	2.59E-06	3.12E-06	6.07E-07	1.35E-05	6.19E-07

Table 15 lists mean values of the lumped radionuclide mobile concentration limits (for the minimum brine volume). Mean values in both brine types decrease in the CRA26_FS for PU238L, PU239L, and AM241L, and remain about the same for U234L. Changes in the inventory of ^{229}Th, ^{230}Th, and ^{232}Th bring about an increase in the TH230L mole fraction (Docherty and Kim 2025, Eq. 11) from 5.8×10^{-3} to 6.5×10^{-3} in the CRA26_FS. The increased mole fraction causes an increase in the CRA26_FS mobile concentration limit for TH230L as indicated in Table 15.

Table 15. Mean Lumped Radionuclide Mobile Concentration Limits in mol/L

Brine	Analysis	PU238L	PU239L	U234L	AM241L	TH230L
ERDA-6	CRA26_IS	4.25E-09	3.20E-06	2.79E-09	1.66E-05	3.62E-09
ERDA-6	CRA26_FS	3.59E-09	2.77E-06	2.94E-09	1.43E-05	4.08E-09
GWB	CRA26_IS	4.27E-09	3.22E-06	2.35E-09	1.67E-05	3.59E-09
GWB	CRA26_FS	3.36E-09	2.59E-06	2.48E-09	1.35E-05	4.03E-09

The PANEL code calculates the concentrations of 26 radionuclides for a period of 10,000 years starting at repository closure. The concentrations are summed for use in determining DBRs (Docherty and Kim 2025, Section 3.1.8). Figure 38 shows mean concentration in EPA units/m^3 as a function of time for ^{241}Am, ^{239}Pu, and ^{240}Pu in ERDA-6 brine and in the minimum brine volume (b = 1) (the mean is taken over the 100 vectors of Replicate 1). The three radionuclides, along with the fast-decaying ^{238}Pu, are the largest contributors to inventory at closure (Figure 37). Also shown in Figure 38 is the mean of the sum of the 26 radionuclides, designated CDBR. Concentrations of ^{239}Pu and ^{240}Pu are reduced in the CRA26_FS, as are concentrations of ^{241}Am until about 7,500 years after closure. An increase in ^{245}Cm inventory in the CRA26_FS increases ^{241}Am concentrations at later times. (^{245}Cm, with a half-life of 8,600 years, decays to ^{241}Pu, which decays rapidly to ^{241}Am). Figure 39 plots the sum of concentrations in ERDA-6 brine for all 100 vectors of Replicate 1.

Information Only

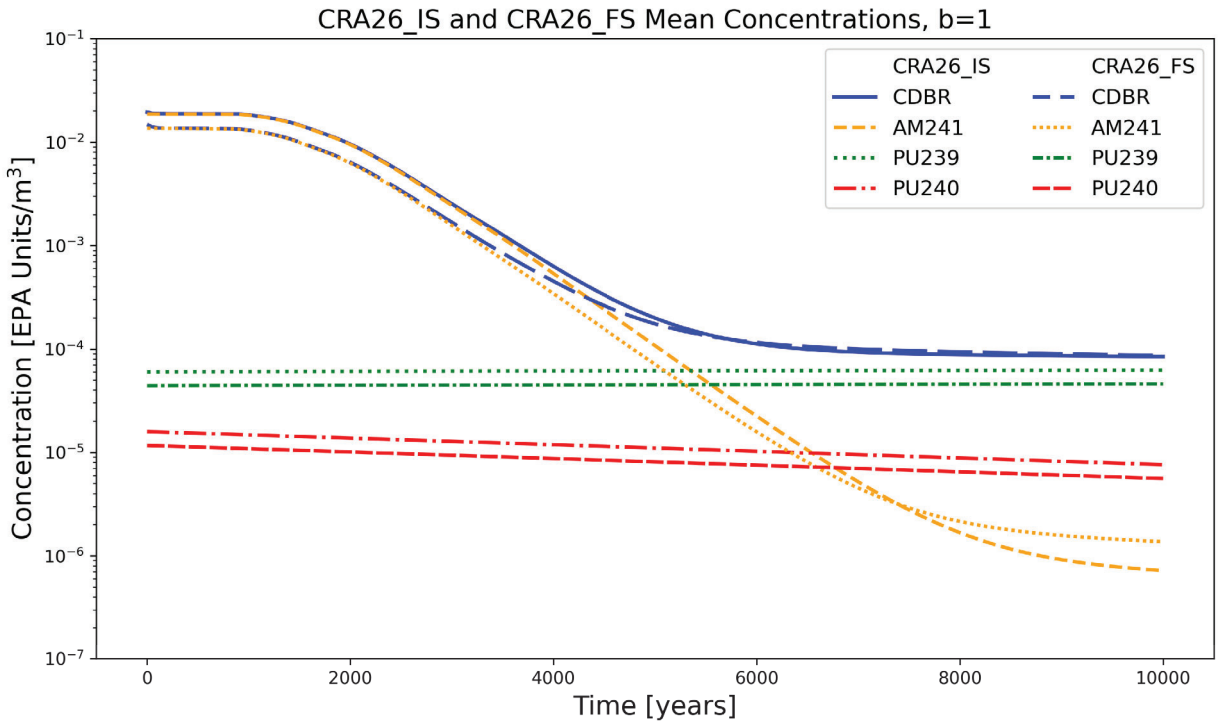


Figure 38. Comparison of Mean Concentrations for Select Radionuclides

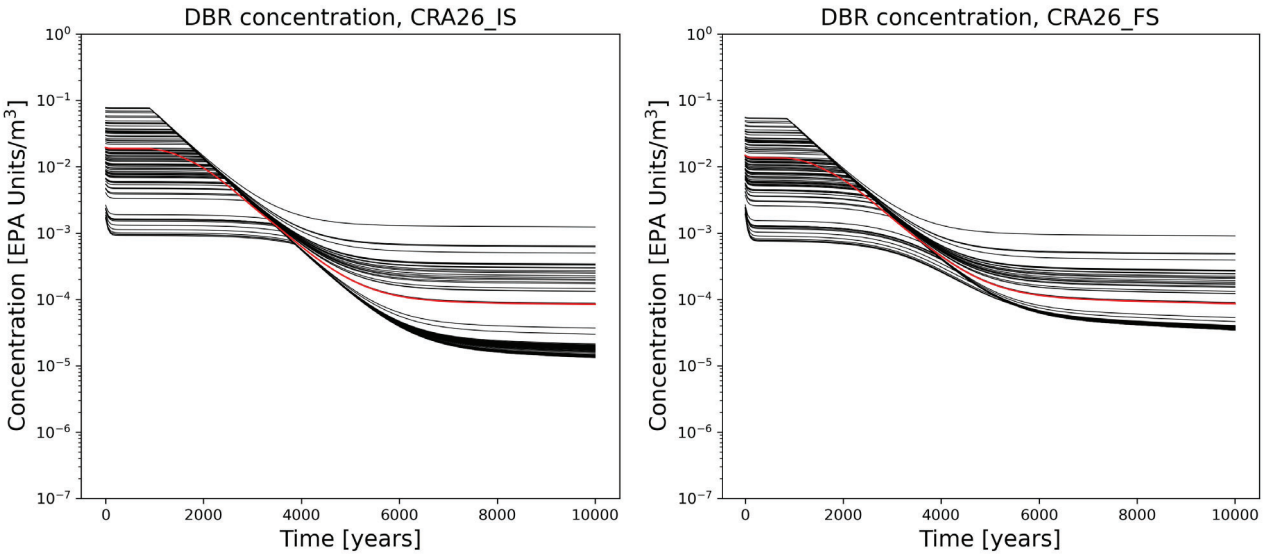


Figure 39. Summed Concentration Versus Time Used for Determining DBRs, all Vectors

Information Only

4.6 Salado Transport

Radionuclide transport up through an intruding borehole is the primary pathway for radionuclide mass transport in the Salado. Releases up the borehole to the Culebra are called *to Culebra* releases (though they are not releases in terms of WIPP regulatory compliance). NUTS determines lumped radionuclide *to Culebra* releases for screened-in vectors in BRAGFLO scenarios S2-BF through S5-BF. No vectors were screened in based on transport in the marker beds across the LWB. Releases for screened-out vectors are set to zero. PANEL determines lumped radionuclide *to Culebra* releases for all vectors in BRAGFLO scenario S6-BF (Table 5). Changes included in the CRA26_FS that were observed to most substantially affect Salado transport as compared to the CRA26_IS are those that affect brine pressure and brine saturation (Section 3.2), and consequently brine flow up the borehole to the Culebra.

Figure 40 shows cumulative *to Culebra* releases at 10,000 years for scenarios S2-BF through S6-BF, as well as total releases for each scenario – obtained by summing the accumulated releases of all five lumped radionuclides. Screened-out vectors have been included when making the box plots and affect the mean values shown (boxes marking 25th through 75th percentiles are absent from the plots where less than 25% of vectors are screened in). For scenarios S4-BF and S5-BF, no vectors were screened in for the CRA26_IS and only a few for the CRA26_FS. Mean cumulative *to Culebra* releases are listed in Table 16.

AM241L and PU239L are the dominant *to Culebra* releases in both analyses. For scenarios S2-BF through S5-BF, the mean cumulative releases of all lumped radionuclides are increased in the CRA26_FS compared to the CRA26_IS. Mean cumulative releases are similar for scenario S6-BF. Scenario S6-BF has the highest total cumulative releases in both analyses. While concentration limits are down for AM241L and PU239L in the CRA26_FS (Table 15), increased brine flow up the borehole can result in more waste delivered to the Culebra. Figure 41 shows cumulative brine flow up the borehole for the CRA26_IS and the CRA26_FS. For scenarios S2-BF and S3-BF in the CRA26_FS, two vectors (vectors 36 and 55) have both the largest cumulative brine flow up the borehole and the largest total cumulative *to Culebra* releases.

The complete history of total cumulative *to Culebra* releases is plotted for scenarios S2-BF through S6-BF in Figure 42. The red lines in the figures are mean total cumulative releases. For most simulations, the majority of the releases occur in the first few hundred years after the borehole plug degrades (plug degradation occurs 200 years after the intrusion). Note that in the CRA26_IS, S4-BF and S5-BF had no screened in vectors, therefore no calculated *to Culebra* releases. For the CRA26_FS, in replicate 1, there are 2 vectors screened in for scenario S4-BF and 1 vector screened in for scenario S5-BF. For scenario S6-BF, where an E2 intrusion at 1,000 years is followed by an E1 at 2,000 years, most of the releases occur after the E1 intrusion.

Information Only

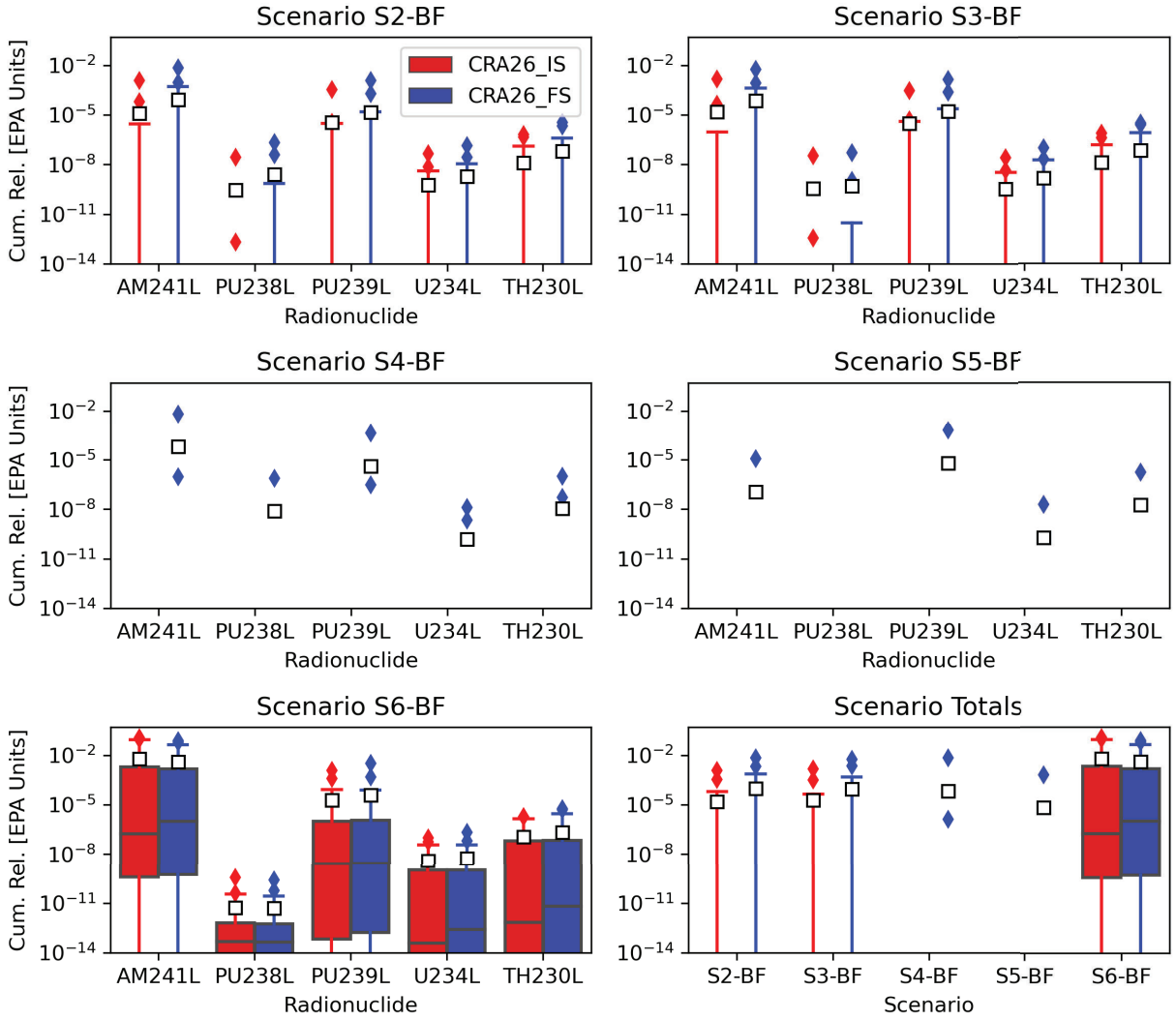


Figure 40. Cumulative Lumped Radionuclide Release

Information Only

Releases

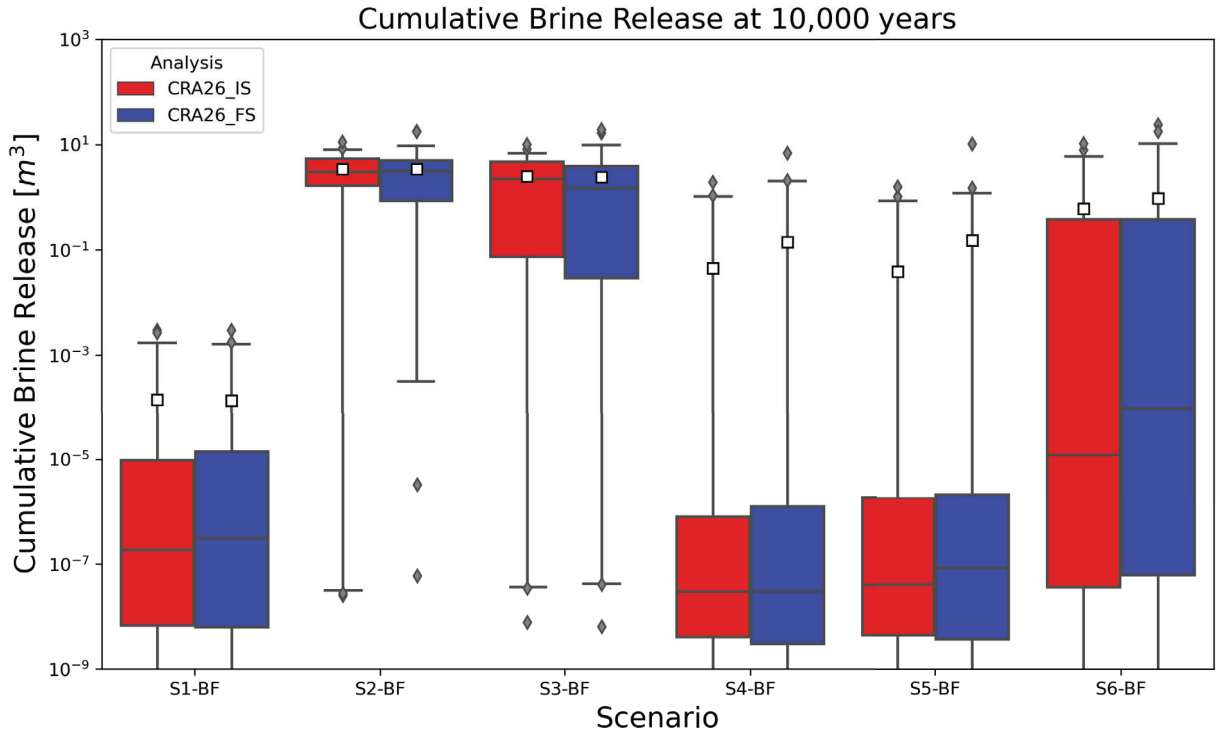


Figure 41. Cumulative Brine Releases up the Borehole

Table 16. Mean Cumulative Lumped Radionuclides Releases Through a Borehole to the Culebra at 10,000 Years in EPA Units

Analysis	Scenario	AM241L	PU239L	PU238L	U234L	TH230L	TOTAL
CRA26_IS	S2-BF	1.23E-05	3.40E-06	2.83E-10	5.71E-10	1.26E-08	1.57E-05
CRA26_IS	S3-BF	1.51E-05	3.13E-06	3.46E-10	3.42E-10	1.30E-08	1.83E-05
CRA26_IS	S4-BF	0.00E+00	0.00E+00	0.00E+00	0.00E+00	0.00E+00	0.00E+00
CRA26_IS	S5-BF	0.00E+00	0.00E+00	0.00E+00	0.00E+00	0.00E+00	0.00E+00
CRA26_IS	S6-BF	5.89E-03	1.88E-05	5.34E-12	3.89E-09	1.14E-07	5.91E-03
CRA26_FS	S2-BF	8.28E-05	1.45E-05	2.48E-09	1.86E-09	6.36E-08	9.74E-05
CRA26_FS	S3-BF	6.94E-05	1.66E-05	5.13E-10	1.45E-09	6.98E-08	8.61E-05
CRA26_FS	S4-BF	6.38E-05	4.08E-06	7.59E-09	1.50E-10	1.08E-08	6.79E-05
CRA26_FS	S5-BF	1.15E-07	6.26E-06	2.05E-19	1.92E-10	1.78E-08	6.39E-06
CRA26_FS	S6-BF	3.90E-03	3.92E-05	4.76E-12	5.30E-09	2.17E-07	3.94E-03

Information Only

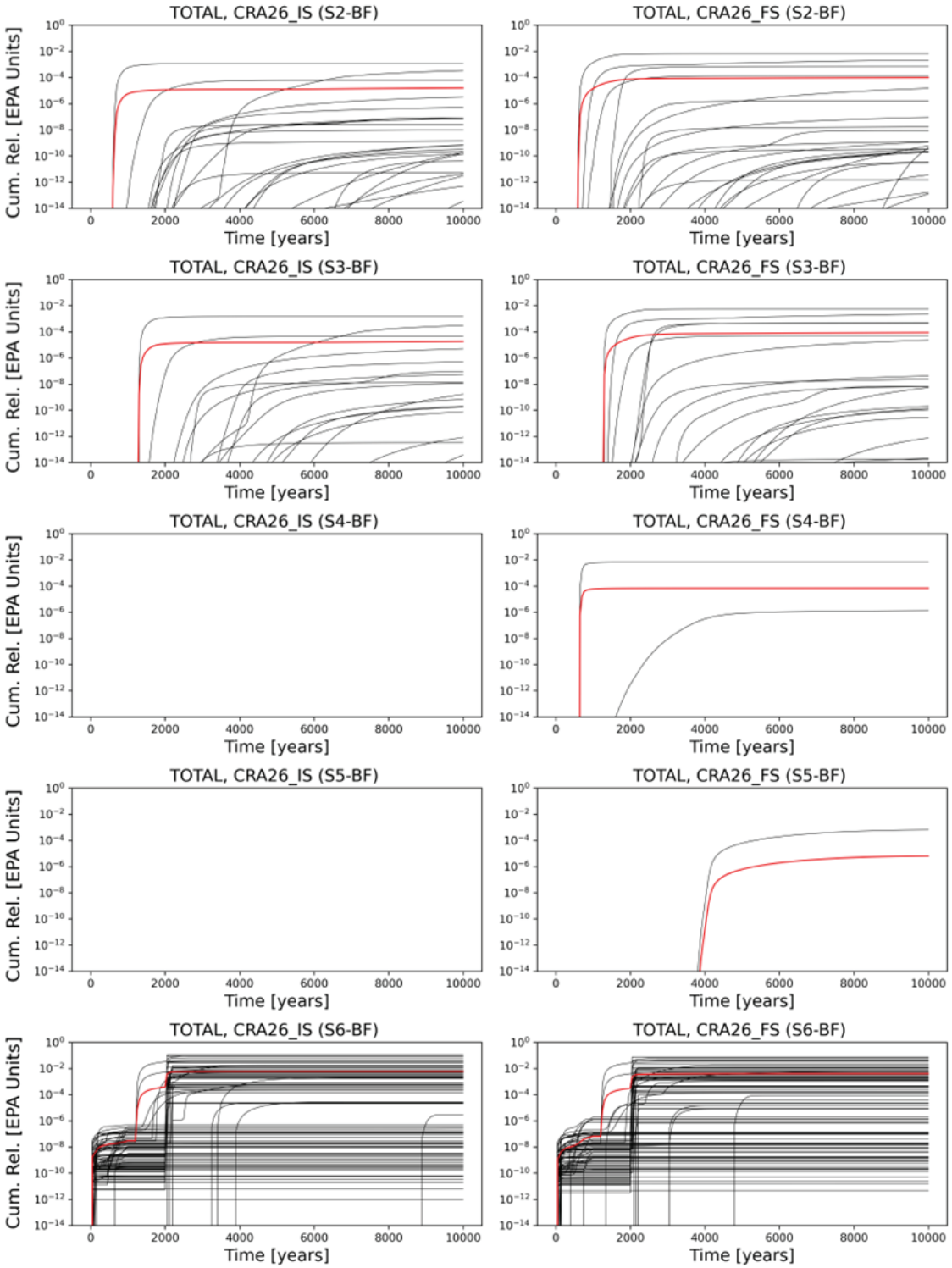


Figure 42. Total Cumulative Radionuclide Releases vs Time

Information Only

4.7 Culebra Flow and Transport

This section presents particle tracking and radionuclide mass transport calculations from the CRA-2026 Culebra flow and transport analysis report, which encompasses results for the CRA26_FS and CRA26_IS. Flow field results are omitted because they are identical to the RPPCR and between the CRA26_FS and CRA26_IS (Wilgus and Bethune 2025). The CRA26_FS considers four CRPs (CRP 1, CRP 2, CRP 3, and CRP 4) while the CRA26_IS only considers CRP 1 and CRP 2. Consequently, CRP 1 and CRP 2 results are identical between the CRA26_IS and CRA26_FS. Relative to the RPPCR, CRA-2026 CRP 1, 3, and 4 results are unchanged. The only modification made in the CRA-2026 since the RPPCR that impacts results was a small change in the location of CRP 2 (see Section 2.8). The relative impacts of the CRP 2 location change are detailed in the Culebra flow and transport analysis report (Wilgus and Bethune 2025) and the interim state summary report (Brunell et al. 2025); since the results are identical, they are also omitted here. A full set of replicate statistics are provided in Wilgus and Bethune (2025).

Figure 43 and Figure 44 show the spatial distribution of all 100 particle tracks alongside the cumulative distribution of the time taken for a particle to reach the LWB from each release point for full and partial mining scenarios, respectively. Time to LWB is shown on a logarithmic scale on the x-axis of the cumulative distribution plots from 10 to 10,000 years. Conceptually, the cumulative particle travel time distribution subplots (plotted as exceedance probability) describe the likelihood of a particle crossing the LWB within the range of observed particle travel times.

As in the RPPCR, particle tracks from release points CRP 1, CRP 2, and CRP 3 show downstream flow generally oriented toward the south. In the full mining scenario, particle tracks show the flow field is typically oriented toward the full mining impacted area to the southeast, then deflects along the mining affected region interface to the southern LWB. The partial mining particle tracks are more broadly distributed across the east-west direction (i.e., not as focused by persistent features across realizations), but are also generally directed toward the south. In contrast, particle tracks from CRP 4 vary significantly between scenarios: the full mining particle tracks continue west then turn sharply to the south near the western edge of the LWB, while the partial mining particle tracks generally lead south.

Travel times to the LWB are shorter in the full mining scenario, with travel times from CRP 4 significantly shorter than the other scenarios across all probability levels. Travel times to the LWB from the CRP 2 and CRP 3 release points are longer than travel times to the LWB from the CRP 1 release points.

Figure 45 and Figure 46 show exceedance probability curves of cumulative mass of each tracked radionuclide reaching the LWB by 10,000 years for full and partial mining scenarios, respectively. Mass discharge is shown on a logarithmic scale on the x-axis from 10^{-9} to 1 kg. Some partial mining scenario subplots display no results due to the low predictions of mass to the LWB.

Cumulative releases at 10,000 years are higher in the full mining scenario than in the partial mining scenario for all radionuclides across all displayed probability ranges. The differences are most apparent in CRP 4 where full mining scenario results are significantly larger than partial mining results. In the full mining scenario, CRP 2 and CRP 3 releases are generally lower than CRP 1, which in turn are lower than CRP 4, for all radionuclides. Amongst the radionuclides, ^{241}Am shows

Information Only

the lowest releases, while ^{234}U, shows the highest releases in both the full and partial mining scenarios.

Information Only

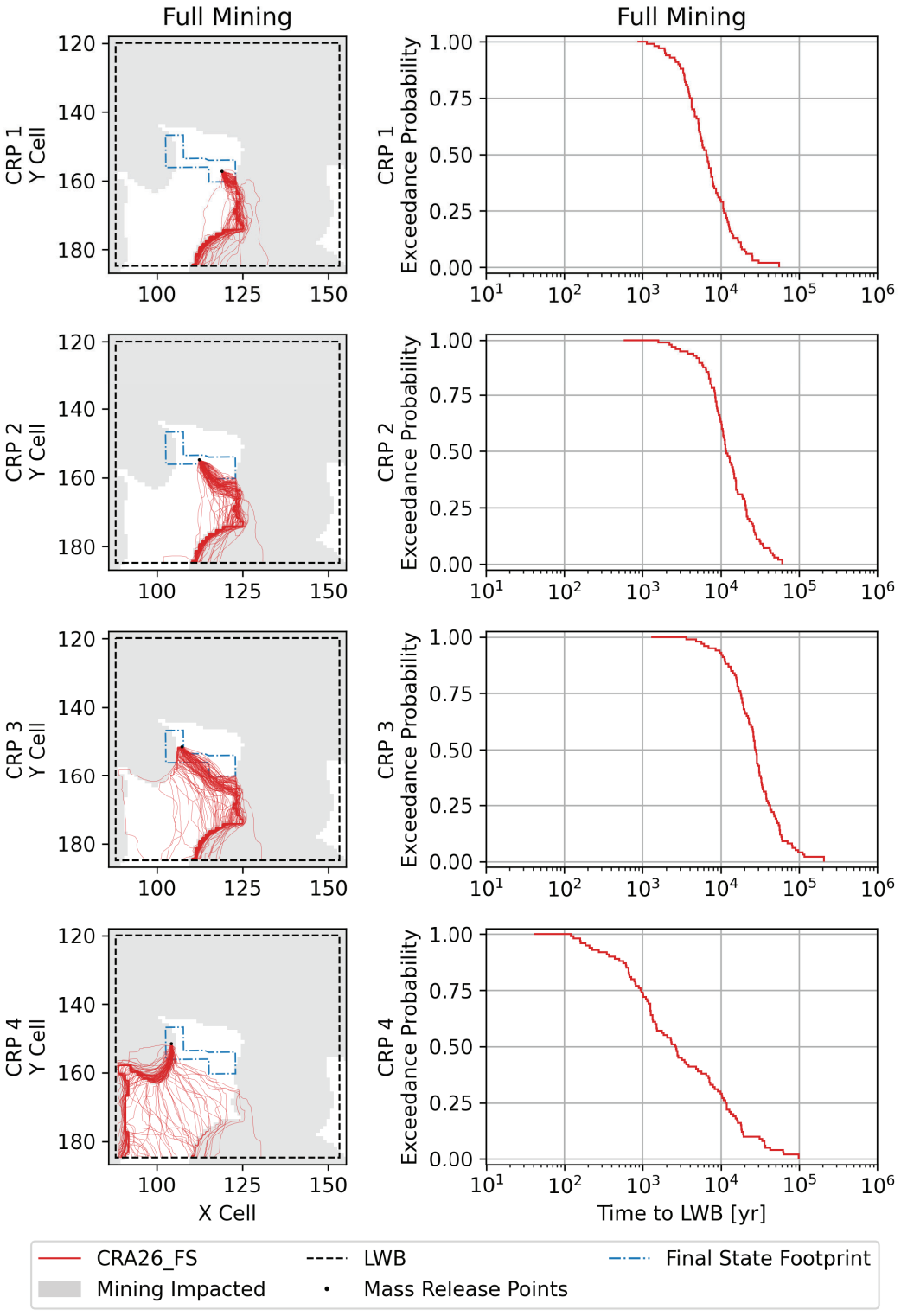


Figure 43. Particle Travel Paths and Travel Time to the LWB Exceedance Probabilities, Full Mining Scenario (Derived from Wilgus and Bethune 2025)

Information Only

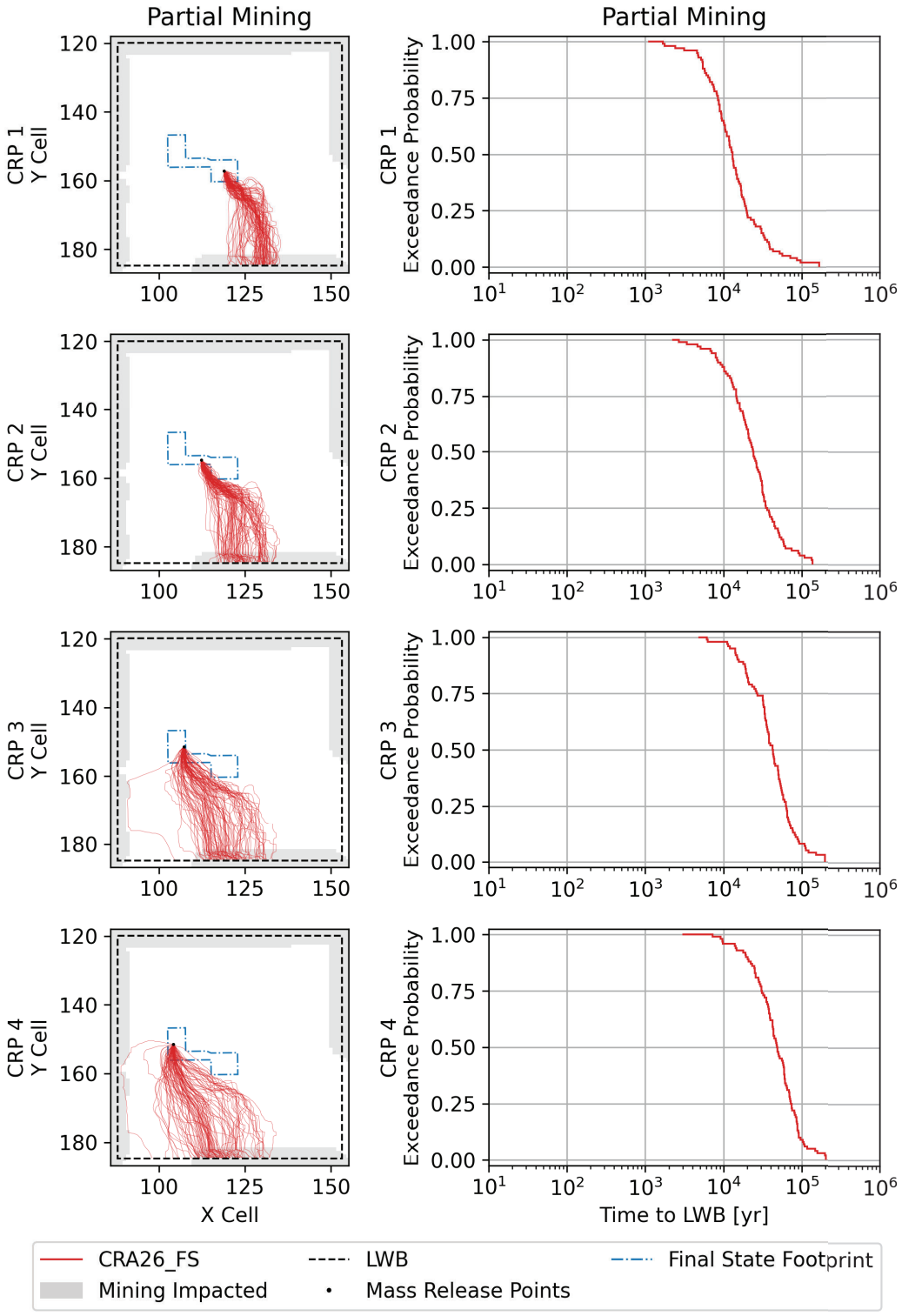


Figure 44. Particle Travel Paths and Travel Time to the LWB Exceedance Probabilities, Partial Mining Scenario (Derived from Wilgus and Bethune 2025)

Information Only

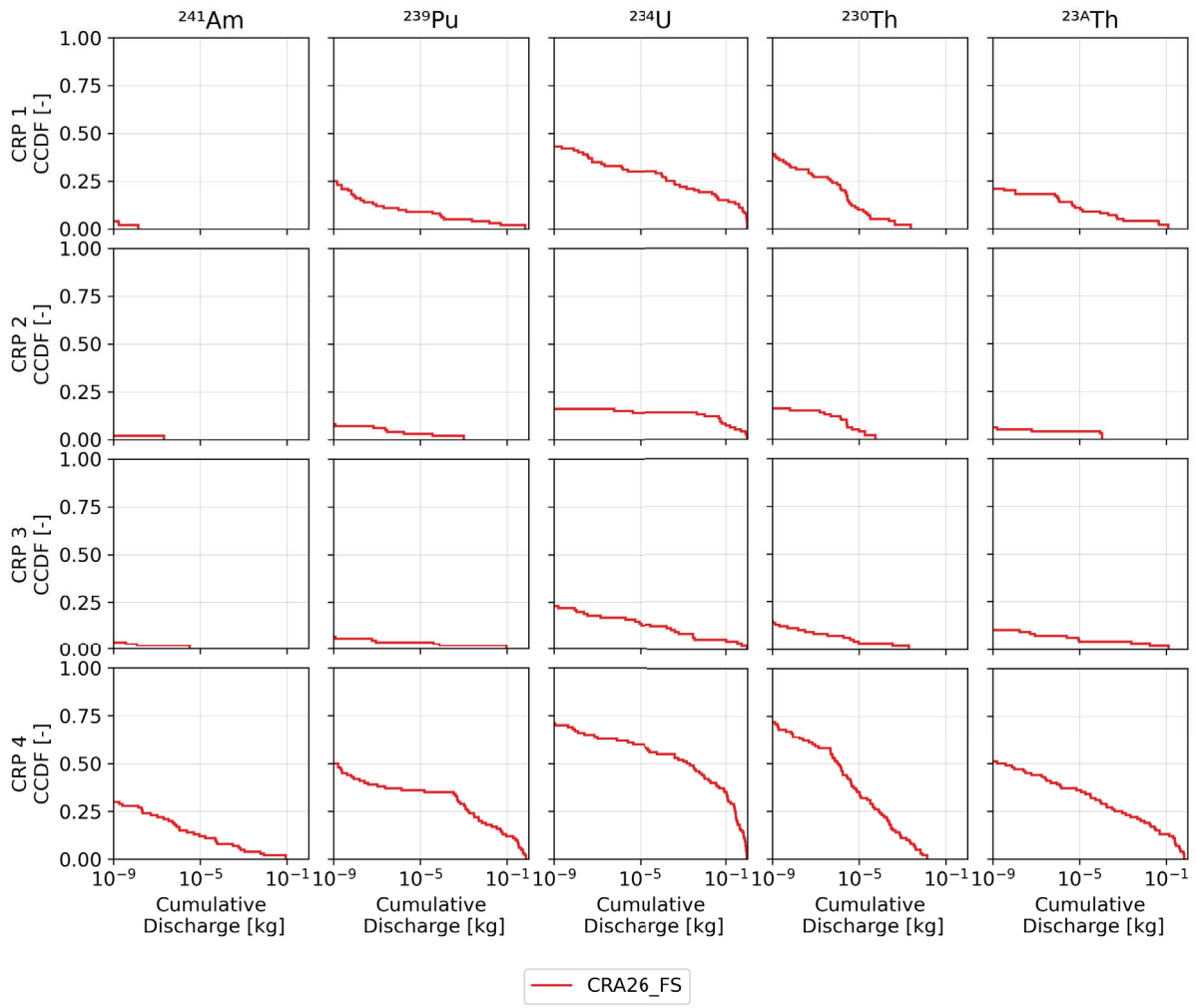


Figure 45. Exceedance Probability of Cumulative Mass to the LWB in 10,000 Years for Full Mining Scenario (Derived from Wilgus and Bethune 2025)

Information Only

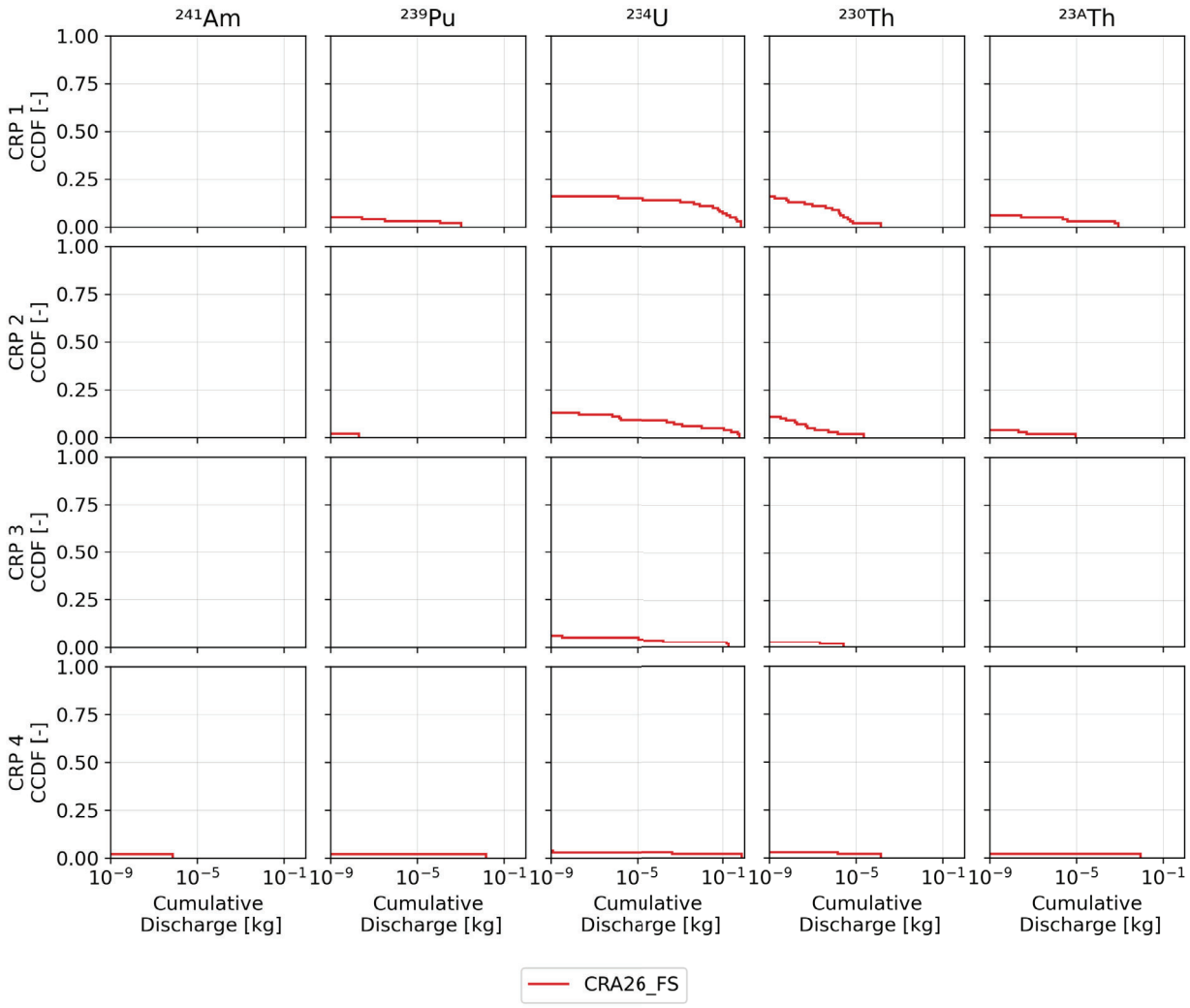


Figure 46. Exceedance Probability of Cumulative Mass to the LWB in 10,000 Years for Partial Mining Scenario (Derived from Wilgus and Bethune 2025)

4.8 Releases by Release Mechanism

This section presents releases for the undisturbed repository and each of the four disturbed repository release mechanisms (cuttings and cavings, spallings, DBRs, and long-term transport releases) that contribute to total releases. In the results that follow, the CCDFs of releases for each release pathway are compared to results from the CRA26_IS calculation. Sensitivities of total releases to uncertain parameters in the WIPP PA are also summarized. Changes included in the CRA26 FS that most substantially affect release results as compared to the CRA26_IS are:

- An increase in the repository footprint, which increases the number of intrusion events but decreases the fractional volume of repository occupied by waste.

Information Only

- A decrease in waste activity concentration, which leads to a decrease in activity of solids releases.
- An increase in brine saturation and brine pressures in the waste areas.

4.8.1 Undisturbed Repository Releases

The undisturbed repository performance scenario includes two potential release pathways: transport through the marker beds and transport up the shaft. Screening runs using a non-sorbing, highly soluble tracer determine which vectors have the potential to transport radionuclides to the accessible environment. Full Salado transport simulations are then performed for all screened-in vectors that have the potential to transport radionuclides to the accessible environment.

As in the RPPCR and CRA26_IS, no vectors in the CRA26_FS exceed the screening criterion for the undisturbed repository. Consequently, no vectors show radionuclide transport through the Salado to the LWB in the CRA26_FS. Similarly, no vectors show radionuclide transport through the shafts to the Culebra. These results demonstrate that radionuclide transport under undisturbed conditions is effectively zero, and no releases from the undisturbed repository are calculated for the CRA26_FS.

4.8.2 Cuttings and Cavings Releases

For each intrusion, cuttings and cavings releases are calculated from the cuttings volume, cavings volume, and radionuclide concentration of the intersected waste. Figure 47 shows the mean CCDFs of cuttings and cavings volume for Replicate 1.

While the cuttings and cavings results reported in Section 4.3 for individual boreholes in the CRA26_FS are unchanged from the CRA26_IS, the larger repository footprint results in a greater number of boreholes per future in the CRA26_FS compared to the CRA26_IS. Consequently, the cuttings and cavings volumes increased from the CRA26_IS to the CRA26_FS (Figure 47). However, the volumes represented in Figure 47 are excavated volumes rather than waste volumes.

The waste volume in cuttings and cavings releases is computed by multiplying the excavated volume by either FVW, which represents the fraction of the repository volume that contains contact-handled waste, or the parameter REFCON:FVRW (FVRW), which represents the fraction of the repository volume that contains remote-handled waste. A decrease in either FVW or FVRW causes a corresponding decrease in waste release volumes from each intrusion. Figure 48 shows the estimated cuttings and cavings excavated volumes for CRA26_IS and CRA26_FS, scaled by their respective values of FVW (0.279 for CRA26_IS and 0.186 for CRA26_FS). The reduction in FVW reduces the waste mass in the cuttings and cavings excavated volume, offsetting the increase in waste area footprint. Comparing Figure 47 and Figure 48 demonstrates the combined effect of the increased repository footprint and the reduction in value of FVW. Note that the CCDFGF code outputs a combined volume for releases of CH and RH waste, which has been scaled by the value of FVW in Figure 48 for comparison purposes only.

Figure 49 through Figure 51 show the CCDFs for cuttings and cavings releases for the CRA26_FS. Figure 52 presents the overall mean cuttings and cavings releases with the 95% confidence interval, and Table 17 provides the statistics for the overall mean cuttings and cavings releases.

Information Only

These results indicate that while the increased repository footprint increases the number of boreholes, the reduction in FVW mitigates to a large extent the impact on waste release volumes. However, the changes associated with the CRA26_FS impact the overall shape of the cuttings and cavings CCDF, particularly at higher probabilities (i.e., greater than 0.5) where releases are increased. The shelf-like plateau that occurs at higher probabilities is associated with the likelihood of at least one intrusion intersecting a surplus plutonium waste stream (SR-KAC-PuOx or SR-KAC-PuOx2). In the CRA26_FS inventory, these waste streams have a combined volume of 2,381.15 m³, or 1.413% of the total CH-waste volume (Van Soest 2025a). In the CRA26_IS inventory, these waste streams have a combined volume of 1,954.74 m³, or 1.251% of the total CH-waste inventory (Van Soest 2025b). The increase in the percentage of CH-waste volume associated with these waste streams, combined with the increased number of intrusions due to the larger repository footprint, raises the probability at which the plateau in the CCDF occurs. At probabilities less than about 0.2, the cuttings and cavings CCDF for the CRA26_FS shows lower releases than the CRA26_IS. The decreased releases in this region can be attributed to the decreased concentration (in EPA Units/m^3) of waste streams associated with the larger repository footprint.

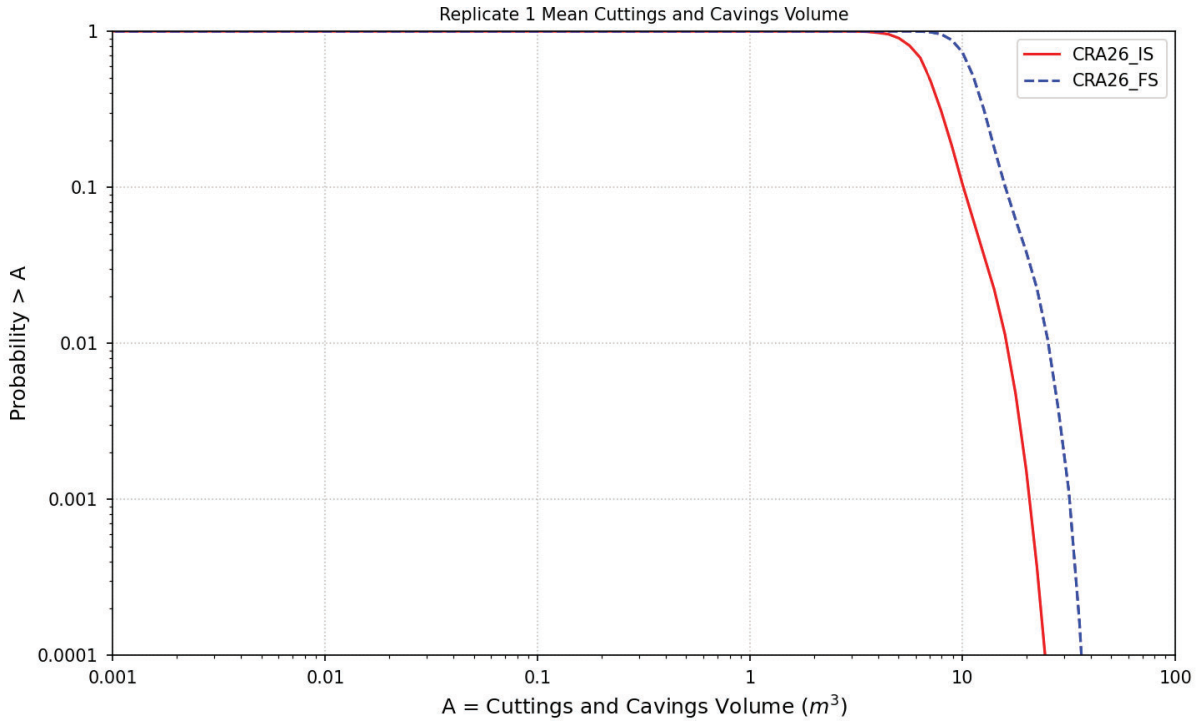


Figure 47. Mean Cuttings and Cavings Excavated Volume for Replicate 1

Information Only

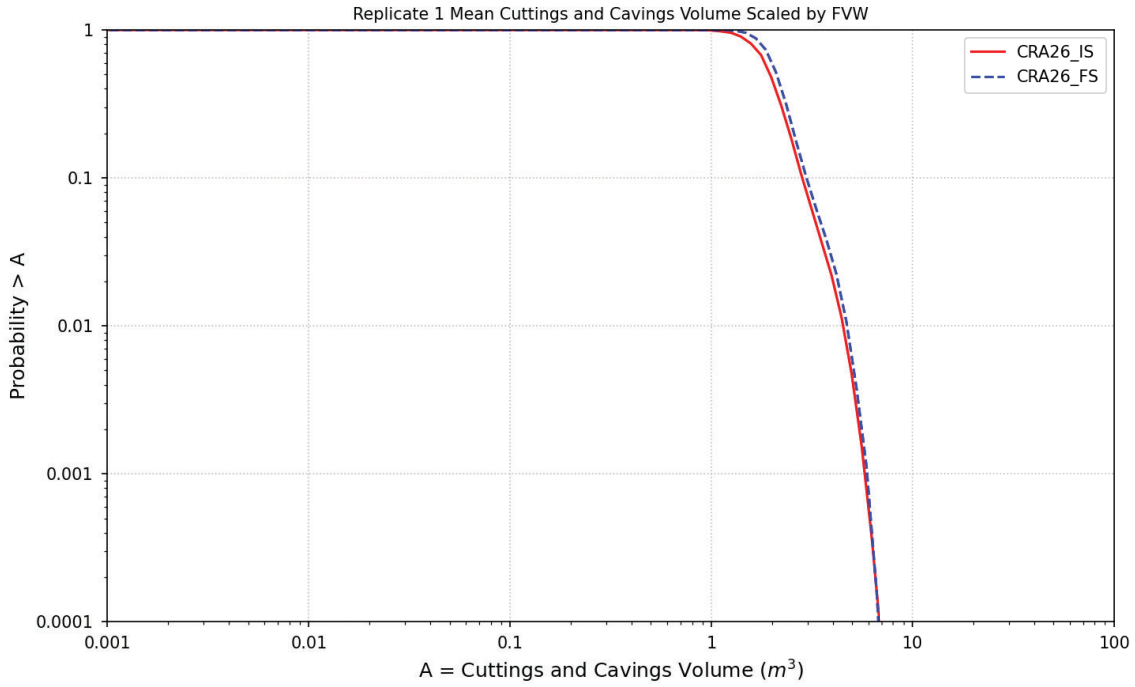


Figure 48. Mean Cuttings and Cavings Excavated Volume Scaled by the FVW Factor for Replicate 1

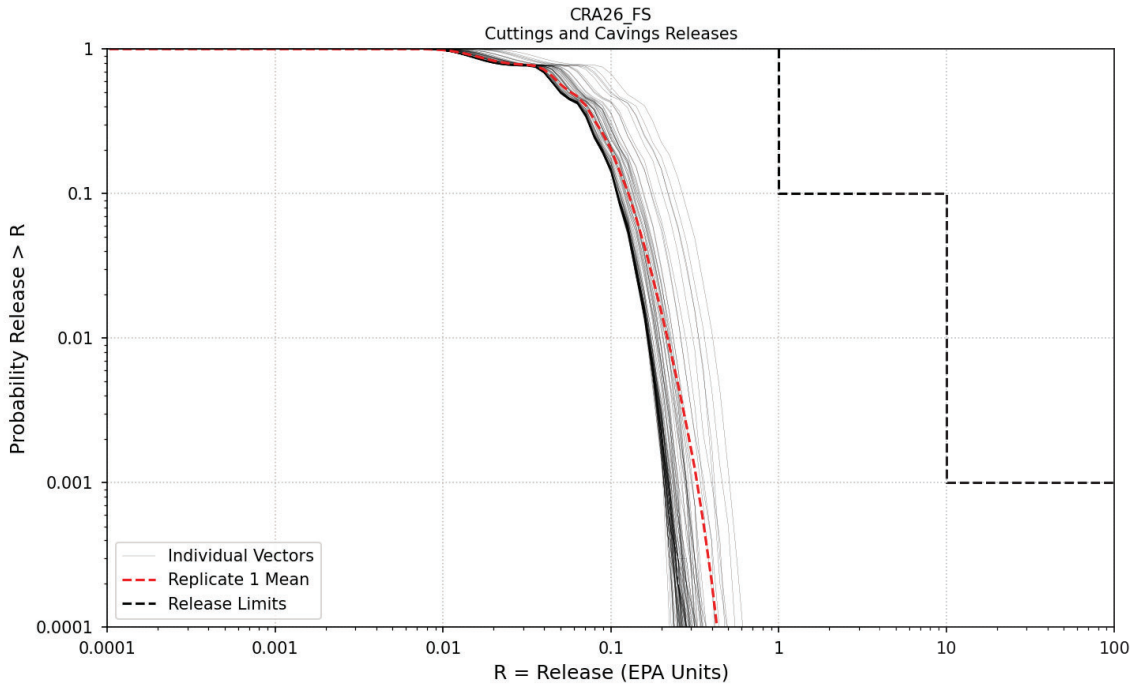


Figure 49. Cuttings and Cavings Releases for Replicate 1 of the CRA26_FS

Information Only

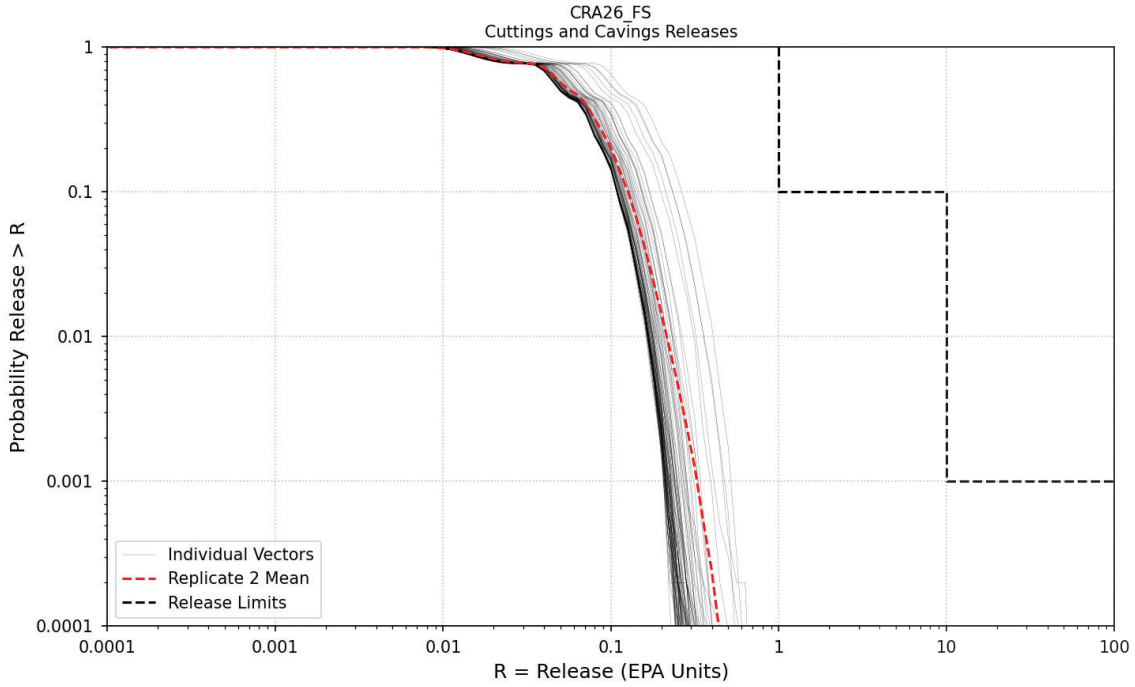


Figure 50. Cuttings and Cavings Releases for Replicate 2 of the CRA26_FS

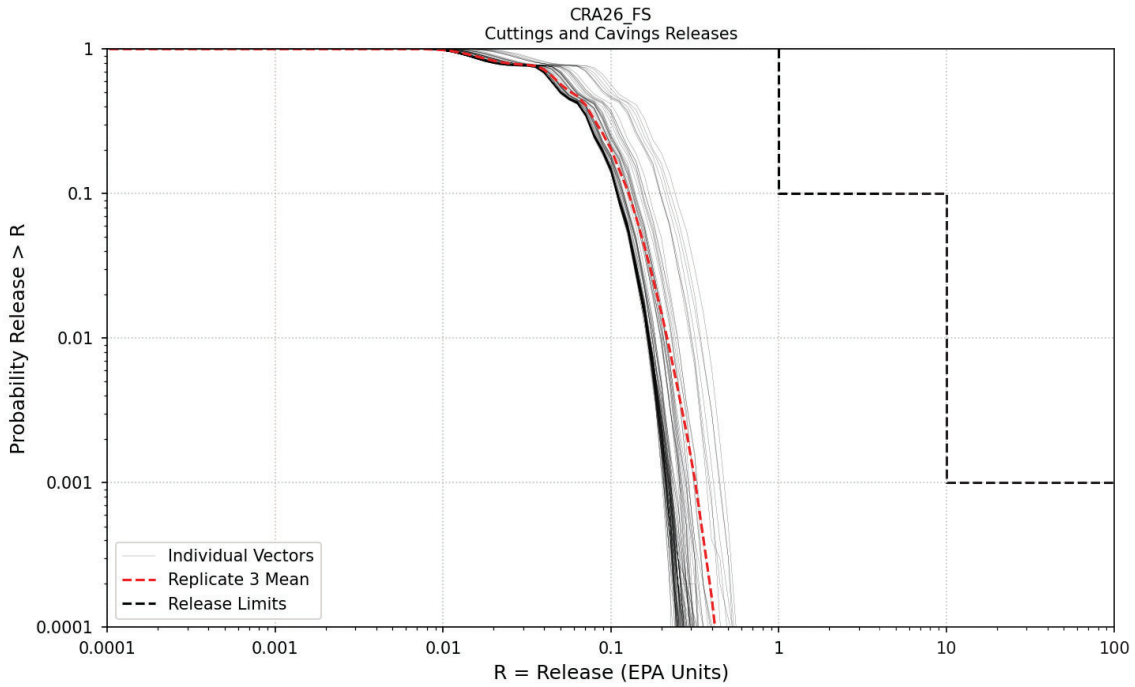


Figure 51. Cuttings and Cavings Releases for Replicate 3 of the CRA26_FS

Information Only

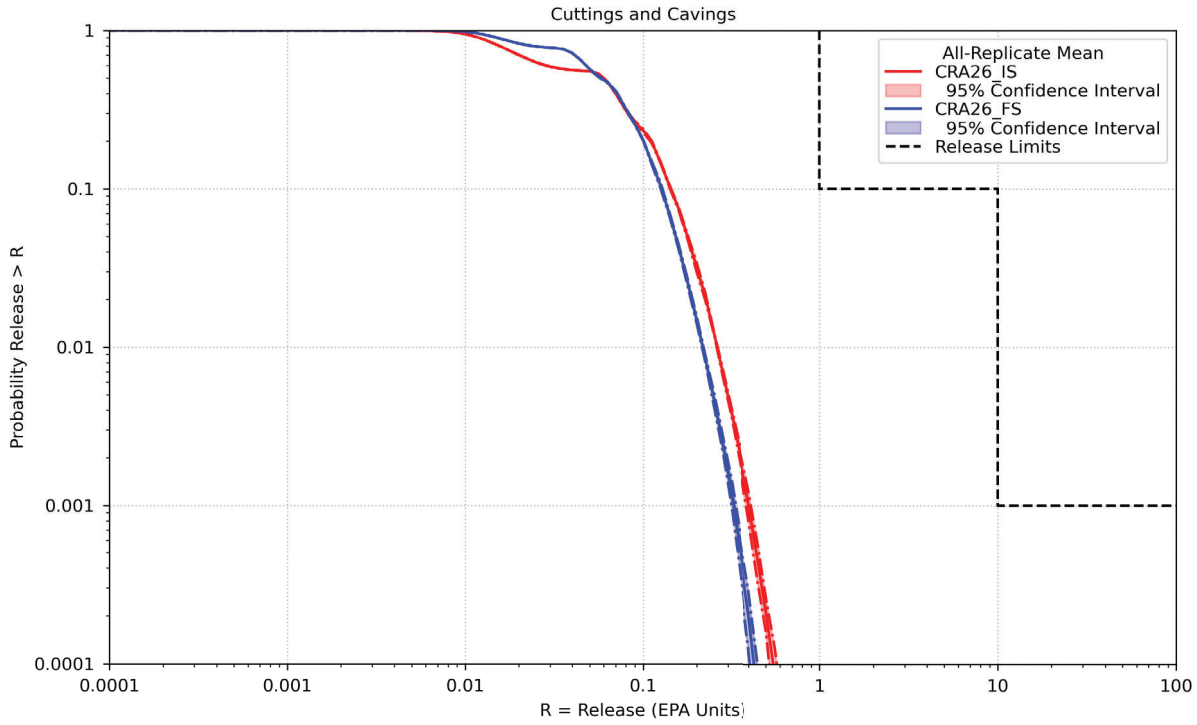


Figure 52. Overall Mean Cuttings and Cavings Releases

Table 17. Statistics on the Overall Mean for Cuttings and Cavings Releases

Analysis	P(R)>0.1 Lower CI (EPA Units)	P(R)>0.1 Mean (EPA Units)	P(R)>0.1 Upper CI (EPA Units)	P(R)>0.1 Release Limit (EPA Units)	P(R)>0.001 Lower CI (EPA Units)	P(R)>0.001 Mean (EPA Units)	P(R)>0.001 Upper CI (EPA Units)	P(R)>0.001 Release Limit (EPA Units)
CRA26_IS	0.1417	0.1429	0.1442	1	0.3898	0.4007	0.4164	10
CRA26_FS	0.1256	0.1273	0.1290	1	0.3149	0.3266	0.3367	10

4.8.3 Spallings Releases

Spallings releases are calculated based on spallings volumes and the average waste activity concentration in contact-handled waste. Spallings volumes from individual intrusions and the likelihood that an intrusion will result in spallings are largely unchanged between the CRA26_IS and CRA26_FS (see Section 4.3.2.1). Figure 53 shows an increase in mean spalled volume for CRA26_FS compared to CRA26_IS, which is attributed to the increased repository footprint of the CRA26_FS.

The volumes comprising spallings are scaled by FVW in Figure 54 to calculate the waste volume in spallings. Overall, the FVW-scaled spallings volumes are comparable to the CRA26_IS volumes (Figure 54), indicating that the reduction in FVW mitigates the impact of the increased

Information Only

repository footprint on waste release volumes. The increased spallings volumes shown in Figure 53 are offset by the decreased spallings radionuclide concentrations shown in Figure 33.

Figure 55 through Figure 57 show the CCDFs for spalling releases for each of the three replicates of CRA26_FS. Figure 58 presents the overall mean spallings releases with the 95% confidence interval for CRA26_IS and CRA26_FS. Table 18 provides the statistics for the overall mean spallings releases. The results demonstrate that spallings releases are similar between the CRA26_IS and CRA26_FS analyses, confirming that the increased repository footprint does not significantly affect spallings releases.

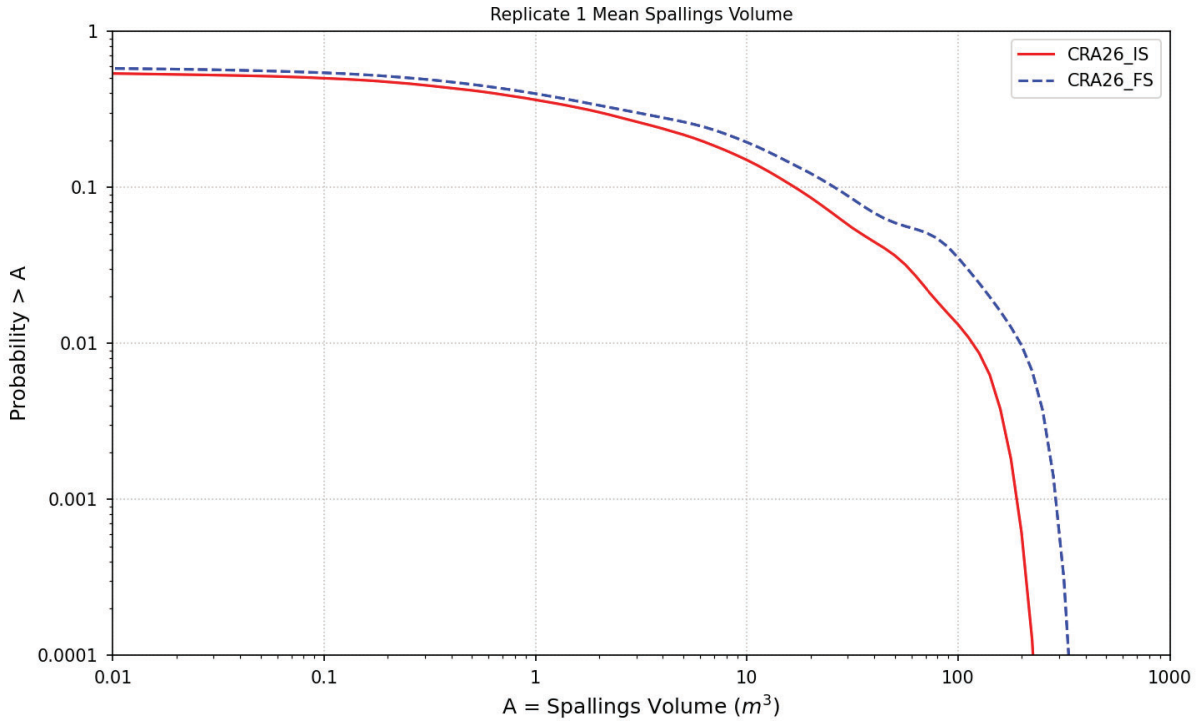


Figure 53. Mean Spallings Volume for Replicate 1

Information Only

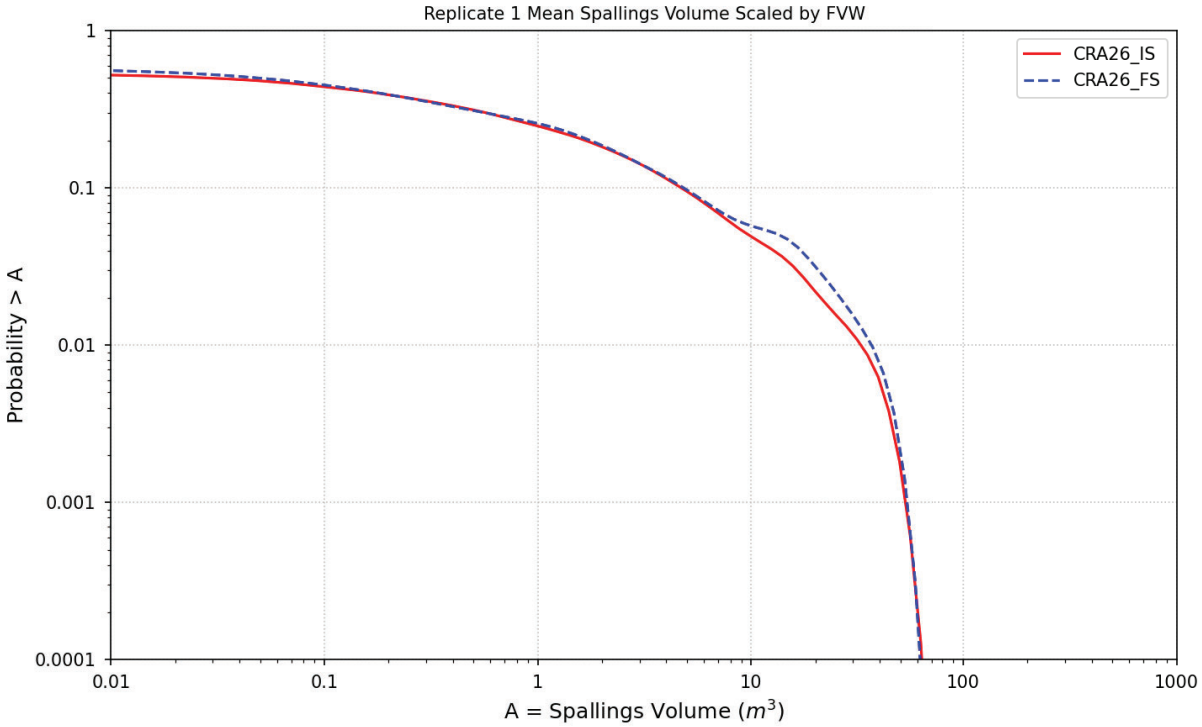


Figure 54. Mean Spallings Volume Scaled by the FVW Factor for Replicate 1

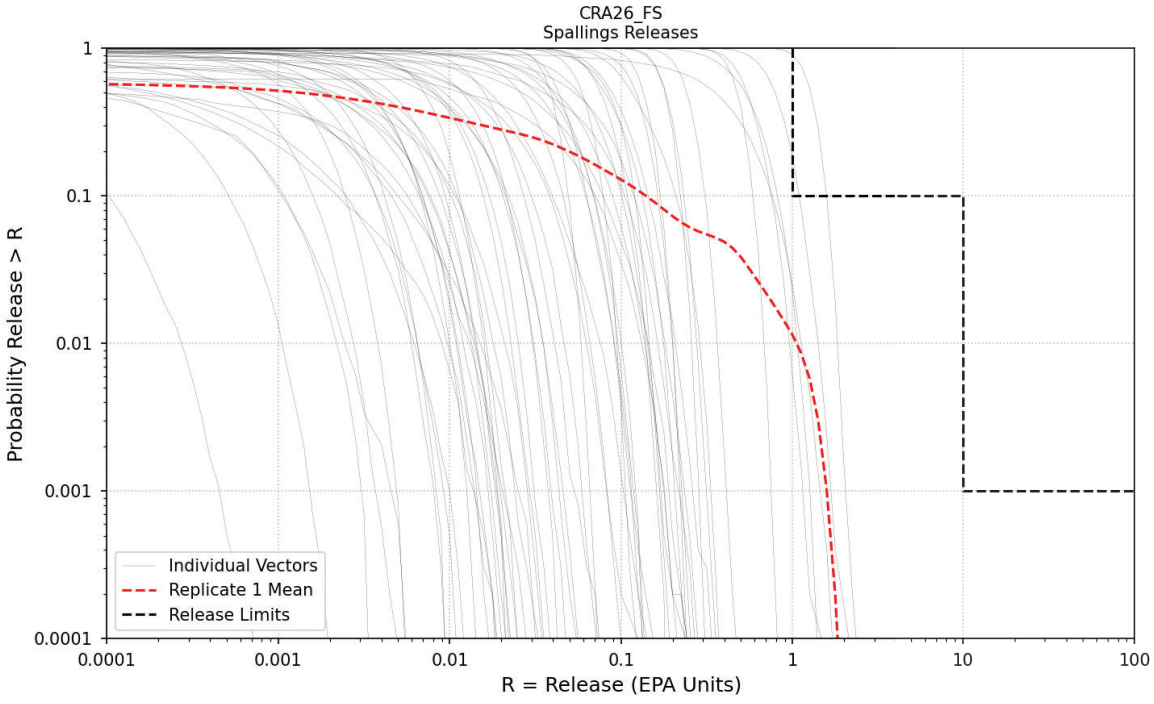


Figure 55. Spallings Releases for Replicate 1 of the CRA26_FS

Information Only

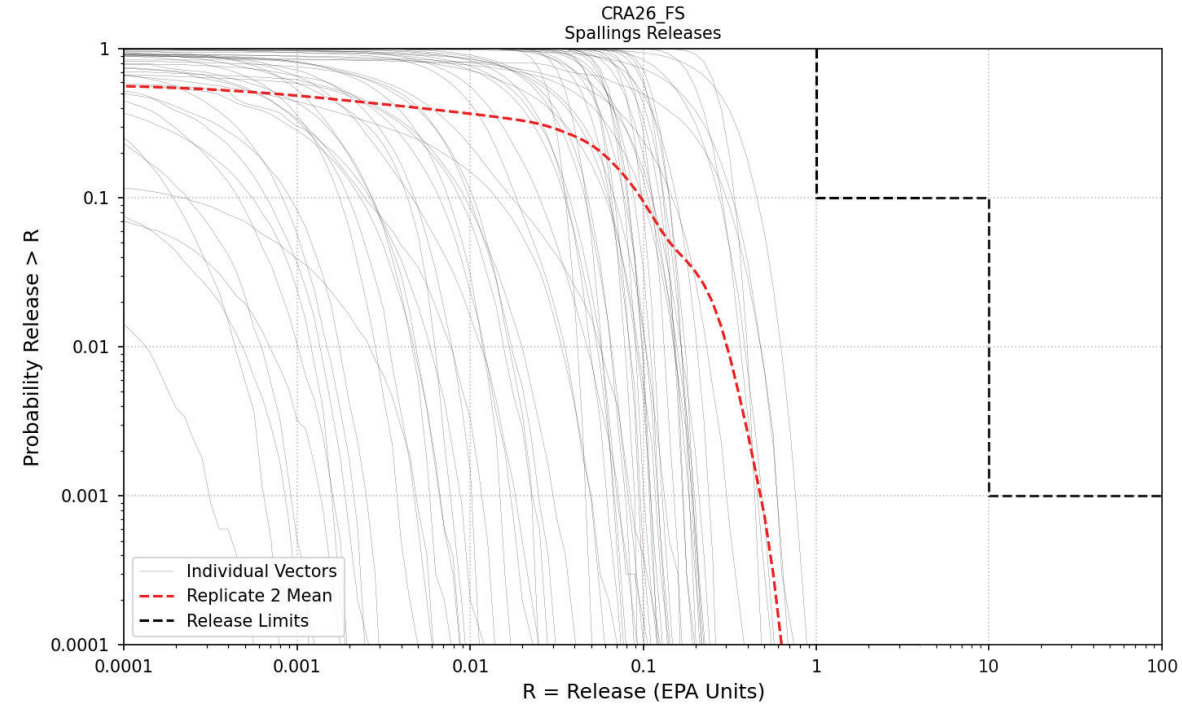


Figure 56. Spallings Releases for Replicate 2 of the CRA26_FS

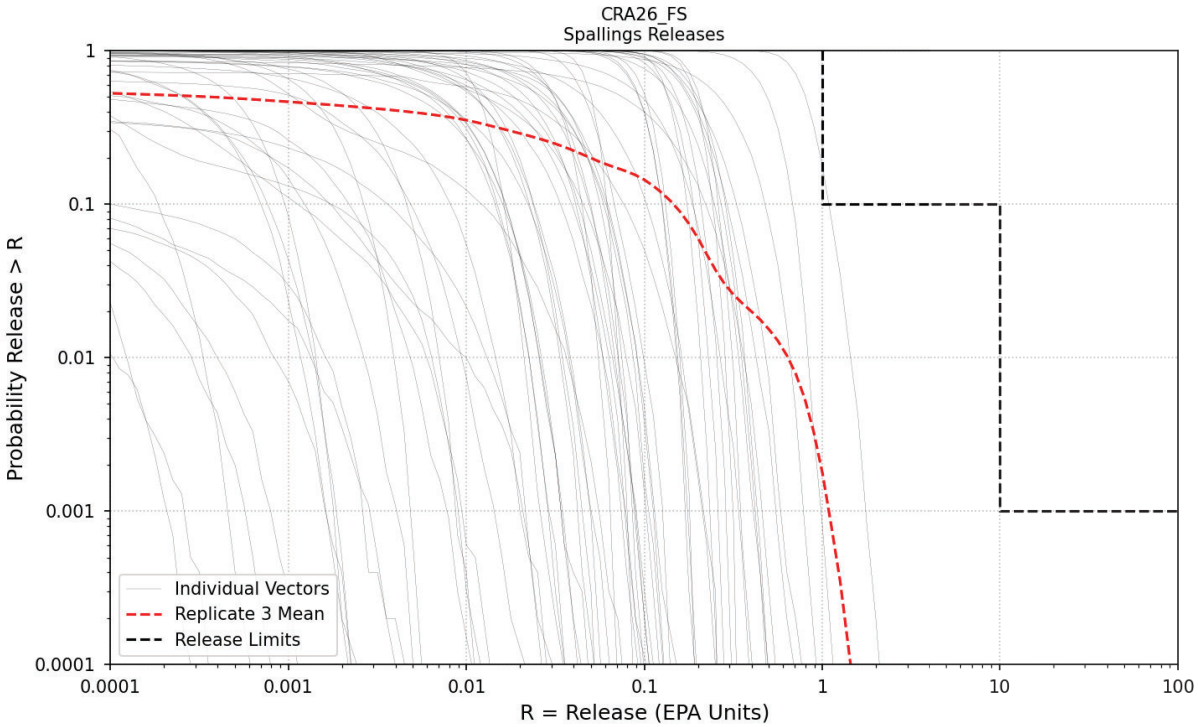


Figure 57. Spallings Releases for Replicate 3 of the CRA26_FS

Information Only

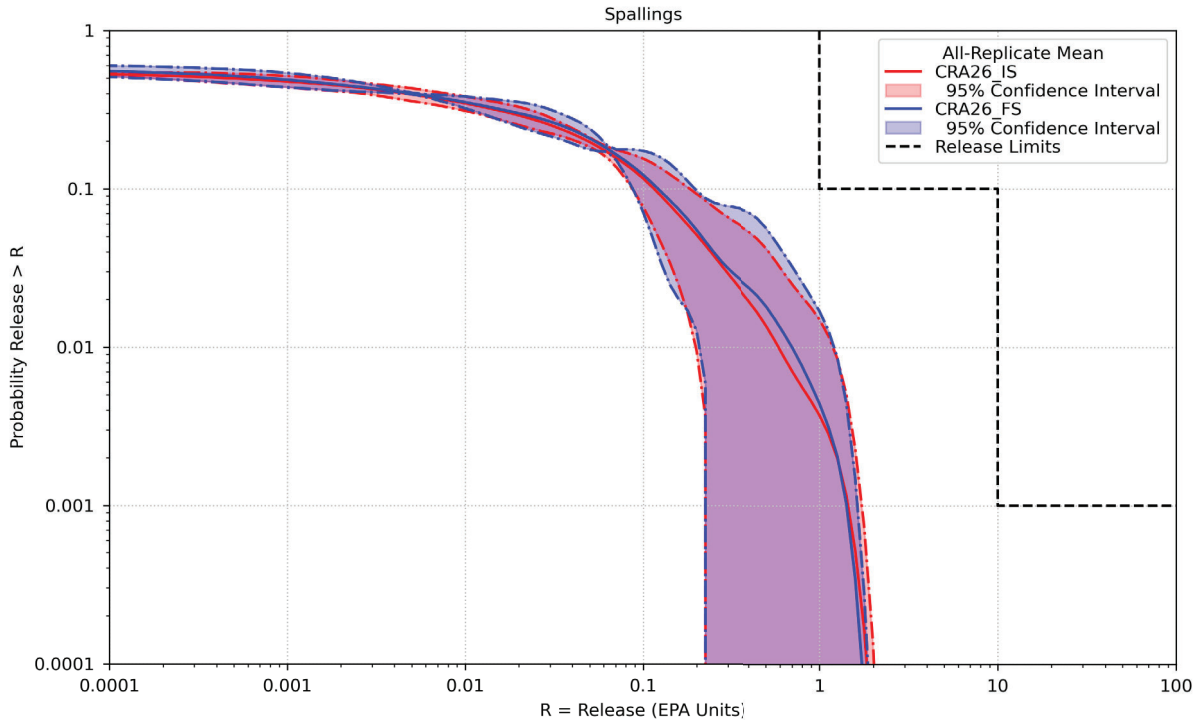


Figure 58. Overall Mean Spallings Releases

Table 18. Statistics on the Overall Mean for Spallings Releases

Analysis	P(R)>0.1 Lower CI (EPA Units)	P(R)>0.1 Mean (EPA Units)	P(R)>0.1 Upper CI (EPA Units)	P(R)>0.1 Release Limit (EPA Units)	P(R)>0.001 Lower CI (EPA Units)	P(R)>0.001 Mean (EPA Units)	P(R)>0.001 Upper CI (EPA Units)	P(R)>0.001 Release Limit (EPA Units)
CRA26_IS	0.0871	0.1153	0.1833	1	0.2389	1.4579	1.7470	10
CRA26_FS	0.0876	0.1217	0.1957	1	0.2395	1.4223	1.6650	10

4.8.4 Direct Brine Releases

Direct brine releases (DBRs) occur when brine migrates up through an intruding borehole under conditions of sufficient brine pressure and saturation. Mean DBR volumes for Replicate 1 are shown in Figure 59. The mean DBR volume is increased due to 1) the increased repository footprint leading to an increased number of intrusions in CRA26_FS; and 2) the increased DBR volumes due to increased brine saturations and brine pressures (Section 4.4).

The CCDFs for DBRs include contributions from DBR volumes (generally increased for the CRA26_FS) and mobilized radionuclide concentrations (generally decreased for the CRA26_FS). Figure 60, Figure 61, and Figure 62 show CCDFs of DBRs for Replicate 1, 2, and 3 respectively. Figure 63 shows the overall mean CCDFs with the 95% confidence intervals. Table 19 gives statistics for the overall mean direct brine release. At most probabilities, mean DBRs are increased for the CRA26_FS, while only at the very lowest probabilities (i.e., less than about 0.003), mean

Information Only

DBRs are decreased. The mixed impact is due to the mixed impacts of DBR volumes and mobilized radionuclide concentrations across the vectors and replicates.

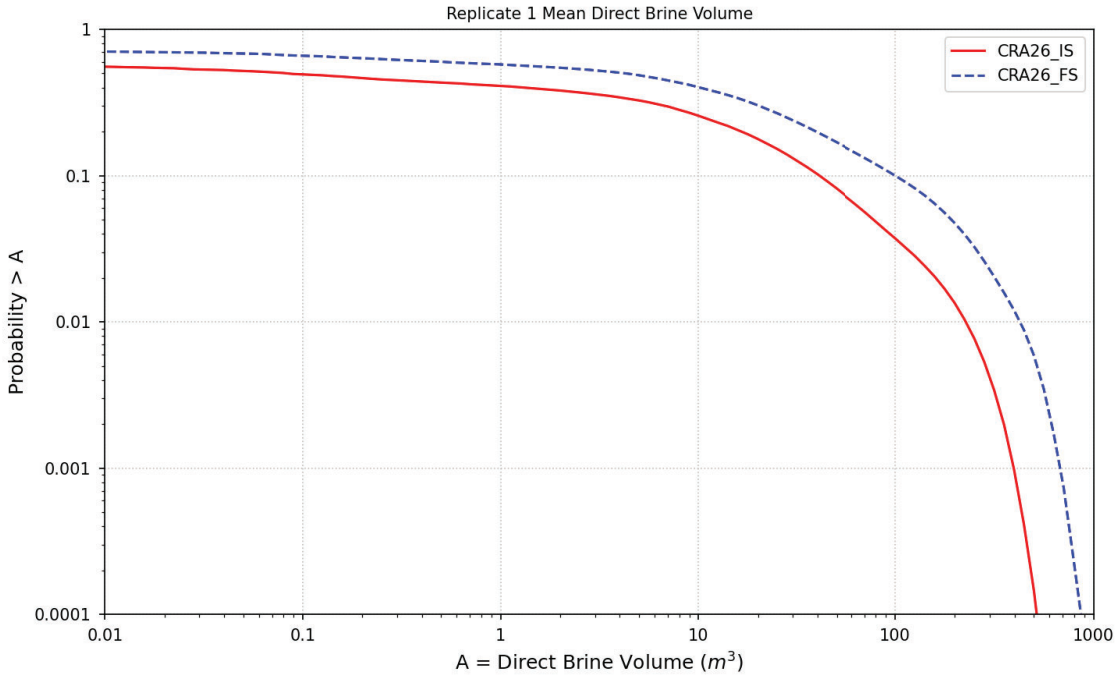


Figure 59. Mean Direct Brine Volume for Replicate 1

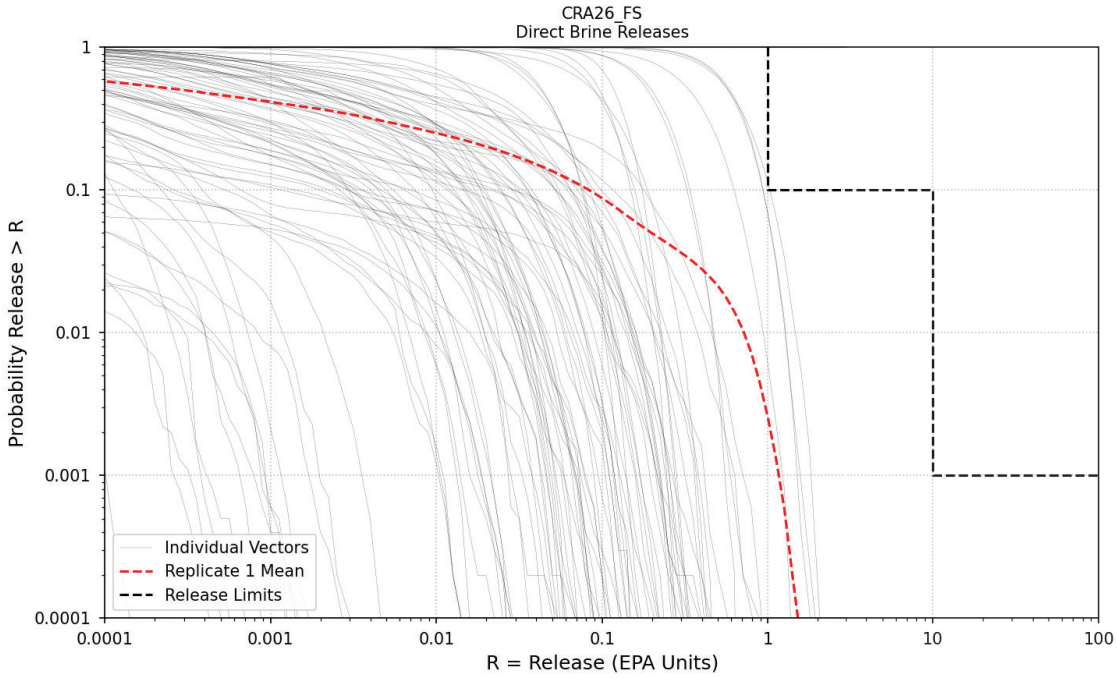


Figure 60. Direct Brine Releases for Replicate 1 of the CRA26_FS

Information Only

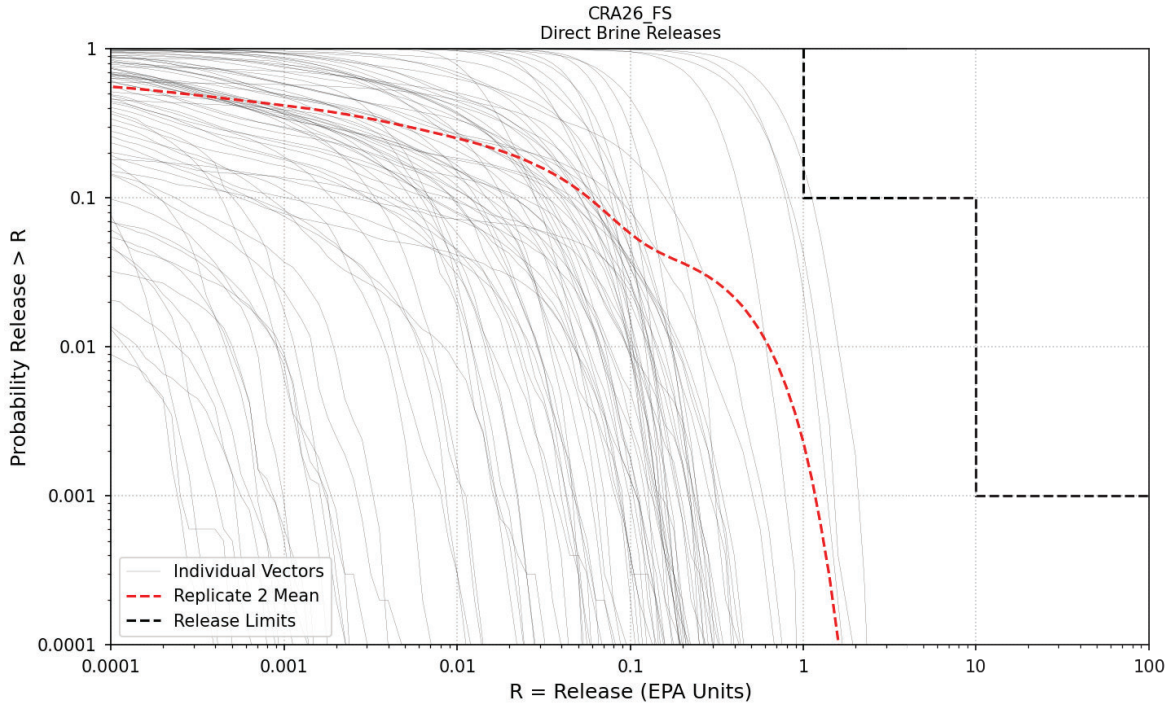


Figure 61. Direct Brine Releases for Replicate 2 of the CRA26_FS

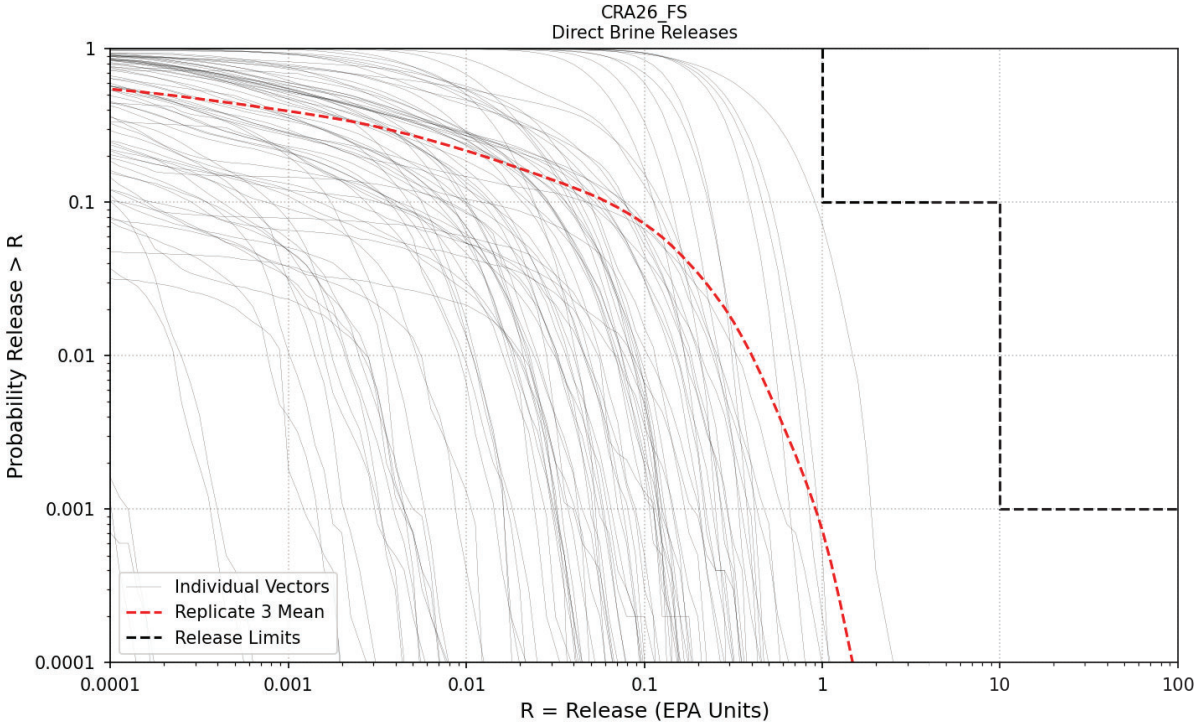


Figure 62. Direct Brine Releases for Replicate 3 of the CRA26_FS

Information Only

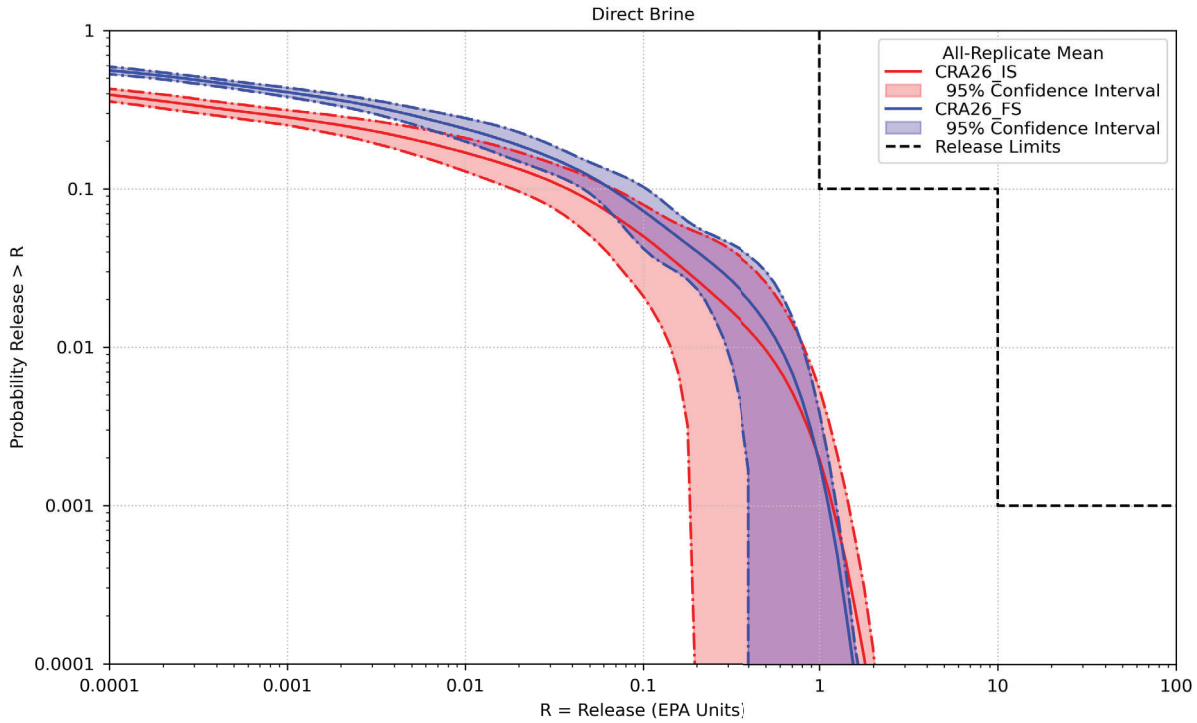


Figure 63. Overall Mean Direct Brine Releases

Table 19. Statistics on the Overall Mean for Direct Brine Releases

Analysis	P(R)>0.1 Lower CI (EPA Units)	P(R)>0.1 Mean (EPA Units)	P(R)>0.1 Upper CI (EPA Units)	P(R)>0.1 Release Limit (EPA Units)	P(R)>0.001 Lower CI (EPA Units)	P(R)>0.001 Mean (EPA Units)	P(R)>0.001 Upper CI (EPA Units)	P(R)>0.001 Release Limit (EPA Units)
CRA26_IS	0.0184	0.0376	0.0685	1	0.1929	1.1927	1.4710	10
CRA26_FS	0.0460	0.0661	0.1043	1	0.4144	1.1237	1.2483	10

4.8.5 Long-Term Radionuclide Transport

Activity entering the Culebra represents the radionuclide source term for transport through the Culebra Dolomite Member of the Rustler Formation. This activity is calculated based on brine flow through boreholes intersecting waste panels and is influenced by repository configuration, brine pressure, and radionuclide mobilization mechanisms. The CCDFs of long-term radionuclide transport releases are calculated via a convolution of the cumulative radionuclide discharges to the Culebra (Section 4.6) and the results of the Culebra radionuclide transport calculations (Section 4.7).

This section first presents CCDFs of radionuclide activity entering the Culebra (i.e., *to the Culebra*), which are not considered releases in terms of regulatory compliance. These results provide insight into the radionuclide transport behavior within the repository system. Following this, CCDFs of releases exiting the land withdrawal boundary (LWB) within the Culebra are presented, which represent the long-term radionuclide transport releases relevant to regulatory compliance.

Information Only

4.8.5.1 Activity Entering the Culebra

Figure 64 shows the mean radionuclide activity entering the Culebra by lumped radionuclide for Replicate 1 of the CRA26_FS. In Figure 64 it can be observed that ^{241}Am dominates the activity entering the Culebra, followed by ^{239}Pu, while ^{230}Th and ^{234}U are minor contributors to the total activity entering the Culebra.

Figure 65 shows the overall mean total activity entering the Culebra with the 95% confidence interval. Table 20 gives the statistics on the overall mean activity entering the Culebra. As the activity entering the Culebra is not a release, there are no release limits associated with Figure 65 or Table 20. At all probabilities, mean releases to the Culebra are increased for the CRA26_FS. The observed increase can be attributed to the increase in number of intrusions due to the increased repository footprint, despite lower radionuclide concentration limits (Section 4.5).

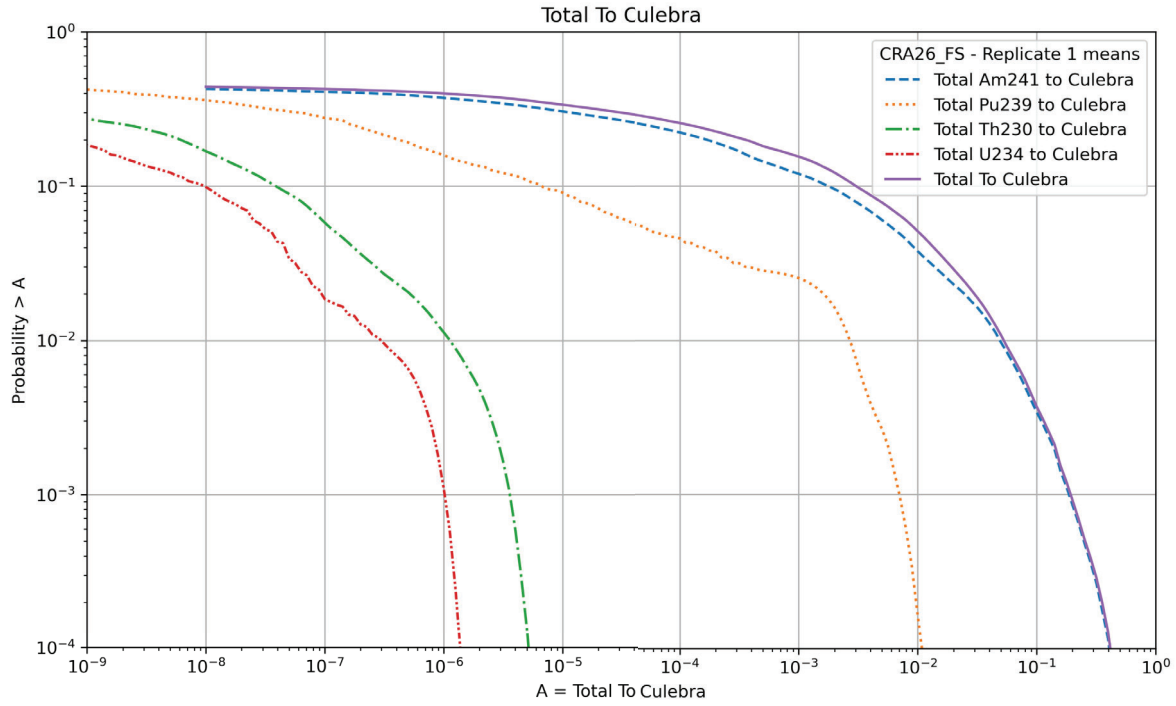


Figure 64. Mean Activity Entering the Culebra by Radionuclide for Replicate 1 of the CRA26_FS

Information Only

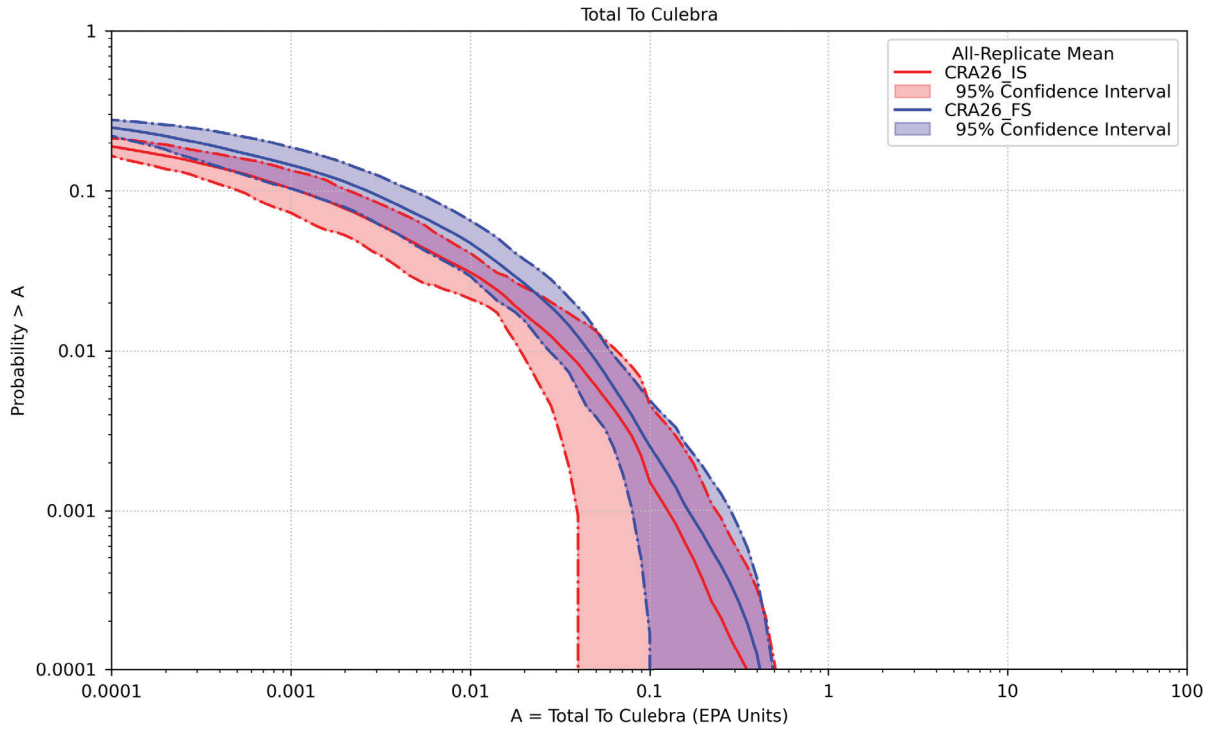


Figure 65. Overall Mean Radionuclide Activity Entering the Culebra

Table 20. Statistics on the Overall Mean for Radionuclide Activity Entering the Culebra

Analysis	P(R)>0.1 Lower CI (EPA Units)	P(R)>0.1 Mean (EPA Units)	P(R)>0.1 Upper CI (EPA Units)	P(R)>0.001 Lower CI (EPA Units)	P(R)>0.001 Mean (EPA Units)	P(R)>0.001 Upper CI (EPA Units)
CRA26_IS	0.0005	0.0011	0.0021	0.0395	0.1263	0.2359
CRA26_FS	0.0011	0.0027	0.0048	0.0800	0.1649	0.2843

4.8.5.2 Releases Through the Culebra

Releases through the Culebra represent radionuclide activity transported from the Culebra Dolomite Member to the accessible environment. These releases are calculated based on radionuclide transport modeling and are influenced by the activity entering the Culebra, transmissivity fields, and radionuclide decay and sorption processes.

Figure 66, Figure 67, and Figure 68 show CCDFs of releases through Culebra for Replicates 1, 2, and 3, respectively. The x-axis in these plots has been extended to lower releases than other CCDF plots due to the relatively smaller releases from long-term transport through the Culebra.

Figure 69 show the mean releases through the Culebra by radionuclide and release point for Replicate 1 of the CRA26_FS. In this plot, it can be observed that radionuclides from CRP 4

Information Only

(Panels 15, 16, 17, and 18) are several orders of magnitude higher than releases from the other Culebra Release Points. Releases from CRP 4 are dominated by ^{241}Am and ^{239}Pu, similar to the activity entering the Culebra (Figure 65). In contrast, releases from CRP 1 and CRP 2 are dominated by ^{234}U, while releases from CRP 3 have nearly equal contributions from ^{234}U, ^{241}Am, and ^{239}Pu.

This behavior is attributed to the faster transport of ^{234}U in the +VI oxidation state, which has a partition coefficient (Kd) value 1 to 2 orders of magnitude lower than that of the other radionuclides, making ^{234}U more mobile in the Culebra. For CRP 1 and CRP 2, ^{234}U longer half-life compared to ^{241}Am helps ensure its activity remains significant over longer travel times, allowing it to dominate releases. For CRP 4, the shorter travel times reduce the impact of uranium's faster transport, and the significantly higher activity of ^{241}Am and ^{239}Pu entering the Culebra leads to their dominance in releases from CRP 4.

Figure 70 shows the overall mean releases through the Culebra with the 95% confidence interval. The overall mean releases for the CRA26_IS is not visible in Figure 70 due to the releases being below the x-axis scale. Table 21 gives the statistics on the overall mean releases through the Culebra. Releases through the Culebra for the CRA26_FS are still very small compared to the other release mechanisms. These releases are increased compared to the CRA26_IS due to: 1) the increased number of release points (i.e., CRP 3 and 4); 2) the shorter particle travel times to the LWB associated with CRP 4; and 3) the increased releases of radionuclides to the Culebra.

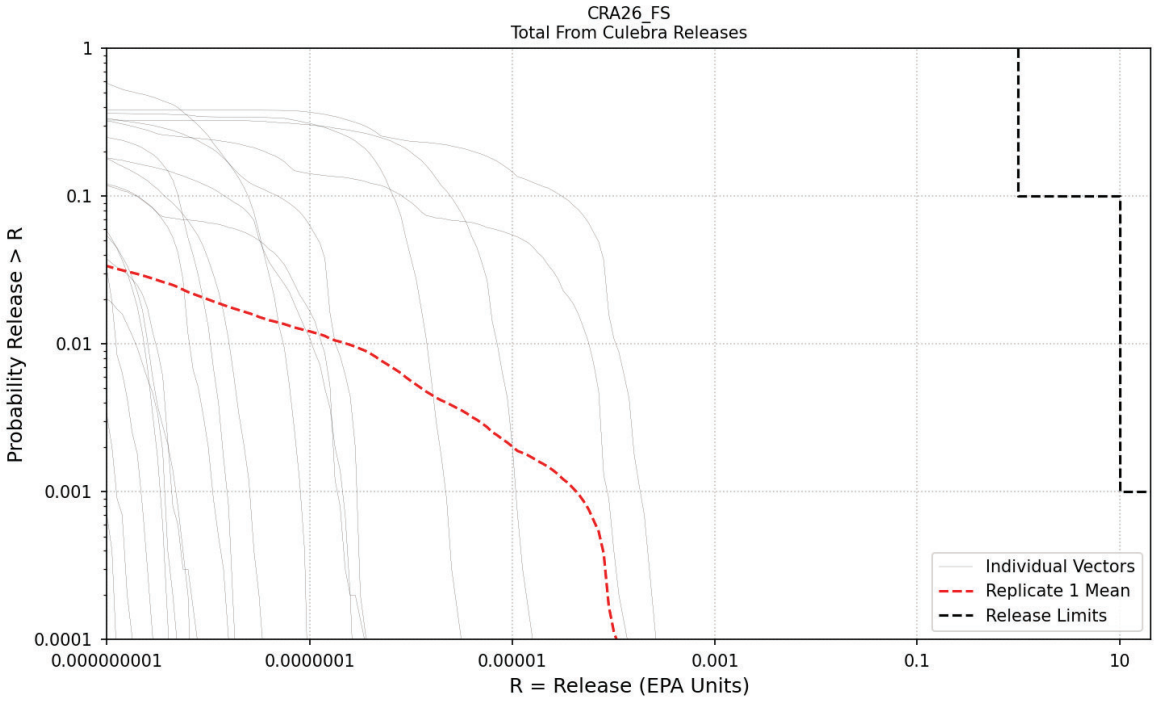


Figure 66. Releases Through the Culebra for Replicate 1 of the CRA26_FS

Information Only

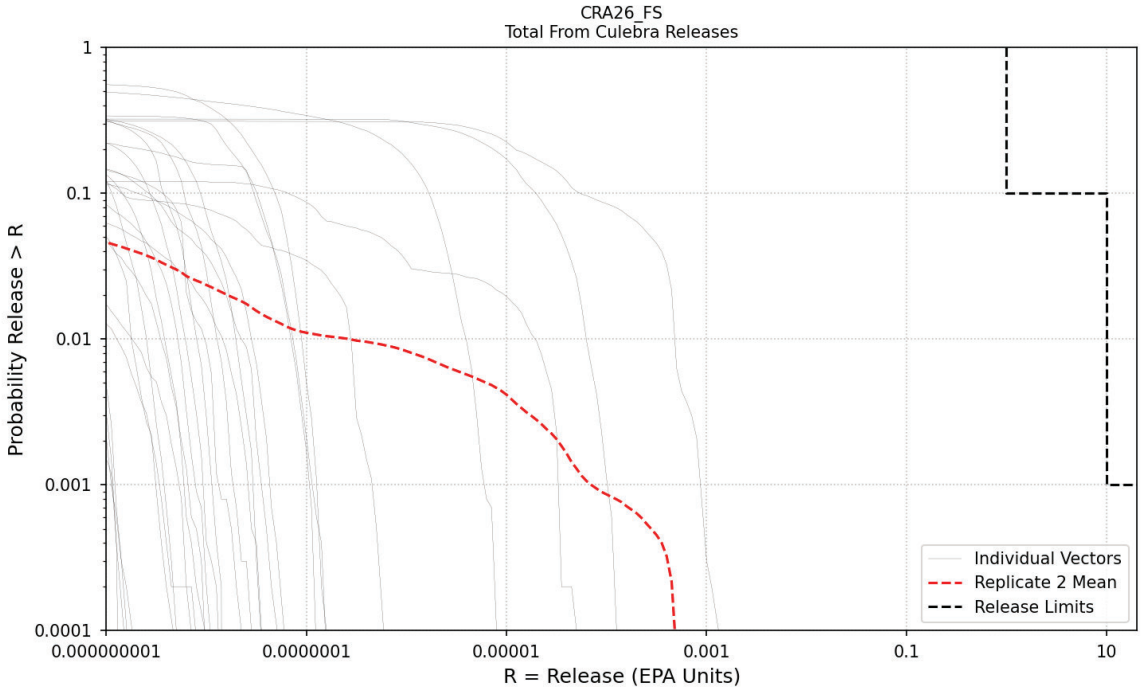


Figure 67. Releases Through the Culebra for Replicate 2 of the CRA26_FS

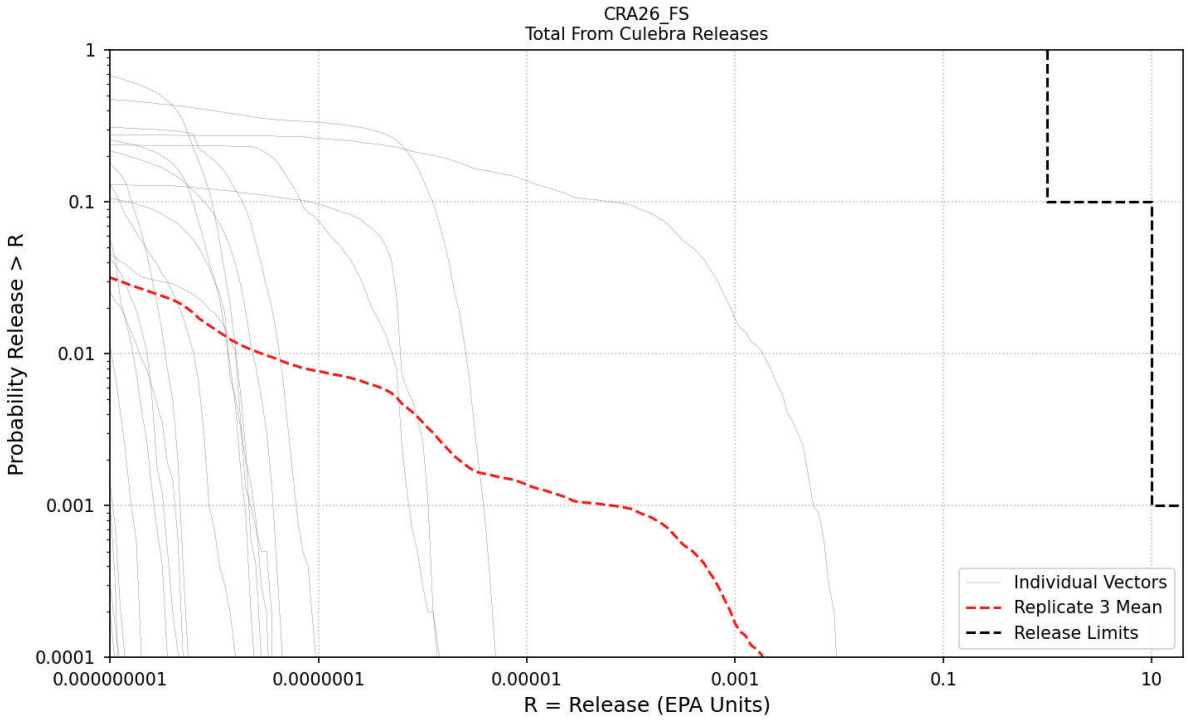


Figure 68. Releases Through the Culebra for Replicate 3 of the CRA26_FS

Information Only

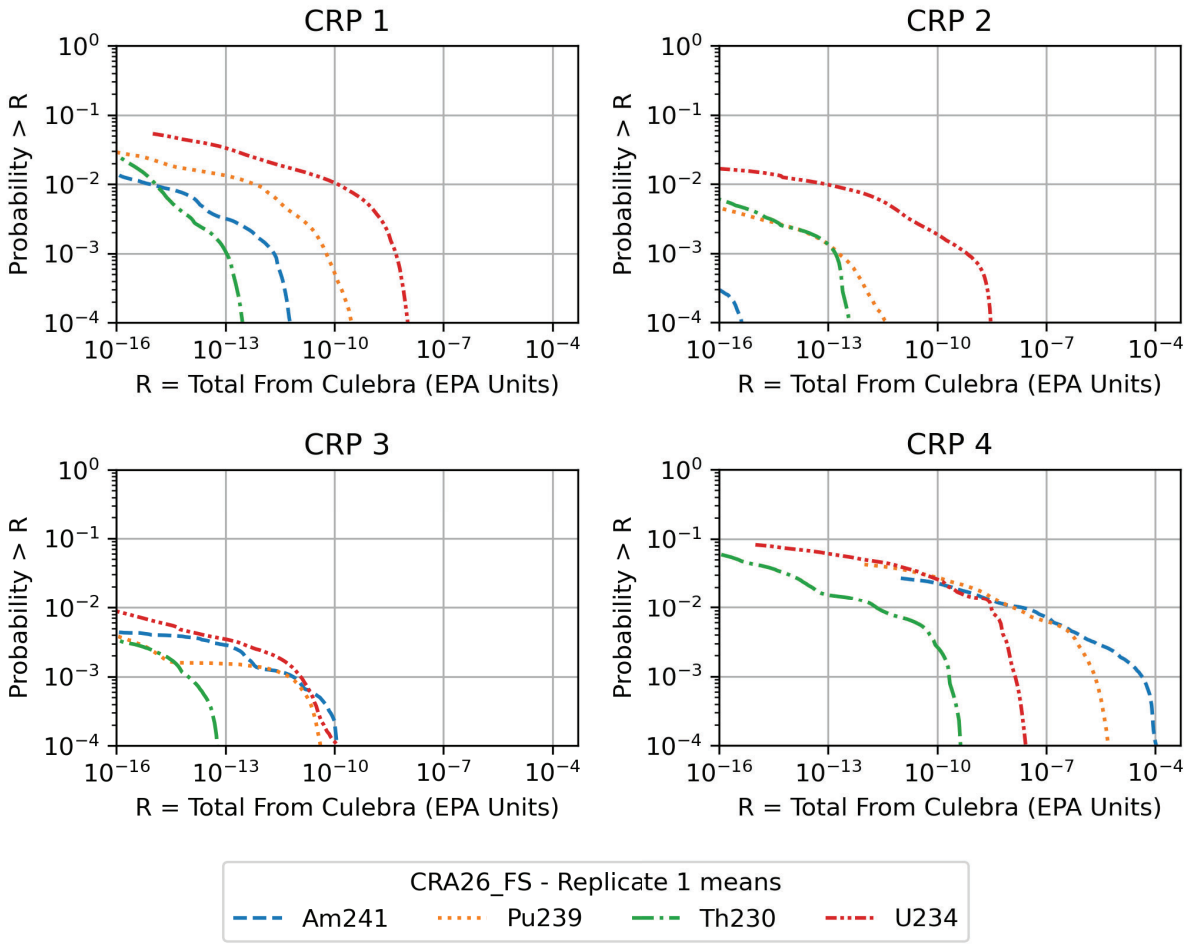


Figure 69. Mean Replicate 1 Releases Through the Culebra by Radionuclide and Release Point

Information Only

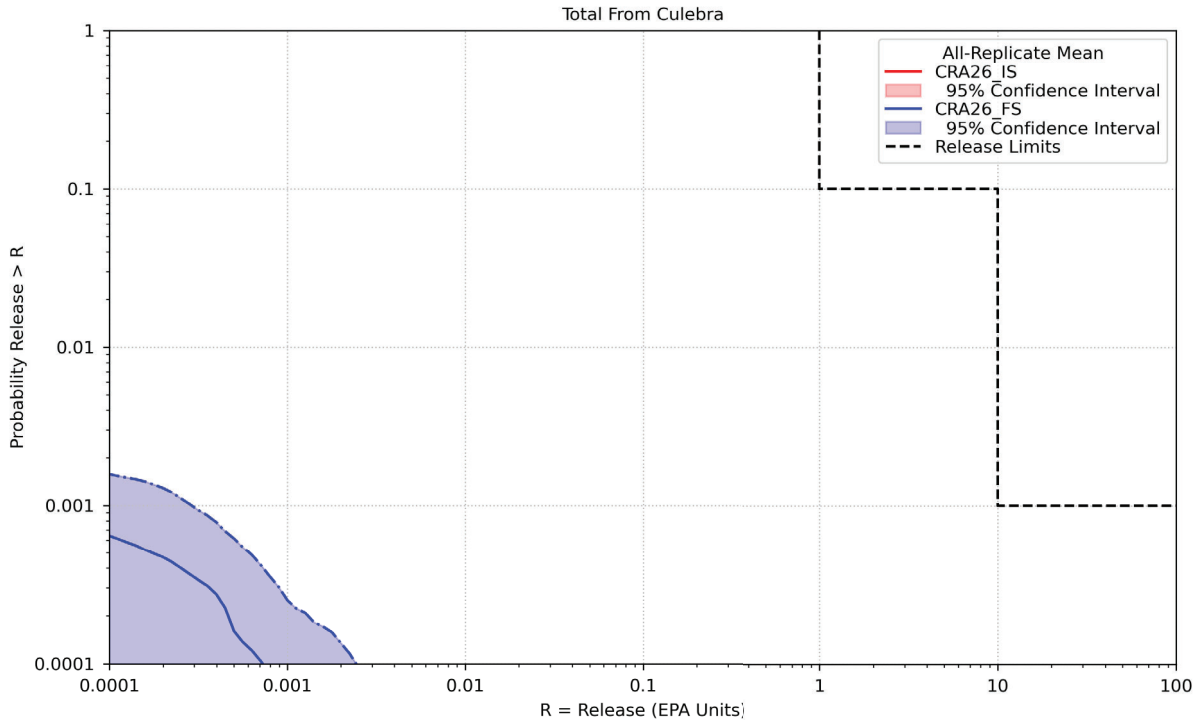


Figure 70. Overall Mean Releases Through the Culebra

Table 21. Statistics on the Overall Mean for Releases Through the Culebra

Analysis	P(R)>0.1 Lower CI (EPA Units)	P(R)>0.1 Mean (EPA Units)	P(R)>0.1 Upper CI (EPA Units)	P(R)>0.1 Release Limit (EPA Units)	P(R)>0.001 Lower CI (EPA Units)	P(R)>0.001 Mean (EPA Units)	P(R)>0.001 Upper CI (EPA Units)	P(R)>0.001 Release Limit (EPA Units)
CRA26_IS	0.0000	0.0000	0.0000	1	0.0000	0.0000	0.0000	10
CRA26_FS	0.0000	0.0000	0.0000	1	0.0000	0.0001	0.0003	10

4.9 Total Releases

Total releases represent the combined radionuclide releases from all release pathways, including cuttings and cavings, spallings, direct brine releases, and releases through the Culebra. Figure 71, Figure 72, and Figure 73 show CCDFs of total releases for Replicate 1, 2, and 3, respectively. While several individual CCDFs exceed the 10% probability release limit of 1 EPA unit, the mean CCDFs remain below the compliance limits for all three replicates.

Figure 74 shows the overall mean total release with the overall mean releases from each release mechanism. This figure demonstrates that total mean releases are mainly composed of cuttings and cavings, spallings, and direct brine releases, while long-term transport releases through the Culebra are a minor component. Cuttings and cavings control total releases at higher probabilities, while spallings and DBRs have an increased impact at lower probabilities. Similar relationships

Information Only

among the release mechanisms contributing to total releases were observed for the CRA26_IS (Brunell et al. 2025).

Figure 75 shows the overall mean total releases with a 95% confidence interval for the CRA26_FS compared to the CRA26_IS. Table 22 gives the statistics for the overall mean total releases. The observed increases in total releases at high probabilities (above about 0.7) are associated with the increases in cuttings and cavings (Section 4.8.2). The observed increases in total releases at probabilities from about 0.005 to 0.1 are associated with the increases in spallings and DBRs. Overall, at probabilities below about 0.7, total mean releases are similar between the CRA26_IS and the CRA26_FS due to the offsetting effects of increased repository footprint and decreased radionuclide concentrations (in both mobilized and nonmobilized forms).

Both Figure 75 and Table 22 confirm that mean total releases are below the regulatory release limits for both the CRA26_FS and CRA26_IS. These results demonstrate that the WIPP repository, in both the interim and final state, remains in compliance with the containment requirements of 40 CFR Part 191.

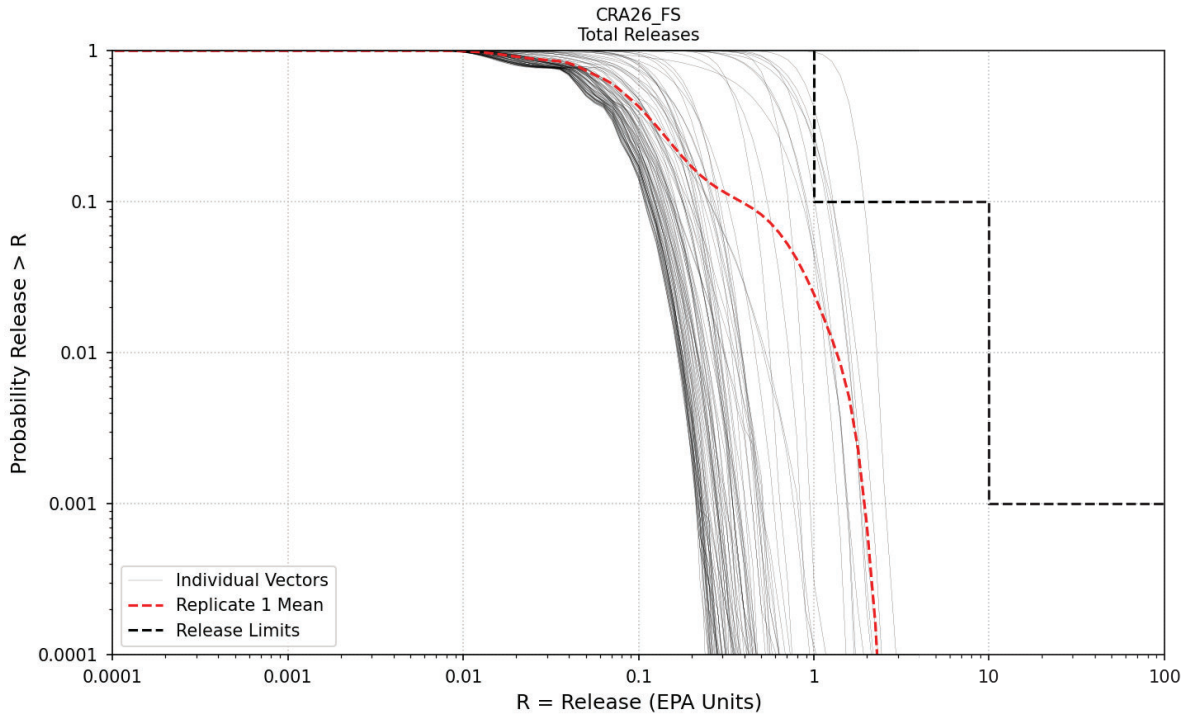


Figure 71. Total Releases for Replicate 1 of the CRA26_FS

Information Only

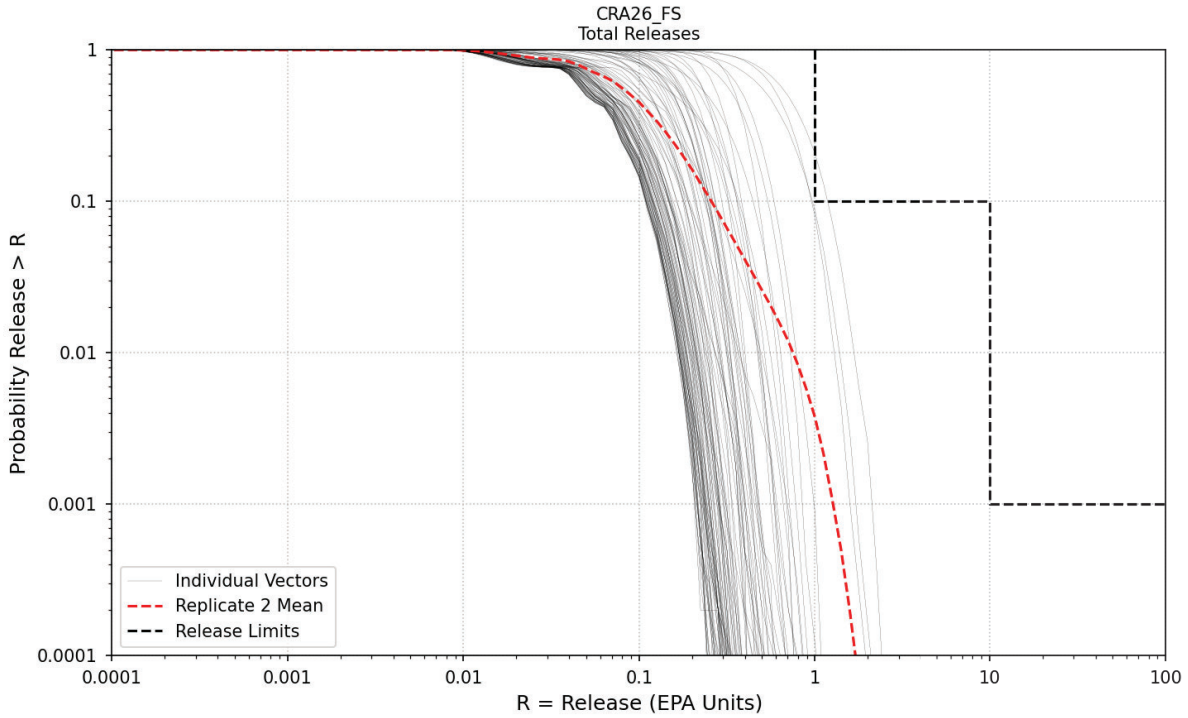


Figure 72. Total Releases for Replicate 2 of the CRA26_FS

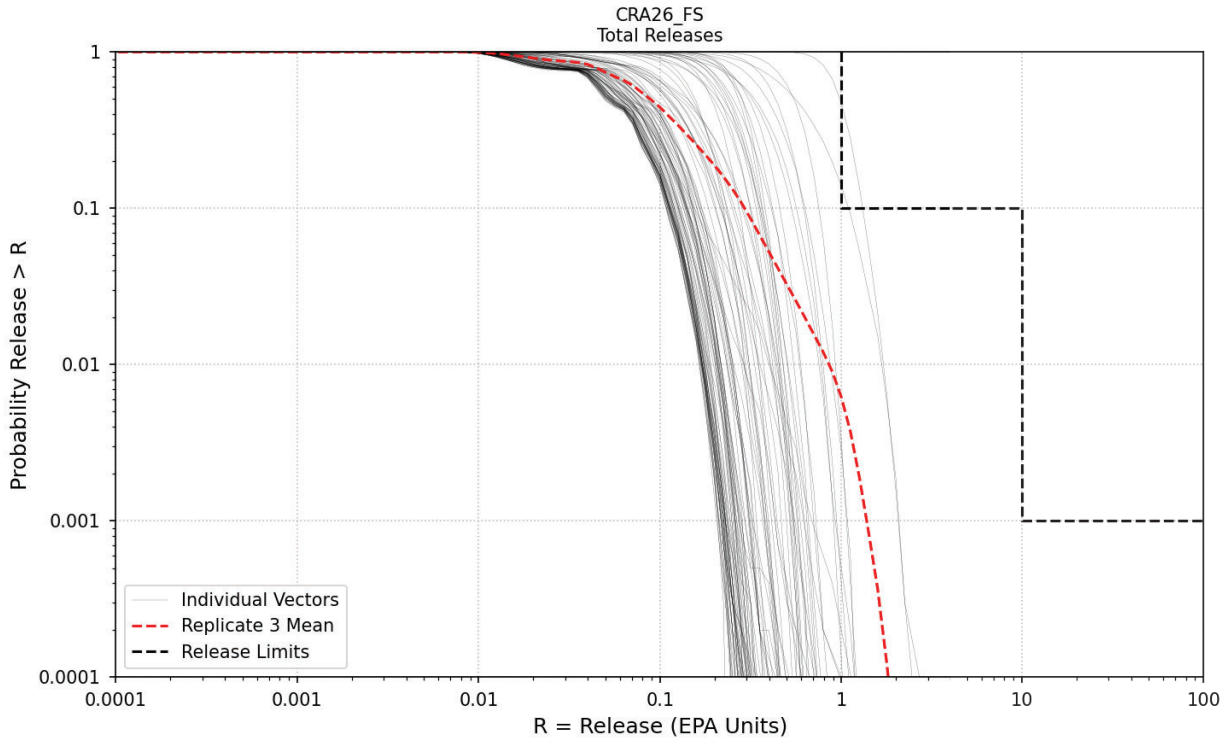


Figure 73. Total Releases for Replicate 3 of the CRA26_FS

Information Only

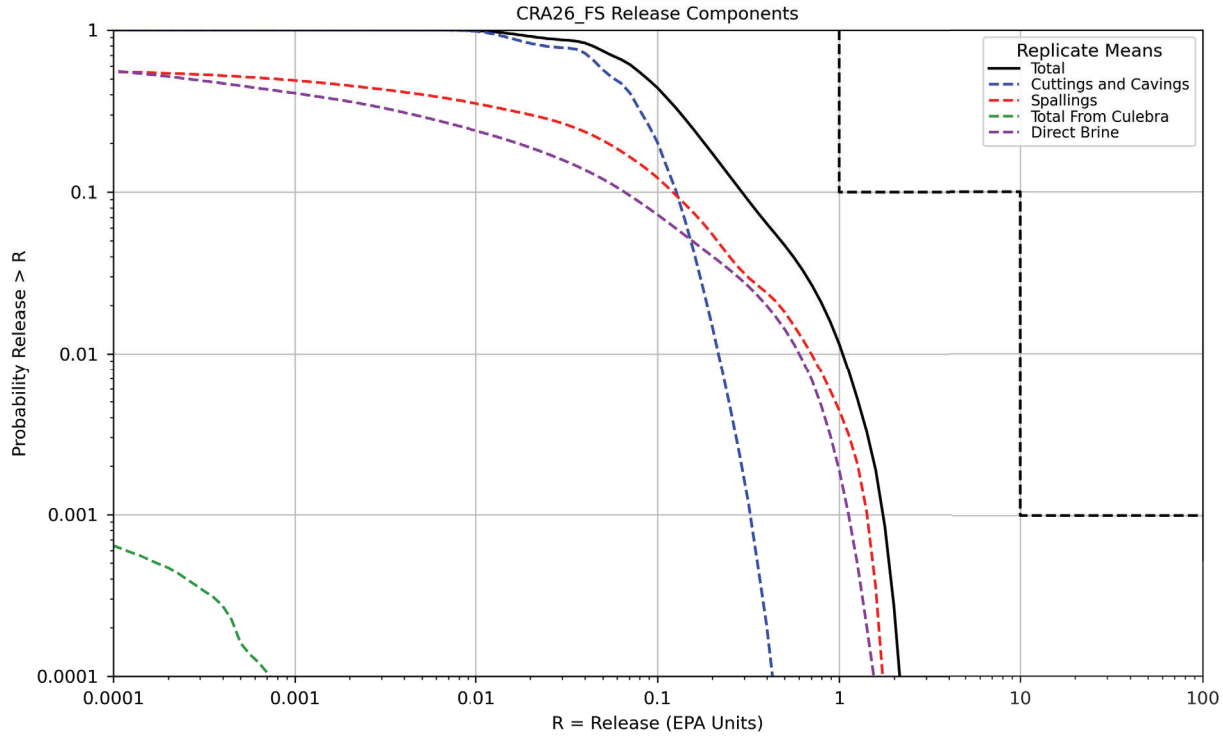


Figure 74. Overall Mean Release Components for the CRA26_FS

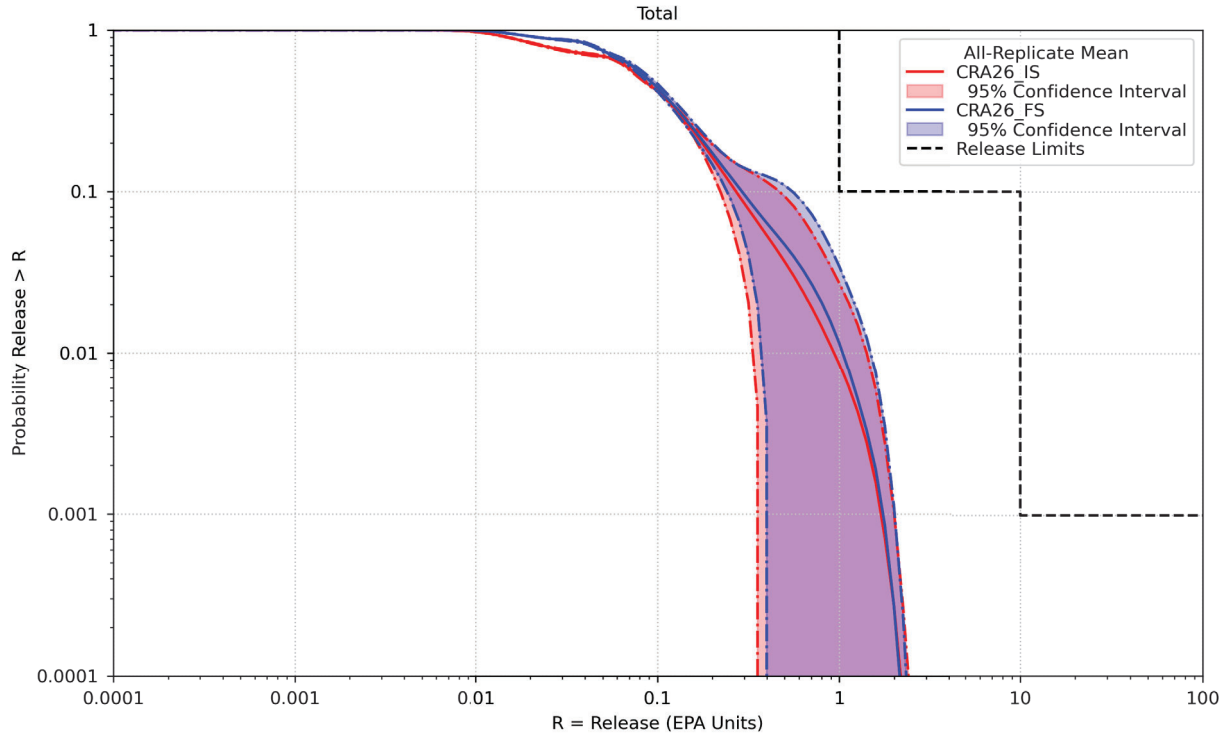


Figure 75. Overall Mean Total Releases for the CRA26_FS

Information Only

Table 22. Statistics on the Overall Mean for Total Releases

Analysis	P(R)>0.1 Lower CI (EPA Units)	P(R)>0.1 Mean (EPA Units)	P(R)>0.1 Upper CI (EPA Units)	P(R)>0.1 Release Limit (EPA Units)	P(R)>0.001 Lower CI (EPA Units)	P(R)>0.001 Mean (EPA Units)	P(R)>0.001 Upper CI (EPA Units)	P(R)>0.001 Release Limit (EPA Units)
CRA26_IS	0.2219	0.2713	0.4679	1	0.3678	1.7121	2.0062	10
CRA26_FS	0.2419	0.2922	0.5516	1	0.4092	1.7489	2.0251	10

4.9.1 Sensitivity Analysis for Total Releases

The methodology of the sensitivity analysis calculations in the CRA26_FS remains consistent with the methodology used in the CRA26_IS. Sensitivity analysis for mean total releases was conducted to identify the parameters contributing most to variability in total releases. In the sensitivity analysis results, the cumulative R^2 value represents the proportion of total uncertainty explained by the fitted rank regression using the listed variables, starting with the greatest contributor to the variance. The number of variables in the regression model is determined by the stepwise regression procedure (King et al. 2025). Regression analyses are conducted for each replicate separately, so results for the CRA26_IS and the CRA26_FS analyses are compared on a per-replicate basis.

To aid in interpretation and discussion of the results, gray highlighting indicates parameters with a change in R^2 greater than 0.05 between the current step and the previous step. While this threshold of 0.05 is somewhat arbitrary, the highlighted parameters are clearly influential and tend to have a more consistent ranking. For a full discussion of STEPWISE, see Appendix A of King et al. (2025). Note the CRA26_FS uses the same sampled input parameters in the STEPWISE analysis as the CRA26_IS.

Table 23, Table 24, and Table 25 compare the sensitivity of mean total releases (mean of each CCDF) to uncertain parameters for each replicate of the CRA26_IS and CRA26_FS analyses. In both analyses, the porosity of the intact Salado halite (S_HALITE:POROSITY) is the dominant parameter controlling variability in mean total releases.

In the CRA26_FS analysis, S_HALITE:POROSITY explains 22–32% of the variability in mean total releases, compared to 18–27% in the CRA26_IS analysis. This parameter's influence is attributed to its significant impact on repository pressure and brine saturation, which directly affect spallings and direct brine release volumes.

Other notable parameters include:

- BOREHOLE:TAUFAIL: This parameter, representing waste shear strength, is the second most influential across both analyses, explaining 6-13% of variability in total releases in the CRA26_IS and 5-15% in the CRA26_FS. Its importance is tied to its role in cuttings and cavings releases.
- SPALLMOD:PARTDIAM: Particle diameter for spallings is similarly influential to BOREHOLE:TAUFAIL, as it contributed 5-17% of variability in the CRA26_IS and 3-13% in the CRA26_FS.

Information Only

- CASTILER:PRESSURE: Initial brine pore pressure in the Castile contributes 3-5% of variability in the CRA26_IS and 4-6% in the CRA26_FS, highlighting its role in influencing repository pressure and brine flow behavior.

The sensitivity analysis underscores the critical role of repository pressure and brine saturation dynamics, driven by S_HALITE:POROSITY, as well as the influence of SPALLMOD:PARTDIAM, which directly impacts spallings releases, in determining total releases, and BOREHOLE:TAUFAIL, which governs cuttings and cavings releases, in determining total releases. These findings align with previous analyses.

Table 23. Stepwise Ranked Regression Analysis for Mean Total Releases for Replicate 1 of the CRA26_IS and CRA26_FS

	CRA26_IS Replicate 1			CRA26_FS Replicate 1		
Step [a]	Variable	R^2	SRRC	Variable	R^2	SRRC
1	S_HALITE:POROSITY	0.27	0.49	S_HALITE:POROSITY	0.33	0.57
2	SPALLMOD:PARTDIAM	0.33	-0.25	BOREHOLE:TAUFAIL	0.38	-0.27
3	BOREHOLE:TAUFAIL	0.39	-0.23	CASTILER:PRESSURE	0.44	0.23
4	CASTILER:PRESSURE	0.43	0.22	SPALLMOD:PARTDIAM	0.48	-0.18
5	STEEL:CORRMCO2	0.47	-0.22	SOLMOD3:SOLVAR	0.51	0.19
6	WAS_AREA:PROBDEG	0.49	0.17	STEEL:CORRMCO2	0.53	-0.17
7	SOLMOD3:SOLVAR	0.52	0.16	PCS_T1:PORE_DIS	0.55	-0.14
8	SPALLMOD:REPIPERM	0.54	0.15	DRZ_PCS:PRMX_LOG	0.57	-0.14

[a] Steps in stepwise regression analysis
[b] Variables listed in order of selection
[c] Cumulative R^2 value with entry of each variable into regression model
[d] Standardized Rank Regression Coefficient

Information Only

Table 24. Stepwise Ranked Regression Analysis for Mean Total Releases for Replicate 2 of the CRA26_IS and CRA26_FS

	CRA26_IS Replicate 2			CRA26_FS Replicate 2		
Step [a]	Variable	R^2	SRRC	Variable	R^2	SRRC
1	S_HALITE:POROSITY	0.24	0.51	S_HALITE:POROSITY	0.32	0.57
2	BOREHOLE:TAUFAIL	0.31	-0.28	BOREHOLE:TAUFAIL	0.39	-0.26
3	GLOBAL:PBRINE	0.37	0.26	CASTILER:PRESSURE	0.45	0.25
4	CASTILER:PRESSURE	0.42	0.23	GLOBAL:PBRINE	0.50	0.24
5	SPALLMOD:PARTDIAM	0.47	-0.23	WAS_AREA:BIOGENFC	0.53	0.17
6	WAS_AREA:BIOGENFC	0.50	0.19	SPALLMOD:PARTDIAM	0.56	-0.17
7	BH_SAND:PRMX_LOG	0.53	-0.15	DRZ_1:PRMX_LOG	0.58	0.16
8	SOLMOD3:SOLVAR	0.55	0.16	SOLMOD3:SOLVAR	0.60	0.15
9	WAS_AREA:GRATMICI	0.58	0.16	SPALLMOD:REPIPOR	0.62	-0.14
10	STEEL:CORRMCO2	0.60	-0.14			

[a] Steps in stepwise regression analysis
[b] Variables listed in order of selection
[c] Cumulative R^2 value with entry of each variable into regression model
[d] Standardized Rank Regression Coefficient

Table 25. Stepwise Ranked Regression Analysis for Mean Total Releases for Replicate 3 of the CRA26_IS and CRA26_FS

	CRA26_IS Replicate 3			CRA26_FS Replicate 3		
Step [a]	Variable	R^2	SRRC	Variable	R^2	SRRC
1	S_HALITE:POROSITY	0.18	0.39	S_HALITE:POROSITY	0.22	0.44
2	SPALLMOD:PARTDIAM	0.35	-0.38	BOREHOLE:TAUFAIL	0.37	-0.37
3	BOREHOLE:TAUFAIL	0.48	-0.35	SPALLMOD:PARTDIAM	0.50	-0.35
4	(Composite):MKD_U	0.51	-0.15	(Composite):MKD_U	0.53	-0.20
5	CASTILER:PRESSURE	0.54	0.18	CASTILER:PRESSURE	0.57	0.19
6	WAS_AREA:SAT_WICK	0.57	0.14	WAS_AREA:SAT_WICK	0.60	0.18
7	WAS_AREA:GRATMICH	0.59	0.15	SOLMOD3:SOLVAR	0.62	0.13
8	WAS_AREA:BIOGENFC	0.61	0.15			
9	SPALLMOD:REPIPOR	0.63	-0.14			
10	S_HALITE:PRESSURE	0.64	-0.13			
11	GLOBAL:PBRINE	0.66	0.13			

[a] Steps in stepwise regression analysis
[b] Variables listed in order of selection
[c] Cumulative R^2 value with entry of each variable into regression model
[d] Standardized Rank Regression Coefficient

Information Only

4.9.2 Comparison to RPPCR

In this section, overall mean total releases from the CRA26_FS are compared to releases from the Replacement Panels Planned Changed Request (RPPCR) PA releases. Releases are illustrated in Figure 76, with corresponding statistics provided in Table 26. Mean total releases for the CRA26_FS have increased compared to the RPPCR.

While there have been updates to the PA model from the RPPCR to the CRA26_FS, such as the refinements to the repository dimensions (Section 2.2) and implementation of a lower bound on capillary pressure in the anhydrite marker beds (Hansen et al. 2025), these changes have little impact on releases.

Two factors are seen as driving the increase in releases for the CRA26_FS. First, since there are no calculated releases from the repository in the undisturbed scenario, all releases are contingent upon drilling intrusions, making release levels highly sensitive to the frequency of drilling events. For the CRA26_FS calculation, the frequency of drilling events (parameter GLOBAL:LAMBDAD) was set at 1.534×10^{-2} boreholes/km^2/yr, an increase from the 1.389×10^{-2} boreholes/km^2/yr value used in RPPCR.

Second is the increase in radionuclide activity since the RPPCR. In the CRA26_FS inventory, the total activity at closure is 9.68×10^6 Ci, with a waste unit factor (WUF) of 8.68, compared the RPPCR inventory with a total activity at closure of 6.51×10^6 Ci and a WUF of 5.59 (Kicker 2025a). Because releases are quantified in EPA units (a measure of activity normalized to the activity at closure), an increase in radionuclide activity does not necessarily lead to increased releases. However, the rise in radionuclide activity since RPPCR is driven by increases in long half-life radionuclides. This results in an increase in normalized activity over time, which in turn contributes to increased releases.

Information Only

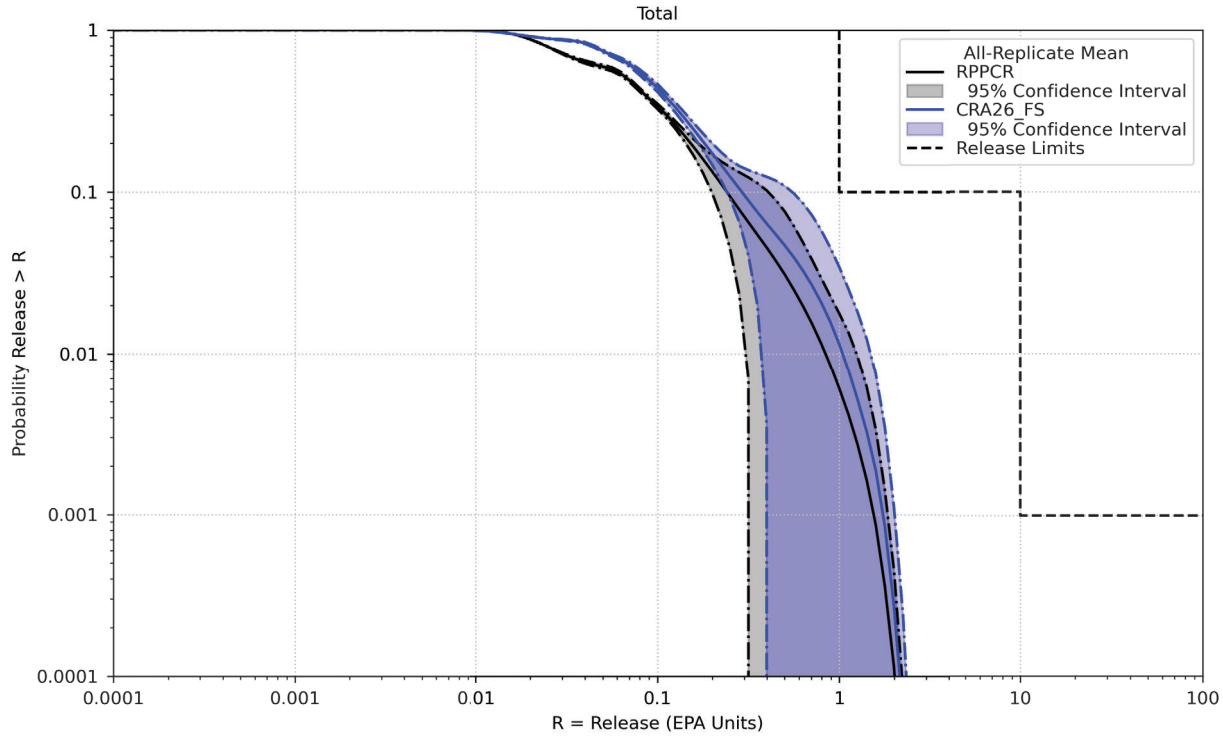


Figure 76. Overall Mean Total Releases

Table 26. Statistics on the Overall Mean for Total Releases

Analysis	P(R)>0.1 Lower CI (EPA Units)	P(R)>0.1 Mean (EPA Units)	P(R)>0.1 Upper CI (EPA Units)	P(R)>0.1 Release Limit (EPA Units)	P(R)>0.001 Lower CI (EPA Units)	P(R)>0.001 Mean (EPA Units)	P(R)>0.001 Upper CI (EPA Units)	P(R)>0.001 Release Limit (EPA Units)
RPPCR	0.1990	0.2418	0.4073	1	0.3360	1.5541	1.8716	10
CRA26_FS	0.2419	0.2922	0.5516	1	0.4092	1.7489	2.0251	10

5.0 CONCLUSIONS

The CRA-2026 Final State Repository Performance Assessment (CRA26_FS PA) supports the DOE's 2026 recertification application with an analysis that considers a repository representation that provides sufficient volume for disposal of the full allowable LWA waste volume. The CRA26_FS repository comprises a total of 19 waste panels (10 original, two replacement, and seven additional panels) and PA results are compared to results of the CRA-2026 Interim State Repository (CRA26_IS) PA which comprises 12 waste panels (10 original, two replacement)..

The primary differences between the CRA26_IS and CRA26_FS are based on the increased footprint and waste inventory associated with the 19-panel repository representation. The changes include: repository volume and footprint area parameters, the computational grid for Salado flow and transport, radionuclide and non-radionuclide waste inventory, baseline actinide solubilities

Information Only

and colloidal enhancement parameters based on the new radionuclide inventory, the minimum brine volume needed for a direct brine release, and additional release points for radionuclide releases from the Culebra formation.

Results from the CRA26_FS analysis are compared to those obtained in the CRA26_IS analysis to assess repository performance impacts due to the inclusion of waste into seven additional waste panels. Mean releases from the CRA26_FS indicate that the additional panels have some impact on cuttings, cavings, spallings, and direct brine releases, as well as releases from the Culebra. Radionuclides entering the Culebra over the four western-most additional panels (Panels 15, 16, 17, and 18) generally travel in a different direction than releases over the existing panels and the other additional and the replacement panels which, under full mining conditions, leads to shorter travel times and a relative increase in releases.

Mean total releases in the CRA26_FS continue to be dominated by cuttings and cavings at high probabilities. Spallings releases show an increased contribution to total releases at lower probabilities, slightly exceeding the impact from direct brine releases; both release mechanisms are dominant at lower probabilities. Direct brine releases are increased at almost all probabilities. Releases from the Culebra are by far the smallest contribution to total releases. Mean total releases have increased in the CRA26_FS compared to the CRA26_IS above probability 0.7 and at probability between 0.005 and 0.1; but are otherwise very similar between the two analyses. Mean total releases have slightly increased in the CRA26_FS compared to the CRA26_IS at the two regulatory release limits. Within the waste panels, brine saturations are increased due to reduced gas generation (pressures are increased or similar), a result of decreased waste concentration across the larger repository footprint. Overall, the changes in releases are relatively minor due to the competing impacts of increased repository footprint and reduced radionuclide concentrations (in both mobilized and nonmobilized forms). For the highest probability releases, increased cuttings and cavings releases can be attributed to the increased probability (associated with the increased repository footprint) of encountering the highest concentration waste streams in the waste inventory. Mean total releases from the CRA26_FS are below the regulatory limits.

Information Only

6.0 REFERENCES

Bethune, J. 2023. Culebra Flow and Transport Analysis Report for the Replacement Panels Planned Change Request (RPPCR). ERMS 579725. Carlsbad, NM: Sandia National Laboratories.

Beauheim, R.L., and Holt, R.M. 1990. Hydrogeology of the WIPP site, in Powers, D.W., Holt, R.M., Beauheim, R.L., and Rempe, N., eds., Geological and Hydrological Studies of Evaporites in the Northern Delaware Basin for the Waste Isolation Pilot Plant (WIPP): Guidebook 14. Geological Society of America (Dallas Geological Society), p. 45-78. ERMS 246378

Bollinger, M. 2024. Letter to Ms. L. Veal. Subject: Planned Change Request for the use of Replacement Panels 11 and 12. March 12, 2024. CBFO:ERCD:MG:SV:24-0168. Carlsbad, NM: U.S. DOE, Carlsbad Field Office.

Bowman, D., R. Kushnereit, M. Pedrazas, P. Johnson, N. Deeds, and J. Pinkard. 2023. Analysis Report Documenting the Data, Generation, and Calibration of T-fields for CRA-2024. ERMS 579507. Carlsbad, NM: Sandia National Laboratories.

Brunell, S. 2025. Update to CRA-2026 PA Input Parameters Due to Revised WIPP Repository Dimensions. EIMS-0004799007. Carlsbad, NM: Sandia National Laboratories.

Brunell, S. and D.C. Kicker. 2025. Analysis Report for Cuttings, Cavings, and Spallings in the 2026 Compliance Recertification Application Performance Assessment: Interim State Repository. EIMS-0005077055. Carlsbad, NM: Sandia National Laboratories.

Brunell, S., B. Day, P. Docherty, D. Kicker, S. Kim, S. King, J. Long, J. Wilgus, and T.R. Zeitler. Summary Report for the 2026 Compliance Recertification Application Performance Assessment: Interim State Repository. Carlsbad, NM: Sandia National Laboratories.

Burgess, A., T. Doe, T. Lowenstein, and J.A. Thies. 2008. Waste Isolation Pilot Plant Culebra Hydrogeologic Conceptual Model Peer Review Final Report. Carlsbad, NM: U.S. Department of Energy. ERMS 551513.

Cranston, C.C. 2009. Minable Potash Ore. ERMS 551120. Carlsbad, NM: Bureau of Land Management.

Day, B. 2025. BRAGFLO Grid Development for CRA-2026. EIMS-0004447000. Carlsbad, NM: Sandia National Laboratories.

Day, B. and S. King. 2025. Analysis Report for Salado Flow in the 2026 Compliance Recertification Application Performance Assessment: Interim State Repository. EIMS-0004944216. Carlsbad, NM: Sandia National Laboratories.

Docherty, P. and S. Kim. 2025. Analysis Report for Actinide Mobilization and Salado Transport in the 2026 Compliance Recertification Application Performance Assessment: Interim State Repository. EIMS-0005110990. Carlsbad, NM: Sandia National Laboratories.

Domski, P. 2025a. Th(IV), Np(V), and Am(III) Baseline Solubilities for the 2026 WIPP Compliance Recertification Application Performance Assessment Final-State Analysis (CRA-2026 FS). EIMS-0004800933. Carlsbad, NM: Sandia National Laboratories.

Information Only

Domski, P. 2025b. Prediction of Baseline Actinide Solubilities for the 2026 WIPP Compliance Recertification Application Performance Assessment Interim-State Analysis (CRA-2026 IS). EIMS-0004838025. Carlsbad, NM: Sandia National Laboratories.

Feng, M. and D.C. Kicker. 2025. Input Parameter Report for the 2026 Compliance Recertification Application Performance Assessment: Final State Repository (CRA-2026 FS). EIMS-0005063812. Carlsbad, NM: Sandia National Laboratories.

Hansen, C., S. King, J. Bethune, and S. Brunell. 2023. Analysis Plan for the Performance Assessment for the Replacement Panels Planned Change Request. AP-204. ERMS 579449. Carlsbad, NM: Sandia National Laboratories.

Hansen, C., S. Brunell, B. Day, S. King, and J. Wilgus. 2025. Analysis Plan for the 2026 WIPP Compliance Recertification Application Performance Assessment. AP-214. Carlsbad, NM: Sandia National Laboratories.

Hart, D.B., R.M. Holt, and S.A. McKenna. 2008. Analysis Report for Task 5 of AP-114: Generation of Revised Base Transmissivity Fields. ERMS 552391. Carlsbad, NM: Sandia National laboratories.

Holt, R.M. 1997. Conceptual Model for Transport Processes in the Culebra Dolomite Member of the Rustler Formation. Carlsbad, NM: Sandia National laboratories. SAND 97-0194.

Kaplan, U., Swanson, J., and Kutahyali-Aslani, C. 2025. LANL ACRSP Parameter Recommendations for CRA-2026 Performance Assessment. Revision 1. LCO-ACP-41. Carlsbad, NM: Los Alamos National Laboratory.

Kicker, D. 2025a. Analysis Report for Radionuclide Inventory Screening in the 2026 Compliance Recertification Application Performance Assessment: Final State Repository. Revision 0. EIMS-0004799526. Carlsbad, NM: Sandia National Laboratories.

Kicker, D. 2025b. Analysis Report for Radionuclide Inventory Screening in the 2026 Compliance Recertification Application Performance Assessment: Interim State Repository. Revision 0. EIMS-0004832100. Carlsbad, NM: Sandia National Laboratories.

Kim, S. and D. Kicker. 2025. Analysis Report for Inventory EPA Units in the 2026 Compliance Recertification Application Performance Assessment: Interim State Repository. Revision 1. EIMS-0004940556. Carlsbad, NM: Sandia National Laboratories.

King, S. 2021. APPA 2D Salado Flow Grid Development. SAND2021-8603PE. Carlsbad, NM: Sandia National Laboratories.

King, S. 2023. Salado Flow Analysis Report for the Replacement Panels Planned Change Request (RPPCR). ERMS 579722. Carlsbad, NM: Sandia National Laboratories.

King, S. 2025. Area for RH waste disposal for the interim state CRA-2026 PA calculation. EIMS-0004801801. Carlsbad, NM: Sandia National Laboratories.

King, S. and T. Zeitler. 2025. Analysis Report for Parameter Sampling in the 2026 Compliance Recertification Application Performance Assessment. EIMS-0004951492. Carlsbad, NM: Sandia National Laboratories.

Information Only

King, S., S. Brunell, and T. Zeitler. 2025. Analysis Report for Normalized Releases in the 2026 Compliance Recertification Application Performance Assessment: Interim State Repository. EIMS-0005040307. Carlsbad, NM: Sandia National Laboratories.

Kirchner, T., A. Gilkey, and J. Long. 2014. Summary Report on the Migration of the WIPP PA Codes from VMS to Solaris. AP-162, Rev. 1. ERMS 561757. Carlsbad, NM: Sandia National Laboratories.

Kirchner, T., A. Gilkey, and J. Long. 2015. Addendum to the Summary Report on the Migration of the WIPP PA Codes from VMS to Solaris. AP-162. ERMS 564675. Carlsbad, NM: Sandia National Laboratories.

Kirkes, G.R. 2024. SP Performing FEPs Baseline Impact Assessments for Planned or Unplanned Changes. Rev. 6. SP 9-4. Carlsbad, NM: Sandia National Laboratories.

Kirkes, G.R. and J. McCormick. 2025. Features, Events, and Processes Assessment for the 2026 Compliance Recertification Application Performance Assessment. EIMS-0004940580. Carlsbad, NM: Sandia National Laboratories.

Kuhlman, K. 2010. Analysis Report for the CRA-2009 PABC Culebra Flow and Transport Calculations. ERMS 552951. Sandia National Laboratories, Carlsbad, NM.

Leigh, C., and J. Trone. 2005. Calculation of Radionuclide Inventories for Use in NUTS in the Performance Assessment Baseline Calculation Revision 0. ERMS 539644. Sandia National Laboratories. Carlsbad, NM.

Long, J. 2025. Computational Code Execution and File Management in the 2026 Compliance Recertification Application Performance Assessment: Final State Repository (CRA-2026 FS). Revision 0. EIMS-0004899943. Carlsbad NM: Sandia National Laboratories.

Lord, D., and D. Rudeen. 2003. Sensitivity Analysis Report: Parts I and II: DRSPALL Version 1.00: Report for Conceptual Model Peer Review July 7–11. ERMS 524400. Carlsbad, NM: Sandia National Laboratories.

Mariner, P. 2025. CRA-2026 FS updates to the WIPP humic colloids models for An(III) and An(IV). EIMS-0004800929. Carlsbad, NM: Sandia National Laboratories.

McCormick, J., Kirkes R., and Hansen C. 2024. Conceptual Models in WIPP Performance Assessment. EIMS-0004385596. Carlsbad, NM: Sandia National Laboratories.

Sanchez, L.C., J. Liscum-Powell, J.S. Rath, and H.R. Trellue. 1997. WIPP PA Analysis Report for EPAUNI: Estimating Probability Distribution of EPA Unit Loading in the WIPP Repository for Performance Assessment Calculations, Version 1.01. WBS 1.2.07.1.1. Albuquerque, NM: Sandia National Laboratories. ERMS 243843.

Shinta, A. A. 1997. User's Manual for NUTS, Version 2.05. Sandia National Laboratories, Albuquerque, NM. ERMS 246002.

U.S. Environmental Protection Agency (U.S. EPA). 1996. 40 CFR Part 194: Criteria for the Certification and Recertification of the Waste Isolation Pilot Plant's Compliance with the 40 CFR Part 191 Disposal Regulations: 61 Federal Register, 5223-5245 (February 9, 1996).

Information Only

U.S. Environmental Protection Agency (U.S. EPA). 1998. 40 CFR Part 194: Criteria for the Certification and Recertification of the Waste Isolation Pilot Plant's Compliance with the Disposal Regulations: Certification Decision. Federal Register, vol. 63 (May 18, 1998): 27354 – 27406.

U.S. Environmental Protection Agency (U.S. EPA). 2025. Letter from Abigale Tardif to Mark Bollinger, Subject: EPA's Review and Approval of DOE's RPPCR for Waste Panels 11 and 12 at WIPP. July 31, 2025. Washington, DC: U.S. EPA.

Van Soest, G.D. 2025a. Full Repository Performance Assessment Inventory Report – 2024. Revision 0. INV-FPA-24. Carlsbad, NM: Los Alamos National Laboratory.

Van Soest, G.D. 2025b. Interim State Performance Assessment Inventory Report – 2024. Revision 0. INV-IPA-24. Carlsbad, NM: Los Alamos National Laboratory.

Wallace, M. 1996. Summary Memo of Record for NS-11: Subsidence Associated with Mining Inside or Outside the Controlled Area. Records Package for Screening Effort NS-11: Subsidence Associated with Mining Inside or Outside the Controlled Area (November 21) (pp. 1–28). ERMS 412918. Albuquerque, NM: Sandia National Laboratories.

Ward, A. 2025. Performance Assessment Inventory for Analysis of a 12-Panel Repository Configuration. Letter to Bill McInroy. March 18, 2025. CBFO:ERCD:AW:RS:25-0197. Carlsbad, NM: Department of Energy Carlsbad Field Office.

Wilgus, J. and J. Bethune. 2025. Analysis Report for Culebra Flow and Transport in the 2026 Compliance Recertification Application Performance Assessment. EIMS-0005101531. Carlsbad, NM: Sandia National Laboratories.

Wilgus, J. and S. Brunell. 2025. Re-Calculation of the Location of Culebra Release Point 2 for Use in WIPP PA Rev. 1. EIMS-0004818700. Carlsbad, NM: Sandia National Laboratories.

Zeitler, T. 2025. Analysis Report for Direct Brine Releases in the 2026 Compliance Recertification Application Performance Assessment: Interim State Repository. EIMS-0004961699. Carlsbad, NM: Sandia National Laboratories.

Information Only

Sandia National Laboratories is a multimission laboratory managed and operated by National Technology & Engineering Solutions of Sandia, LLC, a wholly owned subsidiary of Honeywell International Inc., for the U.S. Department of Energy's National Nuclear Security Administration under contract DE-NA0003525. This research is funded by WIPP programs administered by the Office of Environmental Management (EM) of the U.S. Department of Energy.







Information Only